High Strength and High Modulus Electrospun Nanofibres

Jian Yao

2014

Submitted in partial fulfilment of the requirements of the Degree of Doctor of Philosophy at Queen Mary University of London

Statement of Originality

I, Jian Yao, confirm that the research included within this thesis is my own work or that where it has been carried out in collaboration with, or supported by others, that this is duly acknowledged below and my contribution indicated. Previously published material is also acknowledged below.

I attest that I have exercised reasonable care to ensure that the work is original, and does not to the best of my knowledge break any UK law, infringe any third party's copyright or other Intellectual Property Right, or contain any confidential material.

I accept that the College has the right to use plagiarism detection software to check the electronic version of the thesis.

I confirm that this thesis has not been previously submitted for the award of a degree by this or any other university.

Signature:

Date:

Details of Collaboration and Publications:

1. Yao, J.; Bastiaansen, C.W.; Peijs, T. High strength and high modulus electrospun nanofibers. *Fibers* **2014**, *2*, 158-186.
2. Yao, J.; Jin, J.H.; Pugno, N.M.; Bastiaansen, C.W.; Peijs, T. Electrospinning of PPTA fibres. *Macromolecular Materials and Engineering* **2014**. Submitted.
3. Yao, J.; Pugno, N.M.; Bastiaansen, C.W.; Peijs, T. High performance electrospun co-polyimide nanofibres. *Macromolecules* **2014**. Submitted.
4. Yao, J.; Bastiaansen, C.W.; Peijs, T. Fabrication and Evaluation of co-polyimide nanofibre reinforced composites. *Composites Science and Technology* **2014. S**ubmitted.
5. Yao, J.; Hughes-Brittain, N.F.; Picot, O.T.; Bastiaansen, C.W.; Peijs, T. Electrospinning of reactive mesogens. *Macromolecular Materials and Engineering* **2014**. To be submitted.

Acknowledgements

First of all, I would like to express my sincere appreciation to my supervisors Prof. Ton Peijs and Kees Bastiaansen for giving me the great opportunity to carry out my PhD study in their group. In the last four years, I really appreciate their continuous guidance, trust, patience and last but not the least, their transfer of knowledge. Secondly, I would like to thank my good friends Dr. Nanayaa Bates, Dr. Olivier Picot and Charline Sellam for many valuable discussions, encouragement and generous help.

I wish to thank all the other group members for their friendship and many fruitful discussions. Thanks are especially given to Dr. Emiliano Bilotti, Dr. Wei Tu, Han Zhang, Mai Fang, Pascal Cachelin, Eric Asare, Rui Mao, Zhifei Zhang, Yafet Abbay, Yan Li, and Xi Zhang. Previous group member Dr. Junhong Jin is thanked for his valuable early work and contribution in the electrospinning of rigid polymers (PBO and PPTA) and for his continuous support and care during my PhD career.

I would like to thank Prof. Nicola Pugno for his support and contribution in the mechanical testing and evaluation of single fibres and nanofibre bundles. Dr. Fiorella Pantano and Dr. Emiliano Lepore are thanked for the help with experiments at the University of Trento.

I also wish to make a grateful acknowledgement to all the support staff in the School: to Dr. Rory Wilson for XRD measurements and helpful discussions; to Dr. Zofia Luklinska for her continuous help on SEM and TEM; to Dr. Nima Roohpour and Dr.

Krystelle Mafina for FTIR, DSC and DMA measurements; to Mr. Roger Nelson, Mr. Danny Neighbour, Mr. Vince Ford, Mr. Dennis Lfe, Mr. Dougie Thomson for their valuable technical support.

My sincere thanks are also given to all my friends in the School and Nanoforce: Dr. Xin Bai, Yiran An, Dr. Zhipeng Gao, Dr. Dun Lu, Dr. Huijuan Chen, Dr. Congwei Wang, Menglong Huang, Dr. Yongqiang Tan, Kan Chen and Chunchun Li.

Finally, my special thanks are given to Xin Chen and my parents for their consistent support and understandings.

Abstract

In the last two decades, a rapidly growing polymer processing technology, electrospinning, has attracted great interests as it provides a viable and simple method to create ultra-fine continuous fibres. Despite the potential utilization of electrospun nanofibres in many fields, their success is limited so far due to their poor mechanical properties compared to corresponding textile fibres made from the same polymers, which is mainly ascribed to the low degree of orientation and chain extension of the macromolecules along the fibre axis in such fibres.

In this thesis, first an in-depth review of the mechanical properties of electrospun fibres and recent developed methodologies to generate high strength and high modulus nanofibres will be presented. In the experimental work, electrospinning of rigid polymer PPTA was attempted and mechanical properties of obtained fibres were evaluated (Chapter 3). It was shown that the electrospinning process cannot be easily operated in a controllable and continuous manner although some high performance fibres were obtained. Chapter 4 dealt with the electrospinning of reactive mesogens (liquid crystal monomers) by employing polymers (PMMA and PA6) as matrix. The mechanical properties of the resulting composite nanofibres (PA6/RM257) showed dependence on the reactive mesogen (RM257) content and the phase separation between PA6 and RM257. In Chapter 5, a high performance polymer BPDA/PDA/ODA was synthesized and electrospun; the nanofibres were characterized using FTIR and WAXD and their mechanical tests were carried out based on unidirectional mats and multifilament bundles. A Weibull modulus based

model was introduced to estimate the tensile strength of single nanofibres in such bundles. Subsequently, composites based on BPO nanofibres in a rubbery thermoplastic matrix were fabricated and evaluated in Chapter 7 using composite mechanics theories for off-axis properties and 'Rule of Mixture' which were used to back-calculate the Young's modulus of single BPO nanofibres. From this it could be concluded that the developed co-polyimide BPO nanofibres exhibit among the highest mechanical properties of electrospun nanofibres reported in literature so far. It can be concluded that the electrospun BPO co-polyimide nanofibres and *p*-aramid fibres possess among the highest mechanical properties reported for electrospun fibres so far.

Table of Contents

Table of Contents 8

List of Abbreviations and Acronyms 13

List of Figures 15

List of Tables 23

Chapter 1 24

General Introduction

1.1 Electrospinning and Electrospun Nanofibres 24

1.2 Liquid Crystal Polymers and Reactive Mesogens 27

1.3 High Performance Fibres 28

1.4 Outline of the Thesis 29

1.5 Reference 31

Chapter 2

High Strength and High Modulus Electrospun Fibres

2.1 High Strength and High Modulus Conventional Fibres 34

2.1.1 Basic concepts for high performance fibres 34

2.1.2 High performance fibres based on flexible polymer chains 38

2.1.3 High performance fibres based on rigid polymer chains 40

2.2 Electrospun Nanofibres 43

2.2.1 Basic concepts of electrospinning 43

2.2.2. Electrospun nanofibres based on flexible chain polymers 47

2.2.3. Electrospun nanofibres based on rigid chain polymers 61

2.2.3.1. Electrospun PPTA fibres 61

2.2.3.2. Electrospun polyimide nanofibre 63

2.2.4. Other routes to high performance nanofibres 65

2.2.4.1. CNT reinforced polymer nanofibres 65

2.2.4.2. Electrospun polymer-derived carbon nanofibres 68

2.3. Conclusions 71

2.4. References 72

Chapter 3

Electrospinning of PPTA Fibres

3.1 Introduction 86

3.2. Experimental 88

3.2.1. Solution preparation and electrospinning 88

3.2.2. Tensile testing and fibre characterization 89

3.3. Results and Discussion 90

3.3.1. Electrospinning from isotropic and anisotropic PPTA solutions 90

3.3.2. Feasibility of electrospinning conditions for p-aramid fibres 95

3.3.3. Mechanical properties of electrospun p-aramid fibres 98

3.4. Conclusions 107

3.5. References 108

Chapter 4

Electrospinning of Reactive Mesogens

4.1 Introduction 112

4.2 Experimental 114

4.2.1 Materials and solution preparation 114

4.2.2 Spin-coating, electrospinning and UV-induced photo-polymerization 115

4.2.3 Characterization 116

4.3 Result and Discussion 117

4.3.1 Spinning-coating, electrospinning and characterization of PMMA with RM257 117

4.3.2 Electrospinning and characterization of PA6 with RM257 124

4.4 Conclusions 129

4.5 References 130

Chapter 5

Electrospinning of Co-polyimide Nanofibres 132

5.1 Introduction 132

5.2 Experimental 134

5.2.1 Materials 134

5.2.2 Synthesis of co-polyimide BPDA/PDA/ODA polyamic acid 135

5.2.3 Electrospinning of BPDA/PDA/ODA polyamic acid 135

5.2.4 Conversion from BPDA/PDA/ODA polyamic acid to polyimide 135

5.2.5 Characterization 136

5.3 Results and Discussion 137

5.3.1 Synthesis of BPO polyamic acid 137

5.3.2 Electrospinning of polyamic acid, imidization process and characterization 138

5.3.3 Mechanical properties of co-polyimide nanofibres 142

5.4 Conclusions 150

5.5 References 152

Chapter 6

Co-polyimide Nanofibre Reinforced Composites

6.1 Introduction 155

6.2. Experimental 158

6.2.1. Materials 158

6.2.2. Fabrication of BPO co-polyimide nanofibres UD composites 158

6.2.3. Characterization 159

6.3. Results and Discussion 161

6.3.1. Mechanical properties of UD BPO nanofibre reinforced composites 161

6.3.2. Off-axis properties of UD BPO nanofibre reinforced composites 164

6.3.3. Young's modulus evaluation of single nanofibres 167

6.4. Conclusions 171

6.5. References 171

Chapter 7

Conclusions and Future Work

7.1 Conclusions 175

7.2 Future Work 181

7.3 References 186

List of Abbreviations and Acronyms

BPO	BPDA/PDA/ODA
BPDA	3, 3', 4, 4'-biphenyltetracarboxylic dianhydride
ODA	4, 4'-oxydianiline
PDA	*p*-Phenylenediamine
CNT	Carbon nanotube
DSC	Differential scanning calorimetry
DMF	Dimethylformamide
FTIR	Fourier transform infrared spectroscopy
MWNT	Multi-walled carbon nanotube
OM	Optical microscope
PA6	Polyamide 6
PAN	Polyacrylonitrile
PBO	Poly(phenylene benzobisoxazole)
PEO	Polyethylene oxide
PMMA	Poly(methyl methacrylate)
POM	Polarized optical microscope
PP	Polypropylene
PPTA	Poly(*p*-phenylene terehthalamide)
PS	Polystyrene
PVC	Polyvinylchloride

RM	Reactive mesogen
SANS	Small angle neutron scattering
SEM	Scanning electron microscope
SWNT	Single-walled carbon nanotube
TEM	Transmission electron microscope
UHMWPE	Ultra-high molecular weight polyethylene
WAXD	Wide-angle X-ray diffraction

List of Figures

Figure 1.1. Numbers of research articles, meeting articles, book chapters, etc. from 1999 to 2013 (searching key word: electrospinning; source: Web of Science). 25

Figure 1.2. A typical electrospinning set-up with a grounded collector. 26

Figure 1.3. Specific surface area as a function of fibre diameter in nonwovens. 26

Figure 1.4. Various potential applications of electrospun nanofibres. 27

Figure 1.5. A general classification of high performance fibres, industrial and textile fibres according to their modulus and strength. 29

Figure 2.1. Ideal polymer chains model for producing high strength and high modulus fibres. 36

Figure 2.2. Schematics of the gel-spinning process. 39

Figure 2.3. Molecular orientation during dry-jet wet spinning of PPTA. 42

Figure 2.4. A typical electrospinning set-up with a grounded collector. 44

Figure 2.5. Two scanning electron microscope (SEM) pictures of an electrospun PA6 nanofibre non-woven mat under different magnifications (scale bars of 40 μm and 5 μm, respectively). 45

Figure 2.6. Different fibre morphologies of electrospun nanofibres produced from low solution concentration to high solution concentration of poly(methyl methacrylate) (PMMA) in DMF. 46

Figure 2.7. Novel nanofibre production technologies (a) nozzle-less electrospinning with a rotating head (b) Multi-nozzle electrospinning with a twin-screw extrusion (c) Rotary jet-spinning. 47

Figure 2.8. (a) WAXS pattern of electrospun UHMWPE nanofibre, showing broad reflection arcs typical of a moderately oriented polymer structure. (b) WAXS pattern of solution-spun ultra-drawn UHMWPE fibre with draw-ratio 100, showing intense reflections typical of a highly oriented polymer structure. 48

Figure 2.9. Strain-stress curves electrospun poly(glycolide-co-lactide) of as-spun nanofibre mat and nanofibre mat after a solid-state deformation of 450%. 51

Figure 2.10. Two dimensional (2D) wide-angle X-ray diffraction patterns of electrospun polyoxymethylene (POM) nanofibres with different take up speeds (a) 630m/min (b) 1890 m/min. 52

Figure 2.11. (a) Orientation parameter $<P_2>$ obtained from SANS experiments for as-spun polystyrene fibres as a function of collector speed. Red circles represent uncorrected data for fibre angular alignment on the electrode while black squares are corrected data. Open symbols represent samples collected on static parallel plate electrode. (b) Radius of gyration of polymer chains parallel (black squares) and perpendicular (red circles) to the fibre direction together with bulk data (dashed line). 53

Figure 2.12. PCL nanofibres produced under similar conditions but with different fibre diameters (a) 150 nm (b) 450 nm, showing a thinner nanofibre possessing a more aligned fibrillar and lamellae microstructure. 54

Figure 2.13. Relative Young's modulus E_{rel} ($E_{rel} = E/E_{bulk}$) of electrospun PA 6,6 nanofibres as a function of their diameters. 56

Figure 2.14. (a) Stress-strain curves of electrospun PAN nanofibres with different diameters (b) XRD patterns of nanofiber bundles with various fibre diameters and corresponding degree of crystallinity (inset). 58

Figure 2.15. A single electrospun PPTA fibre together with a single Kevlar®49 fibre. 61

Figure 2.16. Liquid crystalline behavior of PPTA solution, indicating an isotropic phase at concentrations below 12 wt % and an anisotropic phase between concentrations of 12 wt % to 20 wt %. 62

Figure 2.17. Structural formulas of (a) PPTA and (b) BPDA/PDA polyimide. 64

Figure 2.18. A schematic diagram of the imidization process. 64

Figure 2.19. TEM micrograph of an individual MWCNT reinforced electrospun PVA nanofibre, showing an aligned MWCNT in a polymer nanofibre (scale bar 100 nm). 67

Figure 2.20. (a) SEM micrograph and (b) TEM micrograph showing homogenous morphology of carbon nanofibres. 69

Figure 2.21. Mechanical properties of traditional high performance fibres and electrospun nanofibres with respect to Young's modulus and tensile strength. Commercial high-performance fibres show typical tensile strengths of 3–4 GPa and moduli of around 100–300 GPa, while most electrospun fibres typically possess tensile strengths < 0.3 GPa and Young's moduli < 3 GPa. Some high performance

electrospun nanofibres have been reported based on polyimide, polyacrylonitrile and carbon nanofibres from electrospun PAN precursors. 70

Figure 3.1. Schematic illustration of single fibre sample preparation for mechanical tests. 90

Figure 3.2. Schematic illustration of electrospinning set-up of PPTA in concentrated sulphuric acid solutions **Error! Bookmark not defined.**

92**Figure 3.3.** SEM micrographs of fibres 'electrospun' from PPTA solutions with concentrations of (a) 3 wt% (b) 5 wt% and (c) 7 wt%. 94

Figure 3.4. SEM micrographs of fibres 'electrospun' from PPTA solutions with concentrations of (a) 15 wt% (b) 17 wt% and (c) 19.46 wt%. 95

Figure 3.5. Electrospun p-aramid fibres from 19.46 wt% anisotropic solution under crossed polarizer (a) fibre 1 is positioned parallel with one piece of polarizer whilst fibre 2 is positioned at a 45 °angle with the polarizer (b) after 45 °clockwise rotation of sample stage. 99

Figure 3.6. Tensile strength and Young's modulus of electrospun PPTA fibres with varying fibre diameter. 101

Figure 3.7. Stress-strain curves of electrospun PPTA fibres with different diameters. 102

Figure 3.8. Experimental Young's modulus of electrospun PPTA fibres and prediction data based on Equation (3.2). 105

Figure 3.9. Comparison of a smooth PPTA fibre (left) and a PPTA fibre with defects (right). 106

Figure 4.1. Chemical structure of (a) RM257 (b) RM82 and (c) Irgacure184 along with (d) UV-light exposure induced photo-polymerization of RMs in their nematic phase forming an anisotropic structure. 116

Figure 4.2. Optical microscopy pictures of spin-coated films (scale bar 50 μm) of (a) PMMA/RM82 and (b) PMMA/RM257. 118

Figure 4.3. Polarized optical micrographs of electrospun PMMA/RM82 (1/1, weight ratio) fibres (scale bar 50 μm); (a) at 45 ° angle with crossed polarizers (corresponding optical micrograph, inset); (b) at 135 ° angle with crossed polarizers and electrospun PMMA/RM257 (1:1, weight ratio) fibres; (c) at 45 ° angle with crossed polarizers (corresponding optical micrograph, inset); (d) at 135 ° angle with crossed polarizers. 119

Figure 4.4. The stress-strain curves of neat RM257 and RM82 films after UV-light exposure induced photo-polymerization. 120

Figure 4.5. Electrospun PMMA/RM257 nanofibre with RM257 content of 20, 33, 50, and 66 wt% (from top to bottom) before and after UV-curing (from left to right). 122

Figure 4.6. DSC curves of 0, 20, 33, 50, and 66 wt% RM257 in PMMA nanofibre samples along with DSC curves of pure RM257 film (100 wt%). 123

Figure 4.7. DSC traces of PMMA/RM257, showing the shifting of T_g for PMMA with the increasing content of RM257. 124

Figure 4.8. Electrospun PA6/RM257 nanofibre with 20, 33 and 50 w% RM257 in PA6 (from top to bottom) before and after UV-curing (from left to right). 125

Figure 4.9. DSC curves of 0, 20, 33 and 50 wt% RM257 in PA6 nanofibre samples along with DSC curves of pure RM257 film (100 wt%). 126

Figure 4.10. The stress-strain curves of aligned PA6 electrospun nanofibre mat and PA6/RM257 blend nanofibre mats with different RM257 content. 128

Figure 5.1. Low temperature polycondensation and imidization process. 138

Figure 5.2. SEM micrographs of; (a) polyamic acid nanofibres before imidization; (b) polyimide nanofibres after imidization. 139

Figure 5.3. FTIR spectrum of nanofibres before and after imidization. 140

Figure 5.4. WAXD patterns of (a) polyamic acid nanofibres before imidization (b) co-polyimide nanofibres after imidization. 140

Figure 5.5. X-ray intensity versus the azimuth angle for BPO nanofibre mats before (black) and after (red) imidization. 141

Figure 5.6. Stress-strain curves of UD nanofibre mats before and after imidization. 143

Figure 5.7. (a) Schematic illustration of bundle sample preparation for mechanical testing and SEM micrographs of a multifilament nanofibre bundle of 29 filaments (b) before testing and (c) after testing. 147

Figure 5.8. Stress-strain curves of UD nanofibre mats and bundles. 149

Figure 6.1. Schematic of the fabrication process of unidirectional BPO co-polyimide nanofibres reinforced composites. 158

Figure 6.2. Young's modulus of unidirectional BPO co-polyimide nanofibre reinforced composites with different nanofibre volume fractions. 162

Figure 6.3. SEM micrographs showing the surface of unidirectional BPO nanofibre reinforced composite and fracture surface of (a), (b) neat co-polyimide UD nanofibre mat. (c), (d) 25 vol% nanofibre composite. (e), (f) 45 vol% nanofibre composite. 163

Figure 6.4. Young's modulus vs. loading angles for unidirectional BPO co-polyimide nanofibre reinforced composites based on two fibre volume fractions. 166

Figure 6.5. Tensile strength vs. loading angles of unidirectional BPO co-polyimide nanofibre reinforced composite based on two fibre volume fractions. 167

Figure 6.6. Predicted Young's modulus of unidirectional BPO co-polyimide nanofibre reinforced composites with different nanofibre volume fractions based on; (a) perfectly aligned nanofibres (b) aligned nanofibres in a bundle (c) aligned nanofibres in a UD-mat with significant misalignment. 168

Figure 6.7. Histogram representing the average orientation angles of 500 individual nanofibres along the nanofibre alignment direction in electrospun aligned mats. 170

Figure 6.8. Young's modulus vs. loading angles of unidirectional BPO nanofibre composites with perfect alignment (theory) (upper) and non-perfect alignment (experimental mat data) (lower). 170

Figure 7.1. Mechanical property comparison chart of traditional high performance fibres, reported electrospun nanofibres and the nanofibres developed in this thesis with respect to Young's modulus and tensile strength. Commercial high performance fibres show typical tensile strengths of 2–4 GPa and moduli of around 100–300 GPa, while most electrospun fibres typically possess tensile strengths < 0.3 GPa and Young's moduli < 3 GPa. Some high performance electrospun nanofibres have been

reported in literature based on polyimide, polyacrylonitrile and carbon nanofibres from electrospun PAN precursors. 180

Figure 7.2. The Young's modulus of electrospun BPO polyamic acid nanofibres after stretching at different extensions and temperatures. 182

Figure 7.3. The corresponding Young's modulus of stretched electrospun BPO nanofibres after imidization. 183

Figure 7.4. Schematic illustration of the experimental set up for bi-component electrospinning. The insets show the diameter of co-axial spinneret and a core-shell structure of nanofibres. 184

Figure 7.5. SEM micrograph of core-shell nanofibres with RM257 as core and PMMA as shell. 184

Figure 7.6. TEM micrographs of electrospun nanofibres showing clear contrast between core (RM257) and shell structures (PMMA); (a) before UV-curing and (b) after UV-curing. 185

List of Tables

Table 2.1. Theoretical crystal modulus of polymers derived from X-ray diffraction studies. 37

Table 2.2. Mechanical properties of electrospun polyamide (PA) and poly(ethylene terephthalate) (PET) nanofibres. 49

Table 3.1. Viscosity, conductivity and surface tension of anisotropic PPTA solutions compared with common polymer solutions employed in electrospinning. 97

Table 4.1. Mechanical properties of pure RM films and PA6/RM257aligned composite nanofibres along with effective RM257 contributions to the modulus of composite nanofibres. 127

Table 5.1. Mechanical properties of three different types of electrospun polyimide nanofibre unidirectional mats. 145

Table 5.2. Toughness of the three different types of nanofibres from Table 5.1 together with spider silk and Kevlar® 49. 146

Table 6.1. A list of values used for off-axis Young's modulus and tensile strength predictions (V_f is the volume fraction of nanofibre). 165

Table 6.2. A list of values used for predicting Young's moduli as a function of various loading angles. 169

Chapter 1

General Introduction

1.1 Electrospinning and Electrospun Nanofibres

In the last two decades, an old technique – electrospinning – has been extensively used by researchers (Figure 1.1) for the creation of nanomaterials, owing to its simplicity and huge potential of producing nanofibrous materials [1]. Over the years a number of basic electrospinning theories [2-4] have been developed and hundreds of electrospun nanofibres from different polymer systems have been practically produced [5-7].

Electrospinning is a versatile technique that makes use of an - in principle - very

simple experimental set-up. Normally, polymers or polymer mixtures to be used in electrospinning are dissolved in corresponding organic solvents to make homogenous solutions. The spinning solution is usually pumped from a single nozzle with controlled feeding rate. 10-50 kV DC high voltages are applied between two electrodes within a distance of 10-30 cm and an electrostatic field is generated. Consequently, a droplet placed in this filed will be stretched to a Taylor cone first by electrostatic repulsion forces resulting from charges on the solution [8]. A solution jet will be ejected from the deformed cone when the repulsion force exceeds the surface tension of the droplet. In its flight to the counter electrode, it will move in a straight line for a short distance followed by a whipping path accompanied with solvent evaporation and jet stretching until a solid nanofibre is collected on the substrate (Figure 1.2).

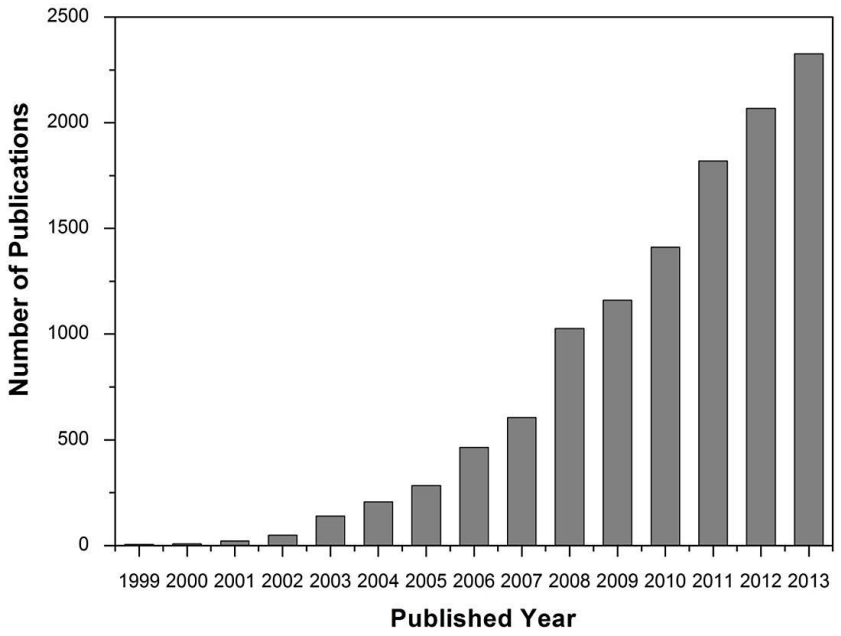

Figure 1.1. *Numbers of research articles, meeting articles, book chapters, etc. from 1999 to 2013 (searching key word: electrospinning; source: Web of Science).*

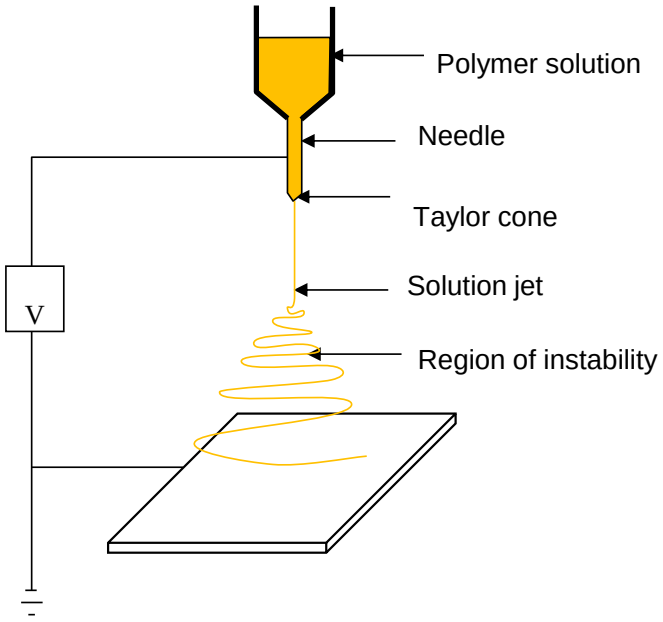

Figure 1.2. *A typical electrospinning set-up with a grounded collector.*

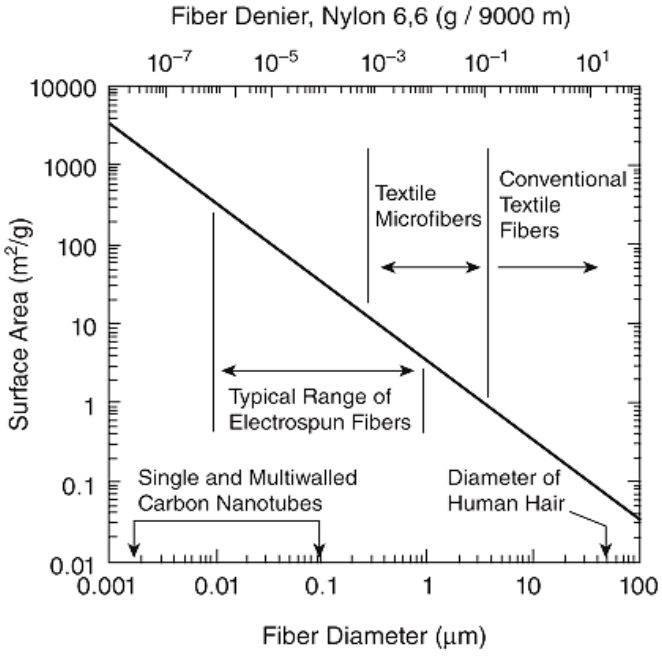

Figure 1.3. *Specific surface area as a function of fibre diameter in nonwovens [9].*

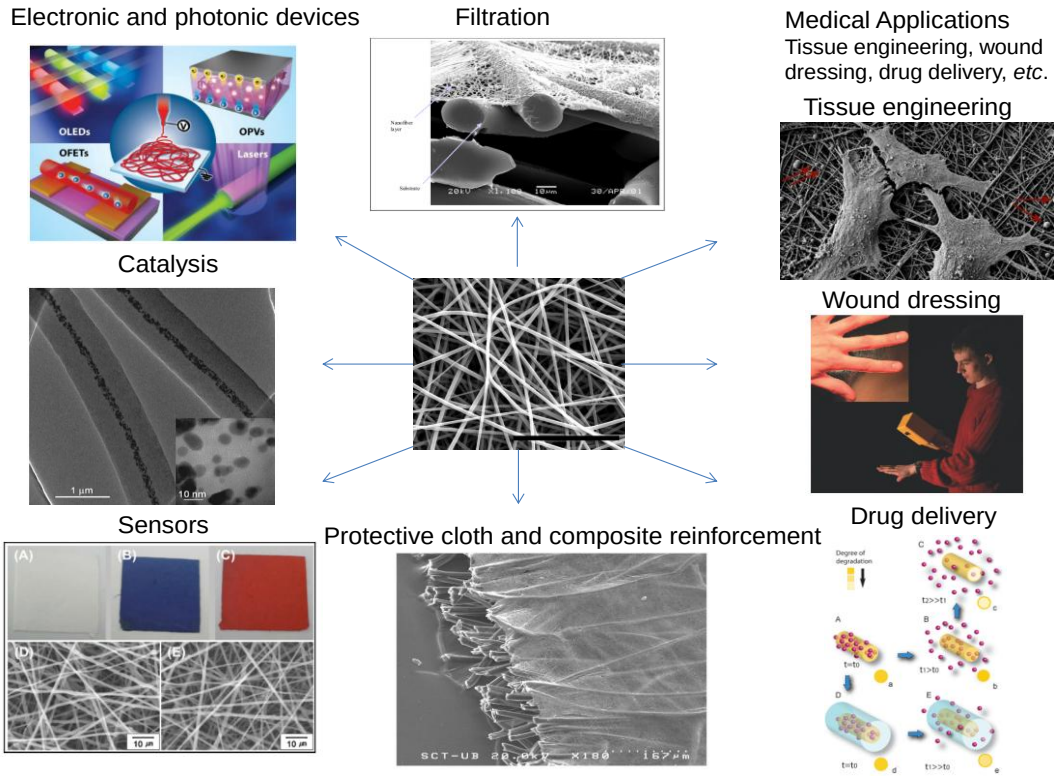

Figure 1.4. *Various potential applications of electrospun nanofibres [8, 10-16].*

The small diameters (usually 10 nm to 1 μm), high specific surface area (tens to hundreds m^2/g, as shown in Figure 1.3), high porosity and small pore size render electrospun nanofibres to a broad range of potential applications (Figure 1.4) in medicine, filtration, sensors, textiles, composite reinforcements, *etc*.

1.2 Liquid Crystals, Liquid Crystalline Polymers and Reactive Liquid Crystals

Liquid crystals are materials that exhibit a state between liquid phase and crystalline phase. They have a certain degree of molecular order as well as liquid properties.

Polymers are referred as liquid crystal polymers (LCPs) when they exhibit liquid crystalline properties either as a function of concentration when dissolved in a solvent (lyotropic LCPs) or heated within a certain temperature range (thermotropic LCPs). In both cases, the polymer chains tend to order themselves along one direction, which results in anisotropy. Traditional high performance fibres such as *p*-aramid fibre and liquid crystal polyester fibre retain their anisotropy properties and thus exhibit high mechanical properties in the direction of the fibre.

Reactive mesogens (RMs) are liquid crystalline monomers having reactive acrylate end groups, which are polymerizable. They tend to orient parallel to each other in their nematic phase. UV-light exposure induced photo-polymerization with the presence of photo-initiator can be used to chemically 'freeze in' such regularly ordered molecular structures, thus leading to highly oriented polymer networks.

1.3 High Performance Fibres

In general, high performance polymer fibres distinguish themselves from industrial and textile grade synthetic fibres in terms of their mechanical properties. Synthetic textile fibres typically have Young's moduli of 5-10 GPa and tensile strengths up to 1 GPa, while this thesis is mainly concerned with high performance polymer fibres of high stiffness (> 50GPa) and tensile strength (> 2 GPa). Usually, due to their superior mechanical properties, high performance polymer fibres have applications in aerospace, ballistic protection, sports equipment, *etc.*

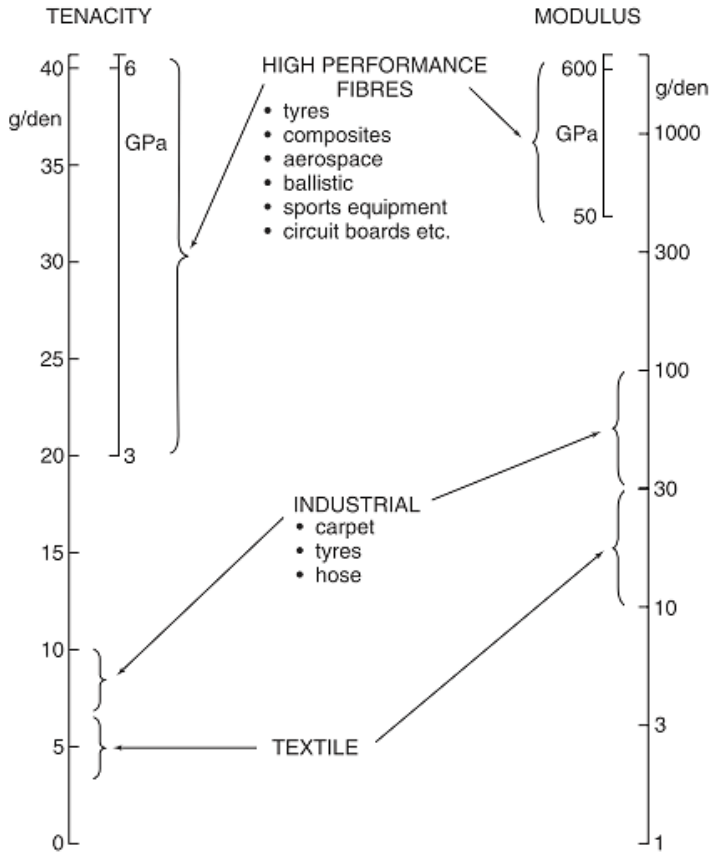

Figure 1.5. *A general classification of high performance fibres, industrial and textile fibres according to their modulus and strength [17].*

1.4 Outline of the Thesis

Many potential applications of electrospun nanofibres require high mechanical property nanofibres, for instance, microfibres are employed in air filtration to support nanofibres since nanofibres are too weak to be used independently [12].

Compared to the corresponding textile fibres made from the same polymers, the mechanical properties of nanofibres are often found to be poor. Electrospun

nanofibres typically display tensile strengths below 300 MPa and Young's moduli below 3 GPa [18-24], which can be mainly ascribed to the low degree of orientation and chain extension of the polymer chains along the fibre-axis. Therefore, the question arises whether it is at all feasible to produce high modulus and high strength electrospun nanofibres. Hence, the objective of this thesis is to investigate potential routes to produce high performance electrospun nanofibres.

A brief review of general concepts employed to produce high modulus and high strength synthetic fibres will be given first in Chapter 2. Then the development of several commonly accepted high strength and high modulus polymer fibres based on flexible and rigid chain polymers are presented. Subsequently, Chapter 2 reviews the various research works on the mechanical properties of electrospun nanofibres, potential ways to produce high modulus and high strength electrospun nanofibres and progress in the area of manufacturing high modulus and high strength electrospun nanofibres.

In Chapter 3 and Chapter 4, the feasibility and challenges of electrospinning of liquid crystal polymer (*p*-aramid) and reactive diarylate mesogens in polymer blends will be studied and discussed, respectively. In both cases, the mechanical properties of obtained fibres are evaluated.

In Chapter 5, co-polyimide BPDA/PDA/ODA nanofibres were produced using a two-step procedure from a precursor fibre. Its mechanical properties based on unidirectional mats and multifilament bundles are fully investigated and evaluated using Weibull statistics. Subsequently, a co-polyimide nanofibre reinforced

composite is fabricated in Chapter 6. The mechanical properties of UD composites at different nanofibre volume fractions are discussed as well as the influence of nanofibre orientation in off-axis composite laminates.

1.5 Reference

1. Doshi, J.; Reneker, D.H. Electrospinning process and applications of electrospun fibers. *Journal of Electrostatics* **1995**, *35*, 151-160.

2. Kim, J.s.; Reneker, D.H. Mechanical properties of composites using ultrafine electrospun fibers. *Polymer Composites* **1999**, *20*, 124-131.

3. Jaeger, R.; Bergshoef, M.M.; Batlle, C.M.I.; Schönherr, H.; Julius Vancso, G. In *Electrospinning of Ultra-Thin Polymer Fibers*, Macromolecular Symposia, 1998; Wiley Online Library: 1998; pp. 141-150.

4. Bognitzki, M.; Czado, W.; Frese, T.; Schaper, A.; Hellwig, M.; Steinhart, M.; Greiner, A.; Wendorff, J.H. Nanostructured fibers via electrospinning. *Advanced Materials* **2001**, *13*, 70-72.

5. Fang, X.; Reneker, D. DNA fibers by electrospinning. *Journal of Macromolecular Science, Part B: Physics* **1997**, *36*, 169-173.

6. Fong, H.; Reneker, D.H. Elastomeric nanofibers of styrene-butadiene-styrene triblock copolymer. *Journal of Polymer Science Part B Polymer Physics* **1999**, *37*, 3488-3493.

7. Ramakrishna, S. *An Introduction to Electrospinning and Nanofibers*; World Scientific Publishing Co. Pte. Ltd: Singapore: 2005; pp. 90-154.

8. Greiner, A.; Wendorff, J.H. Electrospinning: a fascinating method for the preparation of ultrathin fibers. *Angewandte Chemie International Edition* **2007**, *46*, 5670-5703.

9. Wendorff, J.H.; Agarwal, S.; Greiner, A. *Electrospinning: Materials, Processing, and Applications*; John Wiley & Sons: 2012; pp. 1-27.

10. Cho, H.; Min, S.Y.; Lee, T.W. Electrospun organic nanofiber electronics and photonics. *Macromolecular Materials and Engineering* **2013**, *298*, 475-486.

11. Yoon, J.; Kim, J.M. Fabrication of conjugated polymer supramolecules in electrospun micro/nanofibers. *Macromolecular Chemistry and Physics* **2008**, *209*, 2194-2203.

12. Graham, K.; Ouyang, M.; Raether, T.; Grafe, T.; McDonald, B.; Knauf, P. In *Polymeric Nanofibers in Air Filtration Applications*, Fifteenth Annual Technical Conference & Expo of the American Filtration & Separations Society, Galveston, Texas, 2002; 2002; pp. 9-12.

13. Abidian, M.R.; Martin, D.C. Multifunctional nanobiomaterials for neural interfaces. *Advanced Functional Materials* **2009**, *19*, 573-585.

14. Wang, Q.; Yu, X.; Libera, M. Reducing Bacterial Colonization of 3-D nanofiber cell scaffolds by hierarchical assembly of microgels and an antimicrobial peptide. *Advanced Healthcare Materials* **2013**, *2*, 687-691.

15. Faccini, M.; Vaquero, C.; Amantia, D. Development of protective clothing against nanoparticle based on electrospun nanofibers. *Journal of Nanomaterials* **2012**, *2012*, 18.

16. Graeser, M.; Pippel, E.; Greiner, A.; Wendorff, J.H. Polymer core-shell fibers with metal nanoparticles as nanoreactor for catalysis. *Macromolecules* **2007**, *40*, 6032-6039.

17. Hearle, J.W. *High-Performance Fibres*; Woodhead Publishing: Cambridge, England: 2001; Vol. 15, pp. 93-155.

18. Nair, L.S.; Bhattacharyya, S.; Bender, J.D.; Greish, Y.E.; Brown, P.W.; Allcock, H.R.; Laurencin, C.T. Fabrication and optimization of methylphenoxy substituted polyphosphazene nanofibers for biomedical applications. *Biomacromolecules* **2004**, *5*, 2212-2220.

19. Lee, K.; Kim, H.; Khil, M.; Ra, Y.; Lee, D. Characterization of nano-structured poly (ε-caprolactone) nonwoven mats via electrospinning. *Polymer* **2003**, *44*, 1287-1294.

20. Lee, K.H.; Kim, H.Y.; Ryu, Y.J.; Kim, K.W.; Choi, S.W. Mechanical behavior of electrospun fiber mats of poly (vinyl chloride)/polyurethane polyblends. *Journal of Polymer Science Part B: Polymer Physics* **2003**, *41*, 1256-1262.

21. Huang, Z.-M.; Zhang, Y.; Ramakrishna, S.; Lim, C. Electrospinning and mechanical characterization of gelatin nanofibers. *Polymer* **2004**, *45*, 5361-5368.

22. Hansen, L.M.; Smith, D.J.; Reneker, D.H.; Kataphinan, W. Water absorption and mechanical properties of electrospun structured hydrogels. *Journal of Applied Polymer Science* **2005**, *95*, 427-434.

23. Matthews, J.A.; Wnek, G.E.; Simpson, D.G.; Bowlin, G.L. Electrospinning of collagen nanofibers. *Biomacromolecules* **2002**, *3*, 232-238.

24. Greiner, A.; Wendorff, J. Functional self-assembled nanofibers by electrospinning. In *Self-Assembled Nanomaterials I*; Springer Berlin Heidelberg: Berlin, Germany, 2008; pp. 107-171.

Chapter 2

High Strength and High Modulus Electrospun Fibres

2.1 High Strength and High Modulus Synthetic Fibres

2.1.1 Basic concepts for high performance fibres

A century ago, natural fibres like cotton, silk, and wool dominated the market due to their abundance and aesthetic appeal. In the 1920s, Hermann Staudinger was the first to propose the concept of macromolecules [1] and this epoch-making idea greatly influenced the discovery of synthetic fibres with the first synthetic fibre being invented in 1935 by Wallace Carothers, which is known to us as polyamide (PA) or Nylon fibre [2].

The two most commonly used aliphatic polyamide fibres are polyamide 6 and polyamide 6,6 which are made of caprolactam and hexamethylenediamine with adipic acid, respectively. Polyamide (PA) fibres are produced by melt-spinning and are given moderate molecular orientation and crystallinity after post-drawing. Molecular orientation and crystallinity, along with hydrogen bonding between chains provided by the amide group (–NH–CO–) [3] provides them with good mechanical properties and abrasion resistance, which renders them to be one of the most widely used industrial fibres. Polyethylene terephthalate (PET), which is the most important commercial polyester, first appeared on the market in 1953 [4] and is now fully established in textile and technical fibres. PET is produced by polymerization of either dimethyl terephthalate or terephthalic acid with ethylene glycol. Melt-spinning in combination with post-drawing is also applied in the manufacture of PET fibres, with main applications in textiles, ropes, tyres, carpets, and so on. Since these initial developments on PA and PET, more and more synthetic fibres have been investigated and developed.

The tensile strength and Young's modulus of those traditional synthetic fibres are usually limited to below 1 GPa and 15 GPa, respectively. The relatively low mechanical performance of these textile fibres greatly limits their applications in areas such as aerospace, protective clothing, armour, advanced composites, *etc.*

In 1932, Staudinger [5] postulated the basic requirements for producing a high strength and high modulus synthetic fibre. In his structural model for such a fibre, all molecular chains should be fully extended and perfectly aligned along the fibre axis. Simultaneously, few chain end defects should exist as the tensile strength is

determined by secondary bonds rather than primary bonds. The fully extended and oriented polymer chains will provide ultimate stiffness to the fibre while the few chain end defects as in the case of high molecular weight polymers provides high tenacity, the combination of both making the ideal fibre (Figure 2.1).

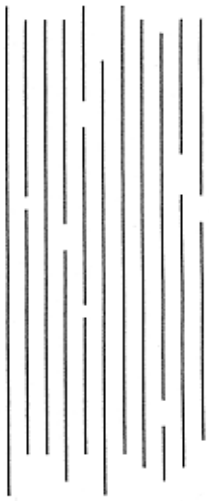

Figure 2.1. *Ideal polymer chains model for producing high strength and high modulus fibres [5].*

It has long been recognized by Meyer and Lotmar [6] that only extended polymer chains will provide high stiffness. In 1960, Treloar [7] estimated the longitudinal modulus of a single extended polyethylene chain to be 182 GPa in comparison to the Young's modulus of isotropic polyethylene being less than 2 GPa [8]. More calculations showed that the Young's modulus of a single extended polyethylene chain can reach even higher values up to 320 GPa [9]. On the other hand, polymers like polypropylene with a helical chain configuration, exhibit a much lower theoretical modulus compared with planar zig-zag configurations as in polyethylene. Elastic modulus of crystalline regions in the direction parallel to the chain axis have

since also been measured experimentally using X-ray diffraction (Table 2.1), providing great insight into the potential of certain polymers to generate high performance fibres [10-12].

Table 2.1. *Theoretical crystal modulus of polymers derived from X-ray diffraction studies [10-12].*

Polymer	**Crystal modulus (GPa)**
Polyethylene (PE)	235
Poly(vinyl alcohol) (PVA)	250
Polyamide 6 (PA 6)	157
Poly(ethylene terephthalate) (PET)	108
Polypropylene (PP)	40
Polyacrylonitrile (PAN)	35–55
Thermotropic polyester (Vectran)	126
Poly(*p*-phenylene terehthalamide) (PPTA)	160
Poly(phenylene benzobisoxazole) (PBO)	478

All the above studies indicated that high modulus and high strength in fibres mainly relies on high polymer chain orientation and extension, combined with sufficient chain length. Inspired by this, polymer scientists have attempted to improve the

mechanical properties of fibres by pursuing two routes to reach Staudinger's ideal model, *i.e.*, flexible chain polymers and rigid chain polymers [13].

2.1.2 High performance fibres based on flexible polymer chains

In the case of flexible chains, notably polyethylene, the chains tend to fold upon crystallization and in order to get the desired level of chain extension necessary to exploit the intrinsic properties of the polymer chain, solid-state drawing at elevated temperature but below the melting temperature is applied [14-16]. Great efforts have been devoted to melt-spinning and later also solution-spinning of polyethylene in the 1970s. Ward *et al.* [17, 18] developed polyethylene fibres using a process of melt-spinning followed by drawing in the solid state. This technique had limitations with respect to the use of high molecular weight polymers and as such the tenacity of the obtained fibres, as spinnability (as a result of the rapidly increasing melt viscosity) and fibre drawability both decreased with increasing molecular weight. An initial breakthrough in the development of high strength polyethylene fibres was the so-called surface growth technique from Zwijnenberg and Pennings [19, 20]. Here, Young's moduli exceeding 100 GPa and tensile strengths over 3 GPa were obtained from ultra-high molecular weight polyethylene. These results were a break-through as this was the first experimental evidence that high modulus and high strength structures could be produced from flexible chain polymers [21].

An industrial breakthrough in the production of high modulus and high strength polymer fibres was achieved by the solution (or gel) spinning process developed at DSM in the Netherlands at the end of the 1970s. Smith and Lemstra [22-25]

discovered that as-spun ultra-high molecular weight polyethylene filaments from solution could be hot-stretched in the solid-state below the melting temperature to very high draw ratios. In the gel-spinning process, a semi-diluted ultra-high molecular weight (Mw > 10^6 g/mol) polyethylene solution of low polymer concentration is squeezed through a spinneret and after quenching in a water bath a gel-like filament is obtained (Figure 2.2). This results in a morphology with a low entanglement density of polymer chains in the as-spun gel-like fibre, which renders them super-drawable.

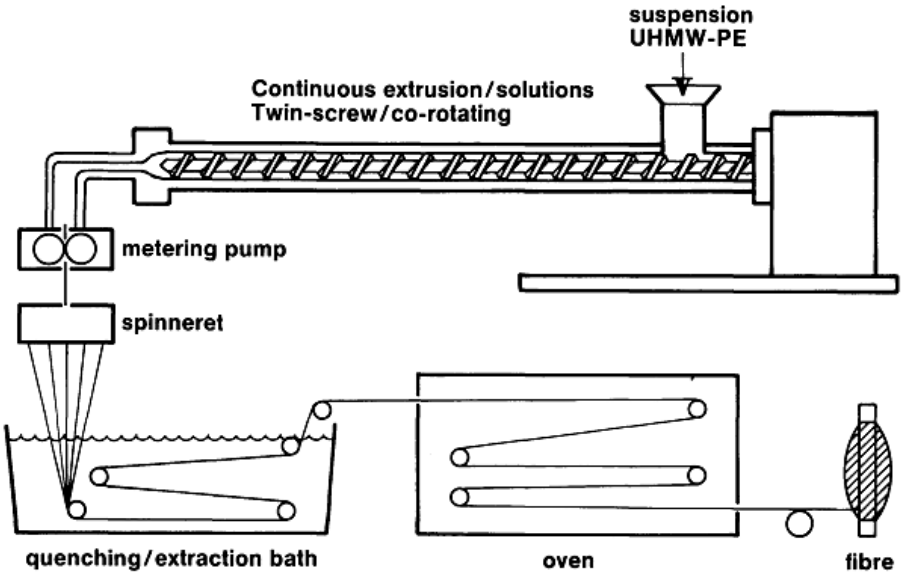

Figure 2.2. *Schematics of the gel-spinning process [15].*

Upon solid-state drawing, the lamellae structure of the as-spun polyethylene fibre will initially orient in the drawing direction. At higher draw-ratios, these lamellae ideally unravel into chain-extended structures approaching ultimate properties (see Table 2.1). In fact, the solid-state drawing step can be regarded as the single most important process step needed to create high performance fibres, based on flexible

chain polymers. Since the relaxation times of flexible chain polymers are typically very short, the elongation flow induced orientation in the as-spun fibres rapidly disappears due to relaxation before solidification. High performance fibres based on flexible chain polymers are therefore typically post-drawn in the solid-state below the melting temperature as this will prevent chain relaxation after orientation and chain extension.

Dyneema® by DSM and Spectra® by its licensee Allied Signal (now Honeywell) are two commercially available high strength and high modulus fibres that use ultra-high molecular weight polyethylene (UHMWPE) as a starting material. These fibres have Young's moduli exceeding 100 GPa and tensile strengths of more than 3 GPa, *i.e.*, 100 times that of bulk polyethylene. In combination with their low density (<1000 kg/m^3), this leads to exceptionally high specific mechanical properties (properties per unit weight), making these UHMWPE fibres of interest for a wide range of applications ranging from maritime ropes to protective gloves, bullet-proof vests, and other advanced composites applications.

2.1.3 High performance fibres based on rigid polymer chains

The discovery of rigid rod polymers to produce high performance fibres originated from the discovery of para-oriented aromatic polyamide [26, 27], notably, poly (*p*-phenylene terehthalamide) (PPTA). Large research efforts led to significant advances in the fundamental understanding of PPTA polymerization [28], spinning solutions [29, 30], spinning process and the structure of para-aramid fibres [29, 31],

taking full advantage of its rigid rod like molecular structure and unique liquid crystalline properties.

Generally, PPTA exhibits lyotropic liquid crystalline properties in proper solvents, *viz.* concentrated sulphuric acid. At low concentrations, the rod-like molecules are randomly distributed but they tend to order and form nematic domains above a certain concentration (see also Section 3.3.1.). As chain extension in rigid chains is already built in by the chemist, it is not essential to post-draw these as-spun filaments, which is the main difference between processing fibres based on rigid and flexible chain molecules.

The melting point of PPTA is higher than its degradation temperature, so melt-spinning is not feasible in the case of PPTA. Dry-jet (air gap) wet spinning [28] was utilized as a novel spinning route for these materials in the 1970s. Anisotropic solutions with concentrations of around 19–20 wt% PPTA in concentrated sulphuric acid at 70–90 °C, *i.e.*, concentrated solutions of moderate viscosities, were used for spinning of these fibres. Orientation with extended chain configuration of the liquid crystalline domains is achieved in the air-gap (Figure 2.3) and fixed in the coagulation bath usually made up of water or diluted sulphuric acid with temperatures in the range of 0-5 °C. The as-spun fibres are then washed, neutralized, and dried afterwards. The degree of chain orientation and crystallinity can be further tuned by changing the draw ratio during spinning and/or by heat treatments.

Para-aramid fibres are manufactured under the trademark of Kevlar® (Du Pont, Wilmington, USA) and Twaron® (Teijin Aramid, Arnhem, The Netherlands). A

combination of properties like light weight, high strength, high modulus, excellent high temperature resistance and good resistance to chemicals, make para-aramid fibres of interest for aerospace composites, anti-ballistic materials, and many other advanced applications.

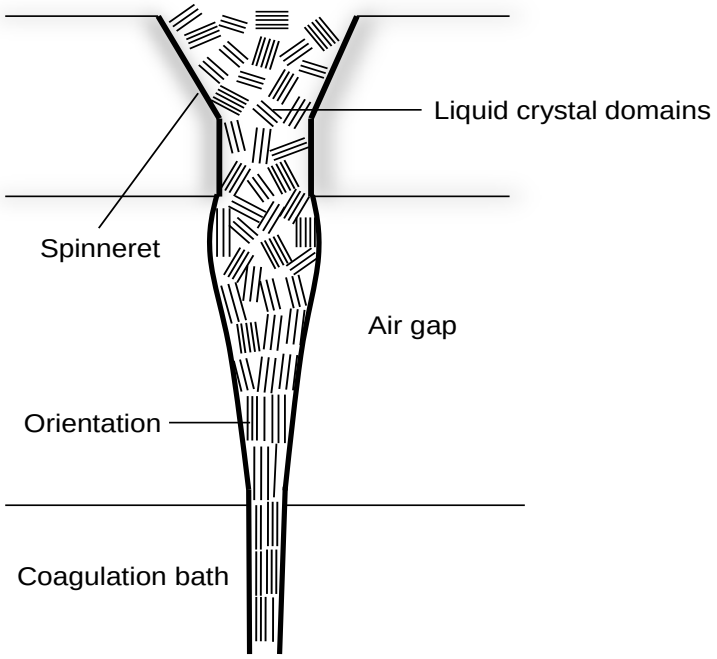

Figure 2.3. *Molecular orientation during dry-jet wet spinning of PPTA.*

Another high strength and high modulus fibre based on (semi) rigid polymer chains is aromatic polyester which exhibits liquid crystalline properties. This thermotropic liquid crystalline polymer (TLCP) fibre was initially developed by Celanese Corporation and became commercially available in the mid-1980s under the trade name Vectran®. Melt-spinning using conventional extrusion practice in combination with moderate draw-down is performed on these thermotropic liquid crystal polyesters to fully exploit their liquid crystalline properties [32].

Other more recent developments in high performance fibres based on lyotropic liquid crystalline rigid rod polymers are poly(phenylene benzobisoxazole) (PBO) from Toyobo Corporation under the trade name Zylon® [33-35] and poly(hydroquinone-diimidazopyridine) ("M-5") [36] from Akzo-Noble with a very similar chemical structure as PBO but exhibiting much better compressive properties [37]. The mechanical properties of all these fibres are later shown in Figure 2.21.

2.2 Electrospun Nanofibres

2.2.1 Basic concepts of electrospinning

Electrospinning is a versatile technique that makes use of an -in principle- very simple experimental set-up. Normally, polymers or polymer mixtures to be used in electrospinning are dissolved in organic solvents to make homogenous spinnable solutions. These spinning solutions are usually pumped from a single nozzle at a controlled feeding rate. 10–50 kV DC high voltages are typically applied between two electrodes within a distance of 10–30 cm to generate an electrostatic field. Consequently, a droplet placed in this field will be stretched to a Taylor cone first by electrostatic repulsion forces resulting from charges on the solution [38, 39]. A solution jet will be ejected from the deformed cone when the repulsion force exceeds the surface tension of the droplet. In its flight to the counter electrode, it will move in a straight line for a short distance followed by a whipping path (Figure 2.4)

accompanied with solvent evaporation and jet stretching until a solid nanofibre mat (Figure 2.5) is collected on the substrate.

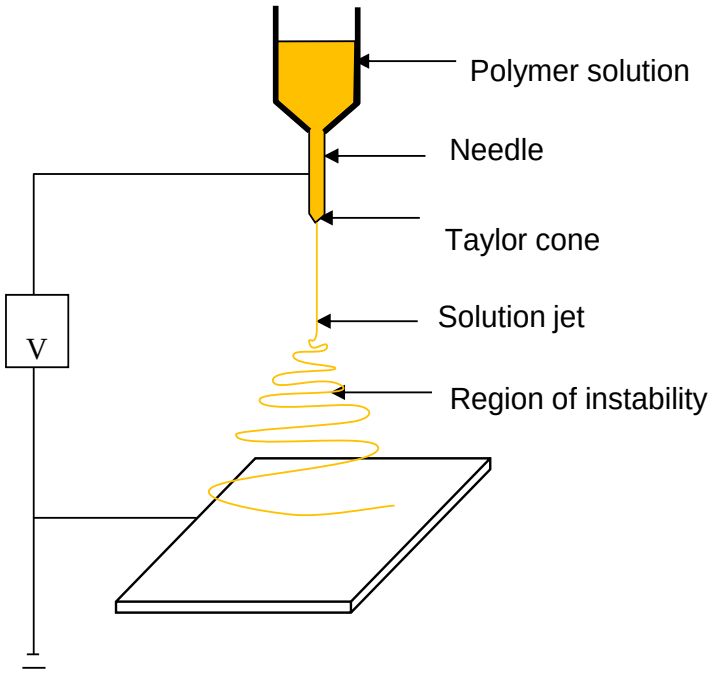

Figure 2.4. *A typical electrospinning set-up with a grounded collector.*

In principle, a numbers of parameters, which can be classified into solution and processing parameters, are believed to affect the electrospinning process. Solution parameters include viscosity (Figure 2.6), molecular weight of polymer, conductivity, surface tension, *etc.* Solution feeding rate, process temperature and humidity, applied voltage, distance between electrodes, and design of collector are typical processing parameters which also influence spinnability and fibre morphology [40].

A significant disadvantage of electrospinning as a mean to create polymer nanofibres has been the low production rate using single needle systems, which have been

typically restricted to a few grams per hour. However, recently, several new technologies have been suggested that tackle this issue.

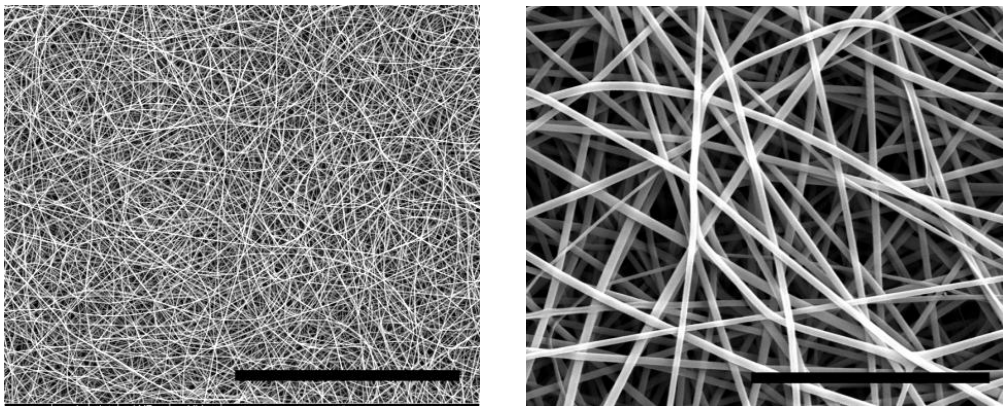

Figure 2.5. *Two scanning electron microscope (SEM) pictures of an electrospun PA6 nanofibre non-woven mat under different magnifications (scale bars of 40 µm and 5 µm, respectively).*

Free liquid surface electrospinning [41] such as the Nanospider® technology applies a nozzle-less electrospinning head instead of a traditional nozzle based set-up. Its rotating electrospinning head can carry a thin layer of polymer solution from a liquid polymer bath and nanofibre layers in a high throughout rate can be produced when the polymer solution is exposed to a high electrical field (Figure 2.7a). Electrospinning has also been combined with traditional polymer processing techniques such as twin-screw extrusion in order to improve the ability to spin more viscous systems including polymer melts [42]. Moreover, such a process can generate high production rates when combined with multi-nozzle spinnerets (Figure 2.7b) [43].

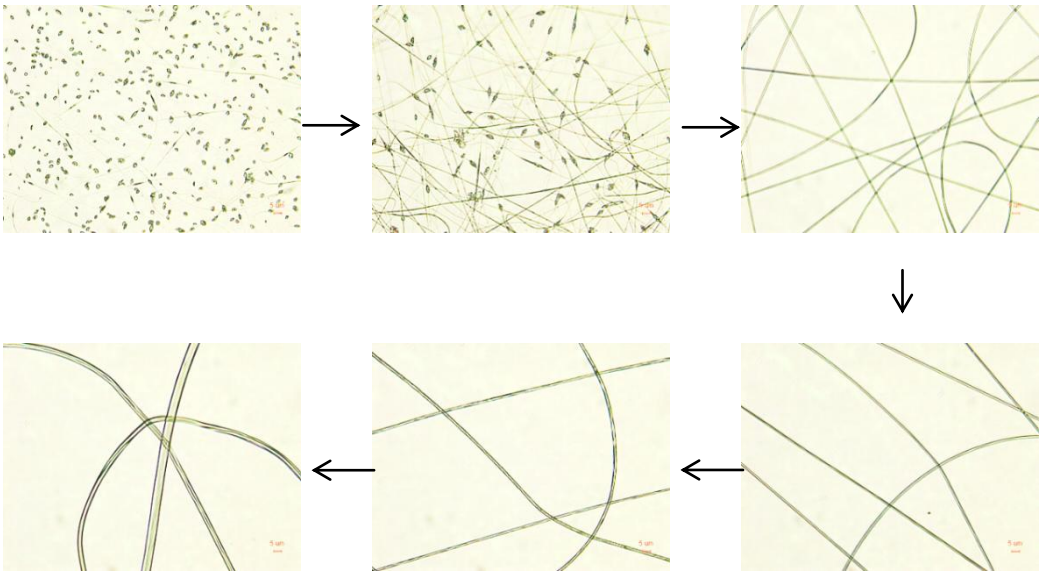

Figure 2.6. *Different fibre morphologies of electrospun nanofibres produced from low solution concentration to high solution concentration of poly(methyl methacrylate) (PMMA) in DMF, nanofibres electrospun from low concentration solutions show beaded morphology while the ones spun from high concentration show homogenous morphology.*

Recently also alternative spinning technologies for nanofibres have been introduced, such as a rotary jet-spinning technology that is capable of high rate spinning [44]. Unlike conventional electrospinning using an electrostatic force as driving force to generate fibres, in rotary jet-spinning nanofibres are fabricated by a centrifugal force caused by high speed rotation of a polymer solution or melt as shown in Figure 2.7c.

To make high performance electrospun nanofibres, in principle, the molecular structures of nanofibres should be oriented with chain extension, and should resemble the ideal polymer chains model described in Figure 2.1. In the next section, recent reports on mechanical properties of electrospun nanofibres are presented

according to their intrinsic chain flexibility, *viz.* flexible chains *versus* rigid chains. Some nanofibres possessing enhanced mechanical properties are highlighted.

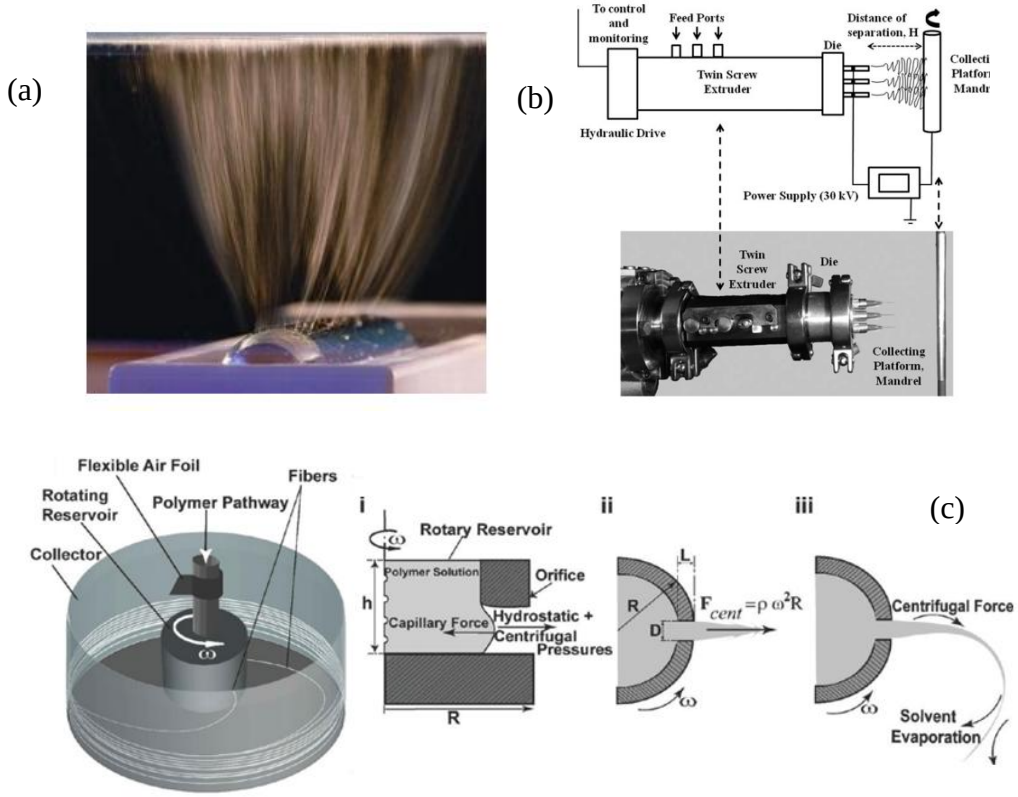

Figure 2.7. *Novel nanofibre production technologies (a) nozzle-less electrospinning with a rotating head [41] (b) Multi-nozzle electrospinning with a twin-screw extrusion [43] (c) Rotary jet-spinning [44].*

2.2.2. Electrospun nanofibres based on flexible chain polymers

Inspired by the success of Dyneema®, Rein *et al.* [45] tried to fabricate UHMWPE fibres using the electrospinning method. The mechanical properties of manually twisted yarn from as-spun nanofibre mats were investigated and a tensile strength of 129 MPa and modulus of 0.4 GPa were reported, which are well below those of

commercial UHMWPE fibres at around 3000 MPa and 100 GPa, respectively [46]. The relatively low strength and modulus of these electrospun UHMWPE fibres can to some extent be explained from their wide-angle X-ray scattering (WAXS) pattern (Figure 2.8). The WAXS data shows a significant difference of the average molecular chain orientation in electrospun and solution-spun ultra-drawn UHMWPE. Where electrospun UHMWPE shows broad (110) and (200) reflection arcs, shows only ultra-drawn UHMWPE greatly intensified reflections typical of a highly oriented polymer fibre.

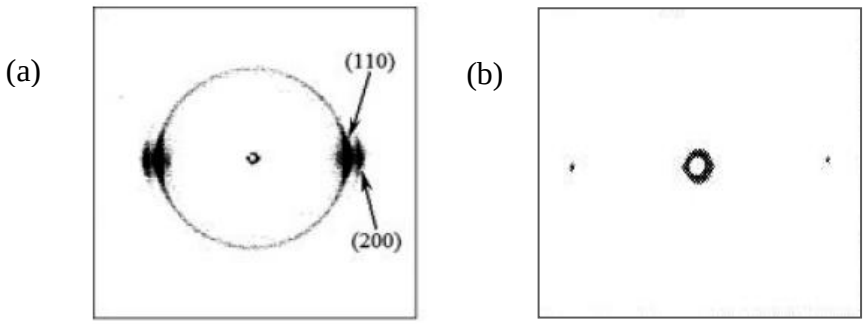

Figure 2.8. *(a) WAXS pattern of electrospun UHMWPE nanofibre [45], showing broad reflection arcs typical of a moderately oriented polymer structure. (b) WAXS pattern of solution-spun ultra-drawn UHMWPE fibre with draw-ratio 100, showing intense reflections typical of a highly oriented polymer structure [14].*

Table 2.2. *Mechanical properties of electrospun polyamide (PA) and poly(ethylene terephthalate) (PET) nanofibres.*

Polymer	**Solvent & concentration**	**Sample**	**Modulus (MPa)**	**Strength (MPa)**	**Refs.**
PA 6	6 wt% in 1,1,1,3,3,3-hexafluoro-2- propanol	Nonwoven nanofibre mat	34 ± 2	7.2 ± 0.5	[47]
PA 6,6	7.5 wt% in 1,1,1,3,3,3-hexafluoro-2- propanol	Nonwoven nanofibre mat	21 ± 1	6.5 ± 0.8	
PA 6	20 wt% in formic acid	Nonwoven nanofibre mat	19	10.5	[48]
		Single nanofibre	902	304	
PA 6,6	20 wt% in formic acid	Single nanofibre	950 ± 390	150 ± 49	[49]
PA 6,6	10 wt% in formic acid & chloroform (75:25 *v*/*v*)	Nanofibre yarn	1216	120	[50]
PA 6	12 wt% in formic acid & acetic acid (50:50 *w*/*w*)	Single nanofibre	1320 ± 152	78.1 ± 6.0	[51]
PA 6	12 wt% in formic acid & acetic acid (50:50 *w*/*w*)	Nonwoven nanofibre mat	418 ± 93	57.7 ± 8.9	[52]
PET	30% (*w*/*v*) in TFA & DCM (70:30 *v*/*v*)	Nonwoven nanofibre mat	60	3.7	[53]
PA 6/6,6	Melt	Bulk	2000–2500	50–80	[4]
PET	Melt	Bulk	2000–3000	50–150	
PA 6/6,6	Melt-spun + drawn	Single fibre	6000	1000	[21]
PET	Melt-spun + drawn	Single fibre	15000	1100	

With respect to the vast amount of research on other electrospun nanofibres based on flexible chain polymers such as aliphatic polyamide and polyester, a relatively limited number of studies involved the mechanical properties of non-woven nanofibre mats or even single nanofibres. According to Table 2.2, the mechanical properties of most electrospun polyamide and polyester fibres are also not comparable with conventional microfibres manufactured by melt-spinning, which again can be ascribed to the low degree of chain orientation in these as-spun nanofibres and the absence of a post-drawing step in the electrospinning process. In fact, in many cases the properties of electrospun fibre properties are even inferior to that of the bulk polymer, which can be attributed to factors, such as residual solvent, plasticization, and porosity.

Although traditional methods to induce high molecular orientation like post-drawing are usually not feasible for single nanofibres, at least for the time being due to technological difficulties, limited stretching or drawing has been attempted to oriented nanofibre mats in order to generate improved molecular orientation and crystallinity. Zong *et al.* [54] stretched PLGA nanofibre membranes up to a deformation of 450% at 90 ℃. An improvement in mechanical properties after post-drawing was observed as seen in Figure 2.9, although the properties achieved remained low. Wu *et al.* [55] also tried solid-state hot-drawing at 135 ℃ of polyacrylonitrile (PAN) nanofibre sheets. Here, the crystallinity increased from 7.9% for as-spun nanofibre mats to 31.8% for hot-drawn mats, while the tensile strength was raised from 100 MPa to 220 MPa, correspondingly.

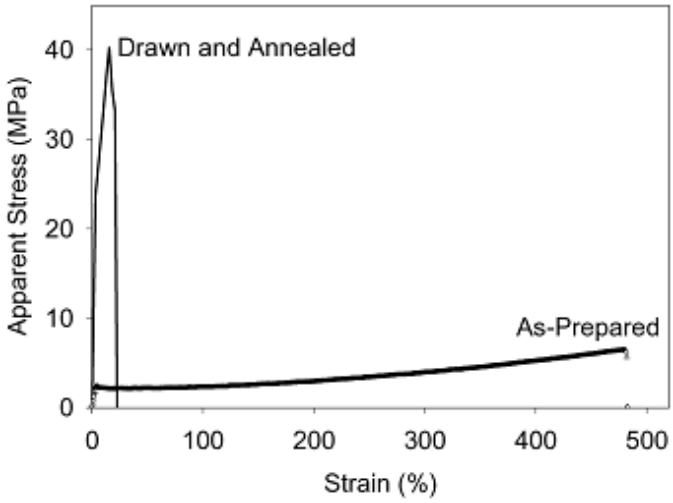

Figure 2.9. *Strain-stress curves electrospun poly(glycolide-co-lactide) of as-spun nanofibre mat and nanofibre mat after a solid-state deformation of 450% [54].*

Kongkhlang *et al.* [56] attempted to induce favourable orientation and increased crystallinity directly into as-spun electrospun nanofibres using a high-speed collector for nanofibres collection. Figure 2.10 exhibits two 2D wide-angle X-ray diffraction patterns of polyoxymethylene (POM) nanofibres electrospun with different take up speeds. It is clearly shown that a higher collecting speed of 1890 m/min induces a higher degree of orientation in these nanofibres. In addition, it should be noted that alignment of the nanofibres within the mat is also vital for achieving high strength and high modulus structures as misalignment will significantly reduce the efficiency of the fibres within a mat and will greatly reduce its mechanical properties [57].

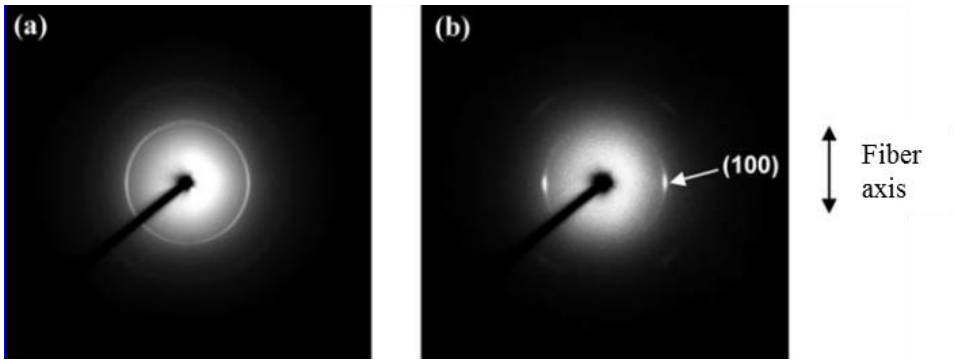

Figure 2.10. *Two dimensional (2D) wide-angle X-ray diffraction patterns of electrospun polyoxymethylene (POM) nanofibres with different take up speeds (a) 630m/min (b) 1890 m/min [56].*

Although it has been shown by various researchers that electrospinning can induce some level of chain orientation in fibres based on flexible chain polymers, these levels are often rather low. An interesting study in this respect was by Mohan *et al.* [58]. Here, small angle neutron scattering (SANS) was used to quantify the size and shape of the chain conformation in electrospun fibres of deuterated atactic polystyrene prepared from solutions. Although the orientation parameter $<P_2>$ was found to increase with increasing collecting speed, the maximum value of about 0.15 (Figure 2.11a) was well below the orientation parameter expected for high performance polymer fibres with values typically approaching 1. When the tangential velocity of the rotating collector was greater than the flight velocity of the fibres some degree of orientation of the polymer coils was induced. However, even at the highest collector speeds the ratio of the radii of gyration increased only by 20% from for bulk (17 nm) to fibres (20 nm), showing limited coil deformation. As the diameters of these fibres was much greater than the polystyrene radius of gyration

these effects can be solely contributed to flow-induced orientation, excluding size or confinement effects as a result of nano-sized fibre diameters.

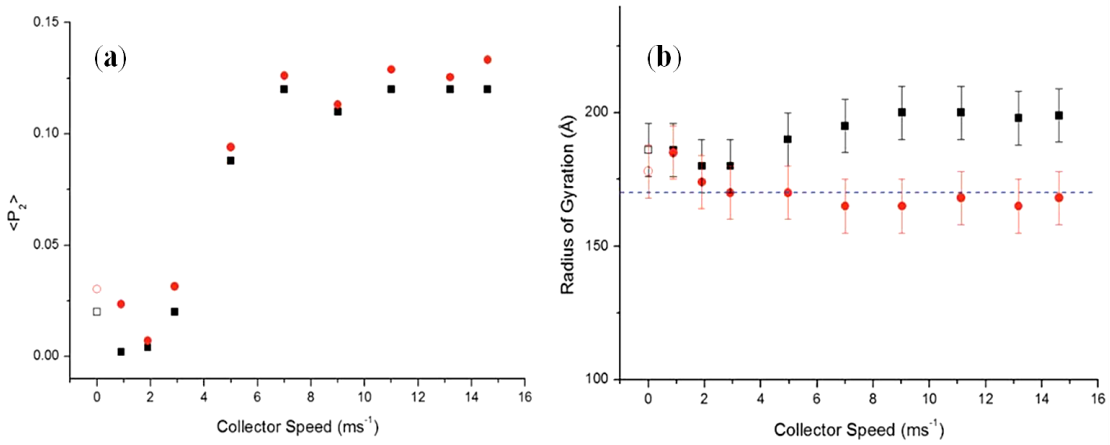

Figure 2.11. *(a) Orientation parameter <P2> obtained from SANS experiments for as-spun polystyrene fibres as a function of collector speed. Red circles represent uncorrected data for fibre angular alignment on the electrode while black squares are corrected data. Open symbols represent samples collected on static parallel plate electrode. (b) Radius of gyration of polymer chains parallel (black squares) and perpendicular (red circles) to the fibre direction together with bulk data (dashed line).*

The influence of size effects on the mechanical properties of electrospun fibres has been studied extensively [59-65] with many studies showing an increase in Young's modulus with decreasing nanofibre diameter. In most cases it is assumed that such an increase is due to confinement of the polymer coils as they are forced to align along the nanofibre axis. Confinement effects are regarded by most researchers as the main reason for property improvement in electrospun nanofibres. However, although some degree of alignment and orientation can be envisaged with decreasing fibre diameter,

particularly if the diameter is reduced to below the coil size, full chain extension as observed in super-drawn high performance fibres will be more difficult to achieve.

Nevertheless, a certain degree of orientation of polymer chains has been observed in electrospun fibres when their diameter is decreased. Figure 2.12a shows improved crystalline and extended amorphous structures in polycaprolactone (PCL) nanofibres for two diameters of 150 nm and 450 nm, produced under similar conditions [60]. Although an increase in mechanical properties with decreasing fibre diameter was reported for these PCL fibres the maximum reported Young's modulus remained low at 2 GPa. Additionally, chain orientation has also been observed in nanofibres that showed birefringence under crossed polarizers [66].

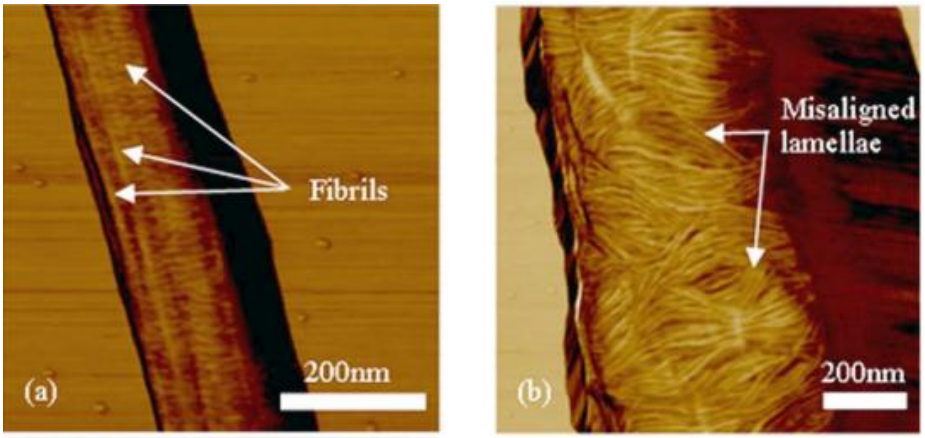

Figure 2.12. *PCL nanofibres produced under similar conditions but with different fibre diameters (a) 150 nm (b) 450 nm, showing a thinner nanofibre possessing a more aligned fibrillar and lamellae microstructure [60].*

Stachewicz *et al.* [67] found that electrospun PVA nanofibres can possess a composite-like core-shell structure, with the shell region being aligned as a result of

rapid solvent evaporation suppressing chain relaxation, and the core region being isotropic. This core-shell structure is used to explain the increase in elastic modulus with decreasing PVA nanofibre diameter as the shell component remained fairly constant at around 30 nm, meaning that the relative contribution of the shell region increases with decreasing fibre diameter. Properties of these PVA fibres indicated an increase in elastic modulus, as measured by single fibre AFM bending tests, for diameters below 300 nm. Elastic moduli up to 13 GPa, six times that of bulk PVA, were reported for fibres with diameters just below 100 nm. Although these values are superior to most reported data for electrospun fibres these values still do not rival solid-state drawn solution-spun PVA fibres possessing Young's moduli up to 70 GPa and tensile strengths of approximately 2 GPa [68].

Arinstein *et al.* [69] related the size of oriented regions in electrospun Nylon 6,6 nanofibres to the rapid increase in Young's modulus and quantified the percolation of the cross-section area required by using a modified Onsager model. A value of about 300 nm for a critical fibre diameter was found, below which a rapid increase in Young's modulus is initiated. Arinstein *et al.* [70] also reported an increase in Young's modulus in electrospun Nylon 6,6 nanofibres with decreasing fibre diameter (Figure 2.13). Here the authors suggest that the rapid increase in Young's modulus with decreasing fibre diameter is not the result of the small increase in observed crystallinity or orientation of the crystallites. Instead they ascribed the increase in mechanical properties to orientation of amorphous regions when their sizes are comparable or smaller than the nanofibre diameter.

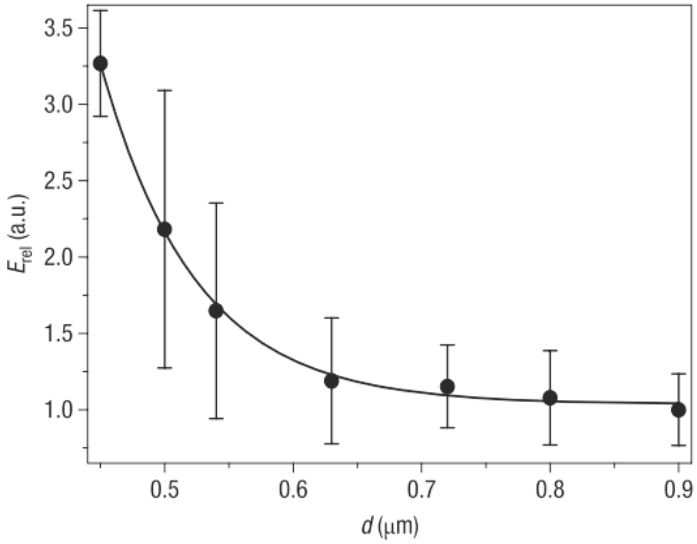

Figure 2.13. *Relative Young's modulus E_{rel} (E_{rel} = E/E_{bulk}) of electrospun PA 6,6 nanofibres as a function of their diameters [70].*

Most studies show similar results to those reported by Arinstein *et al.* [70], *i.e.*, a three-fold increase in Young's modulus of thin electrospun fibres compared to that of the bulk polymer. Naraghi *et al.* reported an increase in Young's modulus for electrospun PAN fibres smaller than 300 nm, with a three-fold increase in modulus for diameters ranging from 100–200 nm [71]. Pai *et al.* reported a similar increase in Young's modulus of individual electrospun fibres of poly(trimethyl hexamethylene terephthalamide) (PA 6(3)T) [62]. Here, the Young's modulus was found to increase for fibres with diameters smaller than 500 nm, with a maximum modulus value reported of around 6 GPa for 170 nm fibres, *i.e.*, three times the bulk modulus.

One recent example of a more significant property improvement in electrospun fibres that was ascribed to confinement effects was reported for polyacrylonitrile (PAN). Young's moduli up to 48 GPa and tensile strengths up to 1.75 GPa were

reported by Dzenis and coworkers [72] for individual PAN nanofibres, approaching typical values for high performance fibres. Unlike traditional high performance fibres, where an increase in mechanical properties is often accompanied with a sacrifice in strain at break, these ultrafine PAN nanofibres were also simultaneously stiff and ductile. The highest value of toughness was achieved from the thinnest electrospun nanofibre with a diameter of 138 nm. Similar to Arinstein *et al.* their increase in mechanical properties was not ascribed to increased crystallinity (Figure 2.14) as crystallization was restrained by the fast solidification that resulted from the rapid evaporation of solvent. Again it was proposed that the increase in mechanical properties was mainly related to confined molecular orientation of amorphous regions with decreasing nanofibre diameter.

The mechanical properties of these electrospun PAN fibres are particularly impressive, with the reported Young's modulus of 48GPa approaching or even exceeding theoretical values for atactic PAN (55 GPa) [73] or isotactic PAN having a 3/1 helical conformation (35 GPa) [73], although theoretical calculations have indicated that the crystal modulus of PAN taking a planar-zigzag conformation could reach values as high as 130 GPa [74]. In contrast to most other electrospun fibres, including PAN, where confinement effects typically result in a moderate increase in modulus [62, 67, 69, 70]; here a nanofibre modulus is reported that is ~25 times greater than that of bulk PAN. This is in stark contrast to studies of Naraghi *et al.* [71], who reported only a three-fold increase in Young's modulus for electrospun PAN fibres with a maximum value of 7 GPa for a 150 nm fibre. Similarly, these high performance PAN nanofibres also outperform most conventional wet-spun high

strength acrylic fibres with typical Young's moduli of 10–20 GPa and tensile strengths of 1–1.5 GPa [75]. In fact, the values reported for these electrospun PAN fibres exceed those of super-drawn solution-spun ultra-high molecular weight PAN fibres by Kanamoto and co-workers who obtained tensile moduli of 35 GPa and strengths of 1.8 GPa for fibres of draw-ratio 80, exhibiting extremely high levels of chain orientation [74].

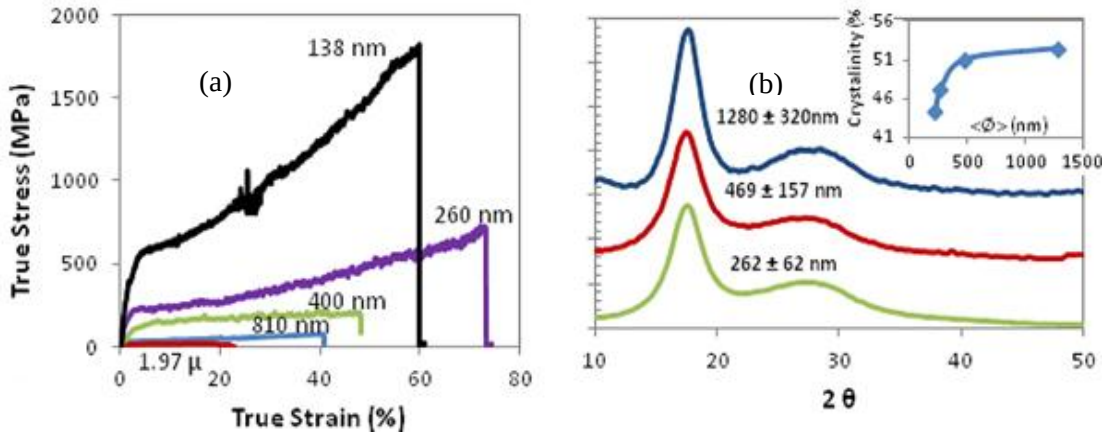

Figure 2.14. *(a) Stress-strain curves of electrospun PAN nanofibres with different diameters (b) XRD patterns of nanofiber bundles with various fibre diameters and corresponding degree of crystallinity (inset) [72].*

The underlying mechanisms of these exceptional properties are therefore still to be debated. The high modulus of the PAN nanofibres seems not related to their crystallinity as the reported crystallinity (< 50%) does not significantly increase with decreasing fibre diameter and is also less than that of conventional PAN fibre (~65%) [76]. Since flow-induced orientation is difficult to achieve during fibre spinning due to fast chain relaxation, and because these fibres are not post-drawn, it is difficult to envisage higher levels of chain extension in these as-spun nanofibres than in the

super-drawn UHMW-PAN fibres by Sawai *et al.* [74]. Moreover, as the estimated coil size of a PAN molecule with a molar mass of 150,000 is of the order of 30–40 nm based on its mean square end-to-end distance ($<R^2> = C_\infty n l^2$) [77, 78] it is also difficult to imagine the extreme confinement effects in 138 nm fibres which are necessary to explain such property improvement. Nevertheless, the reported mechanical properties of these electrospun PAN fibres are very interesting and require further studies.

In summary, the relatively poor mechanical properties of flexible chain based polymer nanofibres are mainly ascribed to two phenomena. The first one is related to the relatively low degree of chain orientation in these systems. Orientation of macromolecules can be usually introduced from a random coil morphology when the product of the polymer chain relaxation time and the strain rate in the electrospinning process is greater than 0.5 [38]. Given that strain rates can be up to 10^5 s^{-1} while viscoelastic relaxation times are found to be tens to hundreds of milliseconds [61, 62], some level of chain orientation can be potentially generated. However, residual solvents in the deposited nanofibres can accelerate chain relaxation and lead to shorter relaxation times [38]. Hence, relaxation of polymer chains could be suppressed by rapid solvent evaporation and fibre solidification [64]. As relaxation times of flexible chain polymers are typically very short, orientation induced in the initial spinning process may rapidly disappear before solidification. It is for this reason that conventional high performance fibres based on flexible chain polymers are post-drawn in the solid state below the melting temperature as this will prevent chain relaxation after orientation. Similarly, low degrees of molecular

orientation are to be expected in electrospun fibres based on flexible chain polymers, explaining their poor mechanical properties. Nonetheless, the mechanics in achieving chain orientation in electrospun fibres is still controversial due to the lack of systematically studies. For instant, most of characterizations on molecular orientation and mechanical properties in electrospun nanofibres are conducted on nanofibre mats or bundles rather than single fibres [81]. Therefore, in future research more attentions should be paid to single fibre characterization in order to establish better structure-processing-property relationships.

The second reason for the relatively poor mechanical properties of electrospun fibres is that full chain extension is nearly impossible to realize during the electrospinning process for flexible chain polymers. This is crucial for obtaining a high performance fibre with properties approaching the theoretical crystal moduli listed in Table 2.1. With the exception Dzenis and co-workers' PAN nanofibre [72], the differences between experimentally reported Young's moduli of electrospun nanofibres and these ultimate values are very large. Assuming the hypothetical case that polymer chain extension from random coil morphology is induced by virtue of reducing the nanofibre diameter to the same level as the size of crystallites or even the size of a single chain one might envisage a high modulus. Respective average crystallite size and chain size of PA 6,6 are around 4 nm and 0.1 nm [69], respectively, and polymer chains could be forced to extent and orient along the fibre axis if fibre diameters would go down to these levels. In such a case the Young's modulus of the fibre would be potentially approaching near theoretical values. However, even in such a hypothetical case it is expected that such ultra-thin fibres would be extremely weak

as there would be insufficient overlap between chains, resulting in poor stress transfer.

2.2.3. Electrospun nanofibres based on rigid chain polymers

2.2.3.1. Electrospun PPTA fibres

While chain extension in the case of flexible chain polymers can effectively be only achieved by solid-state drawing, the extension of polymer chains can be readily build in by polymer scientists when using rigid rod polymers. Rigid rod polymers have a significant advantage over flexible chain polymers as these systems can be oriented during the spinning process without the need of a post-drawing process to induce chain extension.

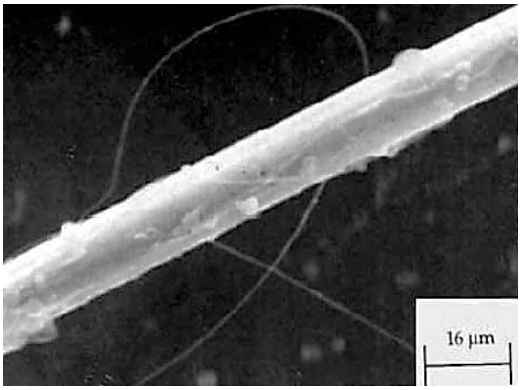

Figure 2.15. *A single electrospun PPTA fibre together with a single Kevlar®49 fibre [82].*

Inspired by the success of high performance aramid fibres the electrospinning of poly(*p*-phenylene terephthalamide) (PPTA) and characterization of the obtained nanofibre structures was carried out by Srinivasan and Reneker [82].

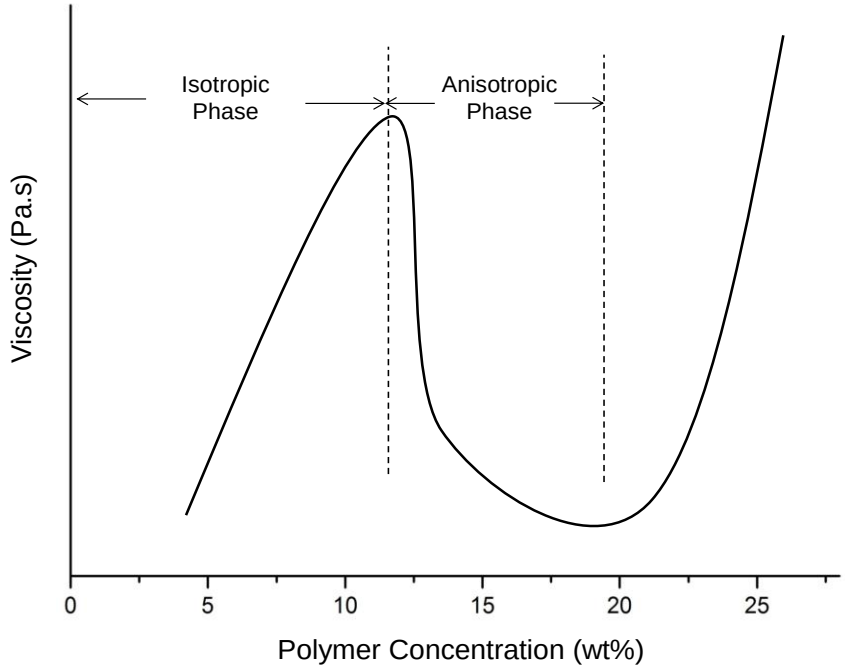

Figure 2.16. *Liquid crystalline behavior of PPTA solution, indicating an isotropic phase at concentrations below 12 wt % and an anisotropic phase between concentrations of 12 wt % to 20 wt %.*

In their studies a homogeneous isotropic solution was formed by dissolving PPTA fibres (Kevlar® 49) at a concentration of 2–3 wt % in a solvent of 95%–98% sulphuric acid. A water bath was used for extracting the solvent and collecting the electrospun nanofibres 12–18 kV high voltages were applied between two electrodes at a distance of 3 cm. Nanofibres with diameters ranging from 40 nm to hundreds of nanometers were produced (Figure 2.15). The meridional and equatorial reflection of the as-spun and at 400 ℃ annealed PPTA nanofibres were shown in dark field mode transmission electron microscopy (TEM) and revealed some order in the fibres. However, only moderate chain orientation in these annealed PPTA nanofibres was

demonstrated using electron diffraction. Moreover, a continuous electrospinning process and mechanical properties of the deposited nanofibres were not reported.

Traditional high performance *p*-aramid fibres are typically produced from anisotropic PPTA solutions with concentrations of around 19–20 wt % as shown in Figure 2.16. However, in the work of Srinivasan and Reneker, spinning solutions employed (2–3 wt %) were in their isotropic phase, which is outside the regime needed for flow induced molecular orientation as in the case of dry-jet wet spinning of high performance *p*-aramid fibres. Nevertheless, electrospinning of rigid rod polymers like aramids could still show promise once anisotropic PPTA solutions are used under optimized conditions, as it avoids problems related to chain relaxation in as-spun fibres.

2.2.3.2. Electrospun polyimide nanofibre

Poly(*p*-phenylene biphenyltetracarboxamide) (BPDA/PDA) is a high performance aromatic polyimide with great mechanical properties but a less rigid structure compared to PPTA [57] (Figure 2.17). Because of the rigid macromolecular backbone, it is insoluble in common organic solvents and thus not directly spinnable from solutions.

However, the precursor of BPDA/PDA, poly(*p*-phenylene biphenyltetracarboxamide acid) (BP-PAA) (Figure 2.18) shows good solubility in common organic solvents and it is therefore feasible to electrospin BP-PAA precursor fibres and subsequently convert them into BPDA-PDA polyimide nanofibres through a heat treatment.

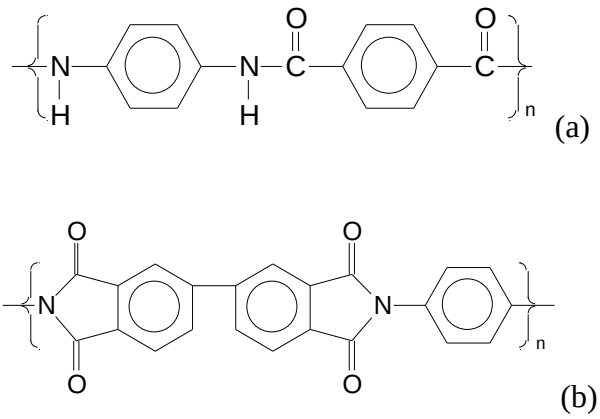

Figure 2.17. *Structural formulas of (a) PPTA and (b) BPDA/PDA polyimide.*

Hou and co-workers [83, 84] investigated the electrospinning process and mechanical properties of these polyimide nanofibres. Under proper spinning condition, a well-aligned BP-PAA nanofibre mat was obtained on a high-speed collector and the aligned polyamic acid nanofibre samples were imidized into polyimide nanofibres. During this imidization process, the rigid-rod molecular chains tend to become oriented and extended along the fibre axis (Figure 2.18).

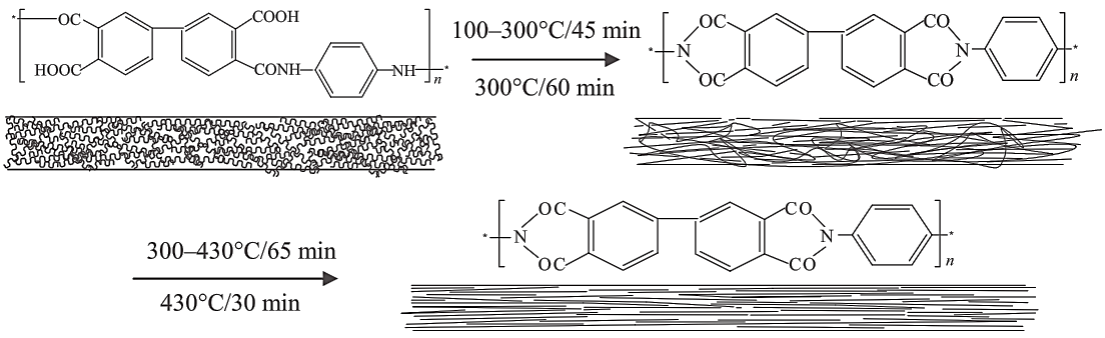

Figure 2.18. *A schematic diagram of the imidization process [57].*

Mechanical tests indicated that the average tensile strength and modulus of these nanofibre mats with fibre diameters of around 300 nm were 660 MPa and 15 GPa,

respectively. Further studies showed that the ultimate tensile strength and Young's modulus could reach values of 1.7 GPa and 76 GPa, which are comparable to conventional BPDA-PDA fibres [85] and are in the region of commercial high performance fibres.

2.2.4. Other routes to high performance nanofibres

2.2.4.1. CNT reinforced polymer nanofibres

Carbon nanotubes, due to their excellent mechanical properties, have been regarded as ideal reinforcement candidates for nanocomposites [86–88]. Basically, the Young's modulus and tensile strength of single-wall carbon nanotubes (SWCNTs) are reported to reach about 1 TPa and tens of GPa [89, 90], respectively, outperforming most other materials.

Generally, CNTs are however prone to aggregation and bundling because of their small diameter and strong Van der Waals interactions, lowering their reinforcing capability. Therefore, three main challenges are encountered when using carbon nanotubes as nano-reinforcements in polymer fibres. Firstly, the creation of a homogenous spinnable dispersion of CNTs; secondly, a good interfacial adhesion and stress transfer, and finally orientation of the CNTs in the polymer fibre [91–93]. Electrospinning is a promising technique to produce CNT reinforced nanofibres since it has the potential to debundle and align CNTs along the fibre axis and thus effectively reinforce the nanofibre [94–96], while interfacial interactions between CNTs and host polymer can be enhanced by functionalization of the CNTs [97].

Sen *et al.* [97] reported on ester-functionalized SWCNTs reinforced electrospun polyurethane (PU) nanofibres. Mechanical tests showed that the tensile strength of these ester-functionalized SWCNT reinforced nanofibre membranes were improved by 104%, while elastic moduli were increased by 250% compared to pure PU membranes, with improvements of these properties being mainly attributed to alignments and improved interfacial interactions between SWCNTs and polymer matrix.

Baji *et al.* investigated the mechanical properties of multi-wall carbon nanotube (MWCNT) reinforced nylon 6,6 nanofibres [98]. In their study, carboxylic acid functional groups modified MWCNTs were mixed together with nylon 6,6 in different concentrations. These mixtures were electrospun into aligned nanofibres using parallel plate electrodes. Mechanical tests showed that the tensile strength and Young's modulus of the composite nanofibres increased with CNT loading, reaching peak values (from about 0.32 GPa and 1.2 GPa to 0.65 GPa and 3.5 GPa, respectively) for CNT concentrations of 7.5 wt%. This significant improvement in mechanical properties was claimed to be due to among others the good dispersion and alignment of the MWCNTs along the nanofibre axis as confirmed by TEM. Other studies involving CNT reinforced nanofibres were reported by Hou *et al.* [99], Jose *et al.* [100], Lu *et al.* [101], and Wang *et al.* [102].

A careful analysis of the reinforcing efficiency of CNTs in the composite fibres should be emphasized here since high reinforcing efficiency of CNTs in composites is generally a good indication of effective dispersion, interfacial interaction and alignment. Wang *et al.* [103] reported on solid-state drawn nanocomposite

PVA/SWCNTs tapes and found a remarkable reinforcing efficiency for systems incorporating up to 1 wt% of SWCNTs. Further studies on nanotube reinforced electrospun PVA nanofibres (Figure 2.19) revealed similar high reinforcing efficiencies, with a back-calculated SWCNT Young's modulus of around 0.85 TPa [102], *i.e.*, close to its theoretical 1 TPa value.

Despite various developments in CNT reinforced nanofibres, in many cases, eliminating agglomeration and achieving homogenous spinnable solutions and good alignment remain a challenge especially at higher CNT concentrations. Moreover, even for systems that report significant property improvements these properties are often still not very impressive when compared to commercial high performance fibres.

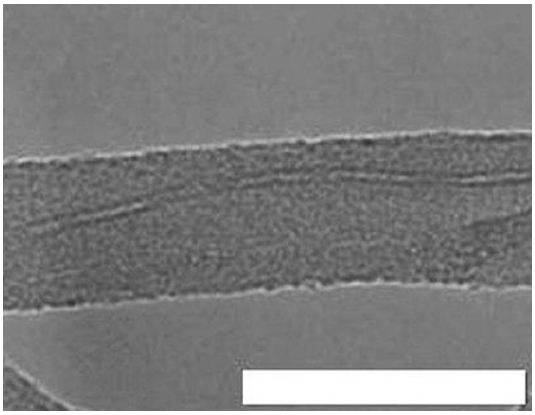

Figure 2.19. *TEM micrograph of an individual MWCNT reinforced electrospun PVA nanofibre, showing an aligned MWCNT in a polymer nanofibre (scale bar 100 nm) [102].*

2.2.4.2. Electrospun polymer-derived carbon nanofibres

Another interesting approach towards high strength and high modulus nanofibres is the development of carbon nanofibres. Polymer nanofibre precursors prepared via electrospinning followed by carbonization have been investigated [104]. Several polymers have been investigated as precursors for carbon fibres. Principally, polyacrylonitrile is used [105–109], while pitches [110, 111], poly(vinyl alcohol) (PVA) [112], polyimide (PI) [113], poly(vinylidene fluoride) (PVDF) [114], and polybenzimidazol (PBI) [115] have also been utilized.

Zussman *et al.* created single electrospun PAN-derived carbon nanofibres with different fibre diameters possessing Young's moduli of 63 ± 7 GP and tensile strengths between 0.32 GPa and 0.9 GPa. The inferior mechanical properties of these electrospun PAN-based carbon nanofibres compared to commercial carbon fibres resulted from the relatively poor molecular orientation and disarrangements in the core-shell structure of the carbon nanofibres [106]. PAN-based carbon nanofibres were also prepared by Zhou *et al.* [109]. Young's moduli of 40 to 60 GPa and tensile strengths of 0.3 to 0.6 GPa for carbon nanofibre bundles were achieved and mechanical properties were found to increase with carbonization temperature. In addition, the authors proposed possible ways to further enhance the mechanical properties of these PAN-based carbon nanofibres, *i.e.*, by post-drawing of precursor fibres; the stabilization and carbonization of nanofibres under tension; and the use of PAN copolymer as a precursor. Optimized process conditions for strong carbon nanofibres based on PAN were reported by Chasiotis and co-workers [116]. Both the PAN precursor nanofibres and carbon nanofibres were smooth and uniform (Figure

2.20). Young's moduli of 191 ± 58 GPa upon carbonization at 1700 °C and tensile strengths of 3.52 ± 0.64 GPa upon carbonization at 1400 °C were reported, and were attributed to an increase in crystallites in the carbon nanofibres, making these fibres approach the mechanical performance of standard high-strength carbon fibres.

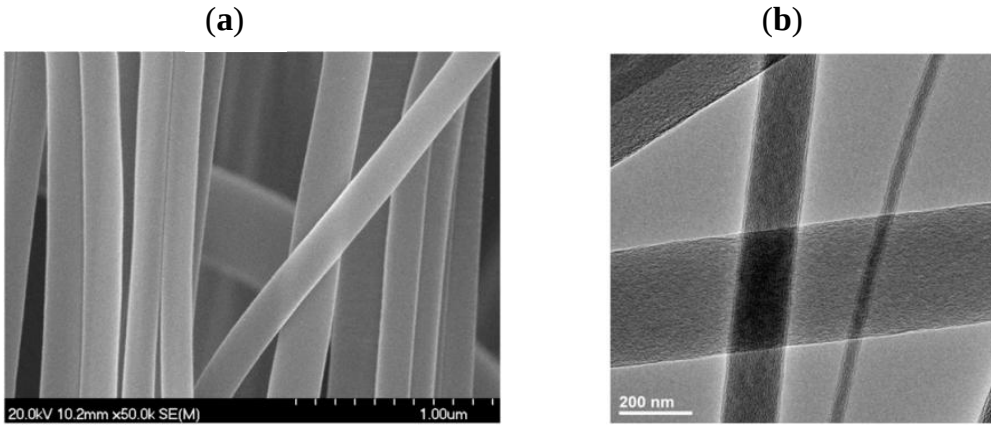

Figure 2.20. *(a) SEM micrograph and (b) TEM micrograph showing homogenous morphology of carbon nanofibres [116].*

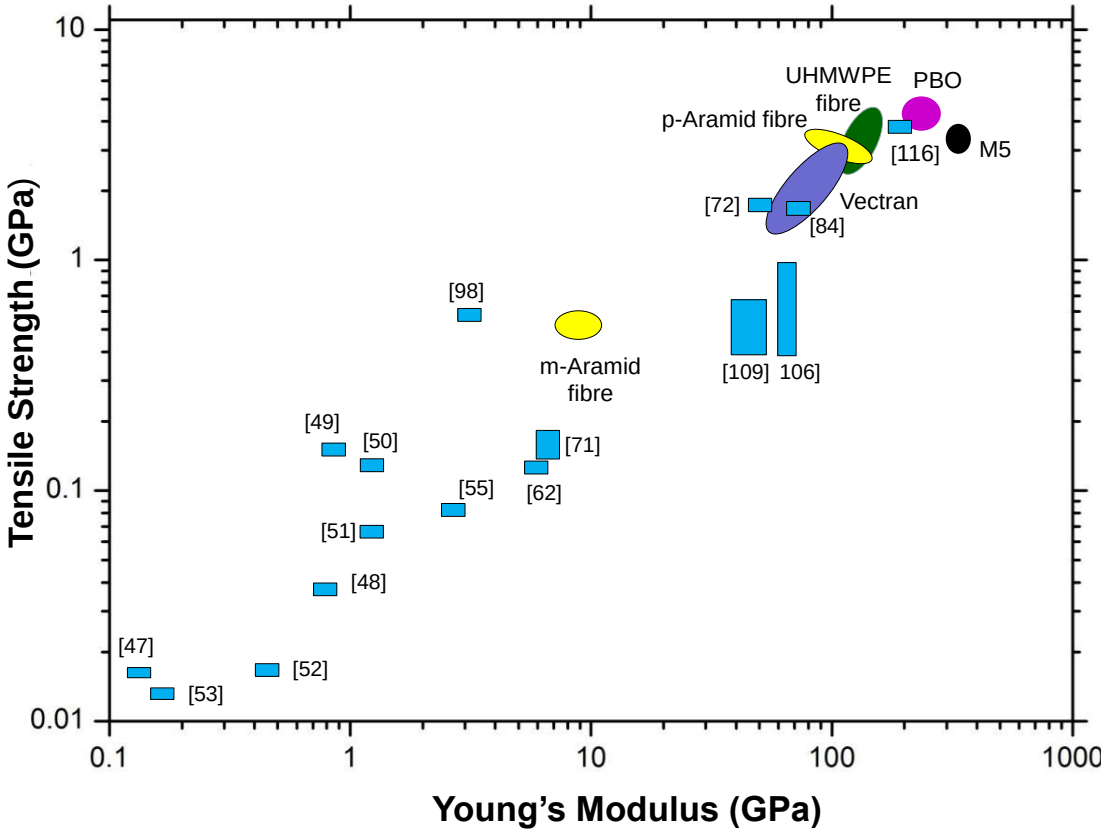

Figure 2.21. *Mechanical properties of traditional high performance fibres and electrospun nanofibres with respect to Young's modulus and tensile strength. Commercial high-performance fibres show typical tensile strengths of 3–4 GPa and moduli of around 100–300 GPa (as shown in the top right hand side), while most electrospun fibres typically possess tensile strengths < 0.3 GPa and Young's moduli < 3 GPa (as shown in the lower left hand side) [47-53, 55]. Some high performance electrospun nanofibres have been reported based on polyimide [84], polyacrylonitrile [72] and carbon nanofibres from electrospun PAN precursors [116].*

2.3. Conclusions

Electrospinning has proven to be an efficient method to produce thin fibres with diameters down to the nano-scale. However, the mechanical properties of these nanofibres are often well below those of fibres made by conventional processes such melt- or solution spinning (see Figure 2.21). The main reason for this is the competition between flow-induced chain orientation and chain relaxation before fibre solidification, leading to low degrees of molecular orientation in as-spun fibres. In conventional polymer fibre processing, chain alignment is induced by drawing the as-spun fibre in the solid-state below the melting temperature into a highly oriented structure as here relaxation times are infinite. In order to achieve similar high levels of chain orientation and chain extension in nanofibres based on flexible chain polymers it is vital to apply a post-stretching step.

Although some evidence exists of confinement induced molecular orientation in the case of ultra-fine nanofibres, the orientation and particularly chain extension achieved is often rather limited, leading to only moderate improvements in Young's modulus (typically 2–4 times bulk polymer), well below those attainable in commercial melt- or solution spun fibres (typically10–100times bulk polymer).

As the introduction of a post-drawing step in commercial electrospinning processes may prove technologically challenging, the use of rigid-rod polymers as an alternative to flexible chain polymers may be more promising as here chains have already build in chain extension and can be readily oriented during spinning. Other

alternative routes worth pursuing are the use of nano-reinforcements such as carbon nanotubes or transforming polymer precursor fibres into carbon nanofibres, with especially the latter showing some great promise for future work.

2.4. References

1. Staudinger, H. Über polymerisation. *Berichte der Deutschen Chemischen Gesellschaft (A and B Series)* **1920**, *53*, 1073-1085. (in German).

2. Heeger, A.J. Nobel Lecture: Semiconducting and metallic polymers: The fourth generation of polymeric materials. *Reviews of Modern Physics* **2001**, *73*, 681-700.

3. Dasgupta, S.; Hammond, W.B.; Goddard, W.A. Crystal structures and properties of nylon polymers from theory. *Journal of the American Chemical Society* **1996**, *118*, 12291-12301.

4. Cook, J.G. *Handbook of Textile Fibres: Man-Made Fibres*; Woodhead Publishing Limited: Cambridge, England: 1984; pp. 192-391.

5. Staudinger, H. Die Hochmolekularen im festen Zustand. In *Die Hochmolekularen Organischen Verbindungen-Kautschuk und Cellulose*; Springer Berlin Heidelberg: 1932; pp. 105-123. (in German).

6. Meyer, K.H.; Lotmar, W.; Pankow, G. Sur le chlorure de poly-phosphornitrile, caoutchouc inorganique. *Helvetica Chimica Acta* **1936**, *19*, 930-948. (in French).

7. Treloar, L.G. Calculations of elastic moduli of polymer crystals: I. Polyethylene and nylon 66. *Polymer* **1960**, *1*, 95-103.

8. Peijs, A.; Jacobs, M.; Lemstra, P. High-performance polyethylene fibers. In *Comprehensive Composite Materials. Vol. 1. Fiber Reinforcements and General Theory of Composites*; Chou, T. W.; Kelly, A.; Zweben, C., Eds.; Elsevier: Netherlands: 2000; pp. 263-301.

9. Hageman, J.; Meier, R.J.; Heinemann, M.; De Groot, R. Young modulus of crystalline polyethylene from ab initio molecular dynamics. *Macromolecules* **1997**, *30*, 5953-5957.

10. Crist, B. The ultimate strength and stiffness of polymers. *Annual Review of Materials Science* **1995**, *25*, 295-323.

11. Manley, T.; Martin, C. Elastic modulus of linear polymer crystals. *Polymer* **1973**, *14*, 491-496.

12. Nakamae, K.; Nishino, T. Crystal moduli of high polymers and their temperature dependence. In *Integration of Fundamental Polymer Science and Technology-5*; Lemstra, P.; Kleintjens, L., Eds.; Springer: Netherlands: 1991; pp. 121-130.

13. Lemstra, P.; Kirschbaum, R.; Ohta, T.; Yasuda, H. High-strength/high-modulus structures based on flexible macromolecules: gel-spinning and related processes. In *Developments in Oriented Polymers-2*; Springer: Netherlands: 1987; pp. 39-77.

14. Lemstra, P.; Van Aerle, N.; Bastiaansen, C. Chain-extended polyethylene. *Polymer Journal* **1987**, *19*, 85-98.

15. Lemstra, P.; Bastiaansen, C.; Meijer, H. Chain-extended flexible polymers. *Die Angewandte Makromolekulare Chemie* **1986**, *145*, 343-358.

16. Bastiaansen, C.W.; Simmelink, J.A.P.M. Solution of ultra-high molecular weight polyethylene. US Patent 5,428,079, filed 30 July 1991, and issued 27 June 1995.

17. Capaccio, G.; Ward, I. Ultra-high-modulus linear polyethylene through controlled molecular weight and drawing. *Polymer Engineering & Science* **1975**, *15*, 219-224.

18. Cansfield, D.; Capaccio, G.; Ward, I. The preparation of ultra-high modulus polypropylene films and fibres. *Polymer Engineering & Science* **1976**, *16*, 721-724.

19. Zwijnenburg, A.; Pennings, A. Longitudinal growth of polymer crystals from flowing solutions III. Polyethylene crystals in Couette flow. *Colloid and Polymer Science* **1976**, *254*, 868-881.

20. Zwijnenburg, A.; Pennings, A. Longitudinal growth of polymer crystals from flowing solutions. IV. The mechanical properties of fibrillar polyethylene crystals. *Journal of Polymer Science: Polymer Letters Edition* **1976**, *14*, 339-346.

21. Ajji, A.; Coates, P.; Dumoulin, M.; Ward, I. *Solid Phase Processing of Polymers*; Carl Hanser Verlag: Munich, Germany: 2000; pp. 85-210.

22. Smith, P.; Lemstra, P.J. Ultrahigh-strength polyethylene filaments by solution spinning/drawing, 2. Influence of solvent on the drawability. *Die Makromolekulare Chemie* **1979**, *180*, 2983-2986.

23. Smith, P.; Lemstra, P.J.; Pijpers, J.P. Tensile strength of highly oriented polyethylene. II. Effect of molecular weight distribution. *Journal of Polymer Science: Polymer Physics Edition* **1982**, *20*, 2229-2241.

24. Smith, P.; Lemstra, P.; Pijpers, J.; Kiel, A. Ultra-drawing of high molecular weight polyethylene cast from solution. *Colloid and Polymer Science* **1981**, *259*, 1070-1080.

25. Smith, P.; Lemstra, P.J. Filaments of high tensile strength and modulus. US Patent 4,430,383, filed 30 September 1982, and issued 7 February 1984.

26. Kwolek, S.L. Optically anisotropic aromatic polyamide dopes. US Patent 3,671,542, filed 23 May 1969, and issued 20 June 1972.

27. Kwolek, S.; Morgan, P.; Schaefgen, J.; Gulrich, L. Synthesis, anisotropic solutions, and fibers of poly (1, 4-benzamide). *Macromolecules* **1977**, *10*, 1390-1396.

28. Yang, H. *Kevlar Aramid Fiber*; John Wiley & Sons: Chichester, NH, USA: 1993; pp. 1-22.

29. Bair, T.; Morgan, P.; Killian, F. Poly (1, 4-phenyleneterephthalamides). polymerization and novel liquid-crystalline solutions. *Macromolecules* **1977**, *10*, 1396-1400.

30. Blades, H. High modulus, high tenacity poly (*p*-phenylene terephthalamide) fiber. US Patent 3,869,430, filed 30 June 1972, and issued 4 March 1975.

31. Dobb, M.; Johnson, D.; Saville, B. Supramolecular structure of a high-modulus polyaromatic fiber (Kevlar 49). *Journal of Polymer Science: Polymer Physics Edition* **1977**, *15*, 2201-2211.

32. Hearle, J.W. *High-Performance Fibres*; Woodhead Publishing: Cambridge, England: 2001; Vol. 15, pp. 93-155.

33. Kumar, S.; Dang, T.D.; Arnold, F.E.; Bhattacharyya, A.R.; Min, B.G.; Zhang, X.; Vaia, R.A.; Park, C.; Adams, W.W.; Hauge, R.H. Synthesis, Structure, and Properties of PBO/SWNT Composites. *Macromolecules* **2002**, *35*, 9039-9043.

34. Kitagawa, T.; Murase, H.; Yabuki, K. Morphological study on poly(p-phenylenebenzobisoxazole) (PBO) fiber. *Journal of Polymer Science Part B: Polymer Physics* **1998**, *36*, 39-48.

35. Choe, E.W.; Kim, S.N. Synthesis, spinning, and fiber mechanical properties of poly (*p*-phenylenebenzobisoxazole). *Macromolecules* **1981**, *14*, 920-924.

36. Sikkema, D.J. Design, synthesis and properties of a novel rigid rod polymer, PIPD or M5: high modulus and tenacity fibres with substantial compressive strength. *Polymer* **1998**, *39*, 5981-5986.

37. Sirichaisit, J.; Young, R. Tensile and compressive deformation of polypyridobisimidazole (PIPD)-based M5 rigid-rod polymer fibres. *Polymer* **1999**, *40*, 3421-3431.

38. Greiner, A.; Wendorff, J.H. Electrospinning: a fascinating method for the preparation of ultrathin fibers. *Angewandte Chemie International Edition* **2007**, *46*, 5670-5703.

39. Ramakrishna, S. *An Introduction to Electrospinning and Nanofibers*; World Scientific Publishing Co. Pte. Ltd: Singapore: 2005; pp. 90-154.

40. Li, D.; Xia, Y. Electrospinning of nanofibers: reinventing the wheel? *Advanced Materials* **2004**, *16*, 1151-1170.

41. Petrik, S.; Maly, M. In *Production Nozzle-less Electrospinning Nanofiber Technology*, MRS Proceedings, 2009; Materials Research Society: 2009.

42. Erisken, C.; Kalyon, D.M.; Wang, H. A hybrid twin screw extrusion/electrospinning method to process nanoparticle-incorporated electrospun nanofibres. *Nanotechnology* **2008**, *19*, 165302.

43. Senturk-Ozer, S.; Ward, D.; Gevgilili, H.; Kalyon, D.M. Dynamics of electrospinning of poly (caprolactone) via a multi-nozzle spinneret connected to a twin screw extruder and properties of electrospun fibers. *Polymer Engineering & Science* **2013**, *53*, 1463-1474.

44. Badrossamay, M.R.; McIlwee, H.A.; Goss, J.A.; Parker, K.K. Nanofiber assembly by rotary jet-spinning. *Nano letters* **2010**, *10*, 2257-2261.

45. Rein, D.M.; Shavit-Hadar, L.; Khalfin, R.; Cohen, Y.; Shuster, K.; Zussman, E. Electrospinning of ultrahigh-molecular-weight polyethylene nanofibers. *Journal of Polymer Science Part B: Polymer Physics* **2007**, *45*, 766-773.

46. Peijs, T.; Rijsdijk, H.; De Kok, J.; Lemstra, P. The role of interface and fibre anisotropy in controlling the performance of polyethylene-fibre-reinforced composites. *Composites Science and Technology* **1994**, *52*, 449-466.

47. Carrizales, C.; Pelfrey, S.; Rincon, R.; Eubanks, T.M.; Kuang, A.; McClure, M.J.; Bowlin, G.L.; Macossay, J. Thermal and mechanical properties of electrospun PMMA, PVC, Nylon 6, and Nylon 6, 6. *Polymers for Advanced Technologies* **2008**, *19*, 124-130.

48. Bazbouz, M.B.; Stylios, G.K. The tensile properties of electrospun nylon 6 single nanofibers. *Journal of Polymer Science Part B: Polymer Physics* **2010**, *48*, 1719-1731.

49. Zussman, E.; Burman, M.; Yarin, A.; Khalfin, R.; Cohen, Y. Tensile deformation of electrospun nylon-6, 6 nanofibers. *Journal of Polymer Science Part B: Polymer Physics* **2006**, *44*, 1482-1489.

50. Sanatgar, R.H.; Borhani, S.; Ravandi, S.A.H.; Gharehaghaji, A.A. The influence of solvent type and polymer concentration on the physical properties of solid state polymerized PA66 nanofiber yarn. *Journal of Applied Polymer Science* **2012**, *126*, 1112-1120.

51. Hang, F.; Lu, D.; Bailey, R.J.; Jimenez-Palomar, I.; Stachewicz, U.; Cortes-Ballesteros, B.; Davies, M.; Zech, M.; Bödefeld, C.; Barber, A.H. In situ tensile testing of nanofibers by combining atomic force microscopy and scanning electron microscopy. *Nanotechnology* **2011**, *22*, 365708.

52. Stachewicz, U.; Peker, I.; Tu, W.; Barber, A.H. Stress delocalization in crack tolerant electrospun nanofiber networks. *ACS Applied Materials & Interfaces* **2011**, *3*, 1991-1996.

53. Veleirinho, B.; Rei, M.F.; Lopes-DA-Silva, J. Solvent and concentration effects on the properties of electrospun poly (ethylene terephthalate) nanofiber mats. *Journal of Polymer Science Part B: Polymer Physics* **2008**, *46*, 460-471.

54. Zong, X.; Ran, S.; Fang, D.; Hsiao, B.S.; Chu, B. Control of structure, morphology and property in electrospun poly (glycolide-co-lactide) non-woven membranes via post-draw treatments. *Polymer* **2003**, *44*, 4959-4967.

55. Wu, S.Z.; Yang, X.P.; Zhang, F.; Hou, X.X. Stretching-induced orientation for improving the mechanical properties of electrospun polyacrylonitrile nanofiber sheet. *Advanced Materials Research* **2008**, *47*, 1169-1172.

56. Kongkhlang, T.; Tashiro, K.; Kotaki, M.; Chirachanchai, S. Electrospinning as a new technique to control the crystal morphology and molecular orientation of polyoxymethylene nanofibers. *Journal of the American Chemical Society* **2008**, *130*, 15460-15466.

57. Huang, C.; Chen, S.; Reneker, D.H.; Lai, C.; Hou, H. High-Strength Mats from Electrospun Poly(*p*-Phenylene Biphenyltetracarboximide) Nanofibers. *Advanced Materials* **2006**, *18*, 668-671.

58. Mohan, S.D.; Mitchell, G.R.; Davis, F.J. Chain extension in electrospun polystyrene fibres: a SANS study. *Soft Matter* **2011**, *7*, 4397-4404.

59. Tan, E.; Lim, C. Physical properties of a single polymeric nanofiber. *Applied Physics Letters* **2004**, *84*, 1603-1605.

60. Lim, C.; Tan, E.; Ng, S. Effects of crystalline morphology on the tensile properties of electrospun polymer nanofibers. *Applied Physics Letters* **2008**, *92*, 141908-141908-141903.

61. Bashur, C.A.; Dahlgren, L.A.; Goldstein, A.S. Effect of fiber diameter and orientation on fibroblast morphology and proliferation on electrospun poly (D, L-lactic-co-glycolic acid) meshes. *Biomaterials* **2006**, *27*, 5681-5688.

62. Pai, C.-L.; Boyce, M.C.; Rutledge, G.C. Mechanical properties of individual electrospun PA 6(3)T fibers and their variation with fiber diameter. *Polymer* **2011**, *52*, 2295-2301.

63. Chew, S.Y.; Hufnagel, T.C.; Lim, C.T.; Leong, K.W. Mechanical properties of single electrospun drug-encapsulated nanofibres. *Nanotechnology* **2006**, 17, 3880.

64. Shin, M.K.; Kim, S.I.; Kim, S.J.; Kim, S.-K.; Lee, H.; Spinks, G.M. Size-dependent elastic modulus of single electroactive polymer nanofibers. *Applied Physics Letters* **2006**, *89*, 231923-231929.

65. Fennessey, S.F.; Farris, R.J. Fabrication of aligned and molecularly oriented electrospun polyacrylonitrile nanofibers and the mechanical behavior of their twisted yarns. *Polymer* **2004**, *45*, 4217-4225.

66. Kim, J.S.; Reneker, D.H. Polybenzimidazole nanofiber produced by electrospinning. *Polymer Engineering & Science* **1999**, *39*, 849-854.

67. Stachewicz, U.; Bailey, R.J.; Wang, W.; Barber, A.H. Size dependent mechanical properties of electrospun polymer fibers from a composite structure. *Polymer* **2012**, *53*, 5132-5137.

68. Schellekens, R.; Bastiaansen, C. The drawing behavior of polyvinylalcohol fibers. *Journal of Applied Polymer Science* **1991**, *43*, 2311-2315.

69. Arinstein, A.; Zussman, E. Electrospun polymer nanofibers: mechanical and thermodynamic perspectives. *Journal of Polymer Science, Part B: Polymer Physics* **2011**, *49*, 691-707.

70. Arinstein, A.; Burman, M.; Gendelman, O.; Zussman, E. Effect of supramolecular structure on polymer nanofibre elasticity. *Nature Nanotechnology* **2007**, *2*, 59-62.

71. Naraghi, M.; Arshad, S.; Chasiotis, I. Molecular orientation and mechanical property size effects in electrospun polyacrylonitrile nanofibers. *Polymer* **2011**, *52*, 1612-1618.

72. Papkov, D.; Zou, Y.; Andalib, M.N.; Goponenko, A.; Cheng, S.Z.; Dzenis, Y.A. Simultaneously strong and tough ultrafine continuous nanofibers. *ACS Nano* **2013**, *7*, 3324-3331.

73. Allen, R.; Ward, I.; Bashir, Z. An investigation into the possibility of measuring an 'X-ray modulus' and new evidence for hexagonal packing in polyacrylonitrile. *Polymer* **1994**, *35*, 2063-2071.

74. Sawai, D.; Fujii, Y.; Kanamoto, T. Development of oriented morphology and tensile properties upon superdawing of solution-spun fibers of ultra-high molecular weight poly (acrylonitrile). *Polymer* **2006**, *47*, 4445-4453.

75. Brandrup, J.; Immergut, E.H.; Grulke, E.A.; Abe, A.; Bloch, D.R. *Polymer Handbook, 4th ed.*; John Wiley & Sons: New York, NY, USA: 1999; Vol. 5, pp. 61.

76. Lewin, M. *Handbook of Fiber Chemistry, 3rd ed.*; Taylor & Francis Group: Boca Raton, FL, USA: 2006; pp. 812-958.

77. Bisschops, J. Gelation of concentrated polyacrylonitrile solutions. II. *Journal of Polymer Science* **1955**, *17*, 89-98.

78. Cleland, R.L.; Stockmayer, W.H. An intrinsic viscosity-molecular weight relation for polyacrylonitrile. *Journal of Polymer Science* **1955**, *17*, 473-477.

79. Reneker, D.H.; Yarin, A.L.; Fong, H.; Koombhongse, S. Bending instability of electrically charged liquid jets of polymer solutions in electrospinning. *Journal of Applied Physics* **2000**, *87*, 4531.

80. Theron, S.; Zussman, E.; Yarin, A. Experimental investigation of the governing parameters in the electrospinning of polymer solutions. *Polymer* **2004**, *45*, 2017-2030.

81. Richard-Lacroix, M.; Pellerin, C. Molecular Orientation in Electrospun Fibers: From Mats to Single Fibers. *Macromolecules* **2013**, *46*, 9473-9493.

82. Srinivasan, G.; Reneker, D.H. Structure and morphology of small diameter electrospun aramid fibers. *Polymer International* **1995**, *36*, 195-201.

83. Huang, C.; Wang, S.; Zhang, H.; Li, T.; Chen, S.; Lai, C.; Hou, H. High strength electrospun polymer nanofibers made from BPDA–PDA polyimide. *European Polymer Journal* **2006**, *42*, 1099-1104.

84. Chen, F.; Peng, X.; Li, T.; Chen, S.; Wu, X.-F.; Reneker, D.H.; Hou, H. Mechanical characterization of single high-strength electrospun polyimide nanofibres. *Journal of Physics D: Applied Physics* **2008**, *41*, 025308.

85. Kaneda, T.; Katsura, T.; Nakagawa, K.; Makino, H.; Horio, M. High-strength–high-modulus polyimide fibers I. One-step synthesis of spinnable polyimides. *Journal of Applied Polymer Science* **1986**, *32*, 3133-3149.

86. Baughman, R.H.; Zakhidov, A.A.; de Heer, W.A. Carbon nanotubes--the route toward applications. *Science* **2002**, *297*, 787-792.

87. Thostenson, E.T.; Ren, Z.; Chou, T.-W. Advances in the science and technology of carbon nanotubes and their composites: a review. *Composites Science and Technology* **2001**, *61*, 1899-1912.

88. Hussain, F.; Hojjati, M.; Okamoto, M.; Gorga, R.E. Review article: polymer-matrix nanocomposites, processing, manufacturing, and application: an overview. *Journal of Composite Materials* **2006**, *40*, 1511-1575.

89. Yu, M.-F.; Files, B.S.; Arepalli, S.; Ruoff, R.S. Tensile loading of ropes of single wall carbon nanotubes and their mechanical properties. *Physical Review Letters* **2000**, *84*, 5552.

90. Shenderova, O.; Brenner, D.; Ruoff, R.S. Would diamond nanorods be stronger than fullerene nanotubes? *Nano Letters* **2003**, *3*, 805-809.

91. Biercuk, M.; Llaguno, M.C.; Radosavljevic, M.; Hyun, J.; Johnson, A.T.; Fischer, J.E. Carbon nanotube composites for thermal management. *Applied Physics Letters* **2002**, *80*, 2767-2769.

92. Xie, X.-L.; Mai, Y.-W.; Zhou, X.-P. Dispersion and alignment of carbon nanotubes in polymer matrix: a review. *Materials Science and Engineering: R: Reports* **2005**, *49*, 89-112.

93. Grossiord, N.; Loos, J.; Regev, O.; Koning, C.E. Toolbox for dispersing carbon nanotubes into polymers to get conductive nanocomposites. *Chemistry of Materials* **2006**, *18*, 1089-1099.

94. Salalha, W.; Dror, Y.; Khalfin, R.L.; Cohen, Y.; Yarin, A.L.; Zussman, E. Single-walled carbon nanotubes embedded in oriented polymeric nanofibers by electrospinning. *Langmuir* **2004**, *20*, 9852-9855.

95. Wan, Y.Q.; He, J.H.; Yu, J.Y. Carbon nanotube-reinforced polyacrylonitrile nanofibers by vibration-electrospinning. *Polymer International* **2007**, *56*, 1367-1370.

96. Kannan, P.; Eichhorn, S.J.; Young, R.J. Deformation of isolated single-wall carbon nanotubes in electrospun polymer nanofibres. *Nanotechnology* **2007**, *18*, 235707.

97. Sen, R.; Zhao, B.; Perea, D.; Itkis, M.E.; Hu, H.; Love, J.; Bekyarova, E.; Haddon, R.C. Preparation of single-walled carbon nanotube reinforced

polystyrene and polyurethane nanofibers and membranes by electrospinning. *Nano Letters* **2004**, *4*, 459-464.

98. Baji, A.; Mai, Y.-W.; Wong, S.-C.; Abtahi, M.; Du, X. Mechanical behavior of self-assembled carbon nanotube reinforced nylon 6, 6 fibers. *Composites Science and Technology* **2010**, *70*, 1401-1409.

99. Hou, H.; Ge, J.J.; Zeng, J.; Li, Q.; Reneker, D.H.; Greiner, A.; Cheng, S.Z. Electrospun polyacrylonitrile nanofibers containing a high concentration of well-aligned multiwall carbon nanotubes. *Chemistry of Materials* **2005**, *17*, 967-973.

100. Jose, M.V.; Steinert, B.W.; Thomas, V.; Dean, D.R.; Abdalla, M.A.; Price, G.; Janowski, G.M. Morphology and mechanical properties of Nylon 6/MWNT nanofibers. *Polymer* **2007**, *48*, 1096-1104.

101. Lu, P.; Hsieh, Y.-L. Multiwalled carbon nanotube (MWCNT) reinforced cellulose fibers by electrospinning. *ACS Applied Materials & Interfaces* **2010**, *2*, 2413-2420.

102. Wang, W.; Ciselli, P.; Kuznetsov, E.; Peijs, T.; Barber, A. Effective reinforcement in carbon nanotube–polymer composites. *Philosophical Transactions of the Royal Society A: Mathematical, Physical and Engineering Sciences* **2008**, *366*, 1613-1626.

103. Wang, Z.; Ciselli, P.; Peijs, T. The extraordinary reinforcing efficiency of single-walled carbon nanotubes in oriented poly(vinyl alcohol) tapes. *Nanotechnology* **2007**, *18*, 455709.

104. Inagaki, M.; Yang, Y.; Kang, F. Carbon nanofibers prepared via electrospinning. *Advanced Materials* **2012**, *24*, 2547-2566.

105. Kim, C.; Yang, K.S.; Kojima, M.; Yoshida, K.; Kim, Y.J.; Kim, Y.A.; Endo, M. Fabrication of Electrospinning-Derived Carbon Nanofiber Webs for the

Anode Material of Lithium-Ion Secondary Batteries. *Advanced Functional Materials* **2006**, *16*, 2393-2397.

106. Zussman, E.; Chen, X.; Ding, W.; Calabri, L.; Dikin, D.; Quintana, J.; Ruoff, R. Mechanical and structural characterization of electrospun PAN-derived carbon nanofibers. *Carbon* **2005**, *43*, 2175-2185.

107. Zussman, E.; Yarin, A.L.; Bazilevsky, A.V.; Avrahami, R.; Feldman, M. Electrospun Polyaniline/Poly (methyl methacrylate)-Derived Turbostratic Carbon Micro-/Nanotubes. *Advanced Materials* **2006**, *18*, 348-353.

108. Kim, C.; Jeong, Y.I.; Ngoc, B.T.N.; Yang, K.S.; Kojima, M.; Kim, Y.A.; Endo, M.; Lee, J.W. Synthesis and characterization of porous carbon nanofibers with hollow cores through the thermal treatment of electrospun copolymeric nanofiber webs. *Small* **2007**, *3*, 91-95.

109. Zhou, Z.; Lai, C.; Zhang, L.; Qian, Y.; Hou, H.; Reneker, D.H.; Fong, H. Development of carbon nanofibers from aligned electrospun polyacrylonitrile nanofiber bundles and characterization of their microstructural, electrical, and mechanical properties. *Polymer* **2009**, *50*, 2999-3006.

110. Park, S.H.; Kim, C.; Choi, Y.O.; Yang, K.S. Preparations of pitch-based CF/ACF webs by electrospinning. *Carbon* **2003**, *41*, 2655-2657.

111. Park, S.H.; Kim, C.; Yang, K.S. Preparation of carbonized fiber web from electrospinning of isotropic pitch. *Synthetic Metals* **2004**, *143*, 175-179.

112. Zou, L.; Gan, L.; Lv, R.; Wang, M.; Huang, Z.-h.; Kang, F.; Shen, W. A film of porous carbon nanofibers that contain Sn/SnO_X nanoparticles in the pores and its electrochemical performance as an anode material for lithium ion batteries. *Carbon* **2011**, *49*, 89-95.

113. Xuyen, N.T.; Ra, E.J.; Geng, H.-Z.; Kim, K.K.; An, K.H.; Lee, Y.H. Enhancement of conductivity by diameter control of polyimide-based

electrospun carbon nanofibers. *The Journal of Physical Chemistry B* **2007**, *111*, 11350-11353.

114. Merino, C.; Soto, P.; Vilaplana-Ortego, E.; Gomez de Salazar, J.M.; Pico, F.; Rojo, J.M. Carbon nanofibres and activated carbon nanofibres as electrodes in supercapacitors. *Carbon* **2005**, *43*, 551-557.

115. Kim, C.; Kim, J.-S.; Kim, S.-J.; Lee, W.-J.; Yang, K.-S. Supercapacitors prepared from carbon nanofibers electrospun from polybenzimidazol. *Journal of The Electrochemical Society* **2004**, *151*, A769-A773.

116. Arshad, S.N.; Naraghi, M.; Chasiotis, I. Strong carbon nanofibers from electrospun polyacrylonitrile. *Carbon* **2011**, *49*, 1710-1719.

Chapter 3

Electrospinning of PPTA Fibres

3.1 Introduction

As discussed in the previous chapter, in order to create high strength and high modulus fibres, it is vital to achieve chain orientation and chain extension along the fibre axis [1, 2]. With respect to electrospun nanofibres, mechanical properties are often found to be poor compared to corresponding synthetic textile fibres made from the same polymers due to their low degree of chain orientation and chain extension. Orientation of macromolecules can be introduced when the product of polymer chain relaxation time and the extension rate in the electrospinning process is greater than 0.5 [3]. Given the fact that the relaxation time of flexible chain polymers is typically very short, orientation induced in the initial spinning process can rapidly disappear due to relaxation before solidification [4]. It is for this reason that high performance

fibres based on flexible chain polymers are typically post-drawn in the solid state below the melting temperature, where relaxation times are nearly infinite. However, such an approach is usually not feasible in electrospinning due to technological difficulties with respect to the post-drawing of nano-sized fibres [5]. Only limited stretching or drawing has been attempted to oriented nanofibre mats in order to induce some levels of molecular orientation and crystallinity, which often remain rather low [6, 7].

An alternative approach to achieve high chain orientation and extension is through the use of rigid chain polymers. The main reason to use rigid rod polymers is that in these systems the chain extension is already built in whilst flow induced chain orientation can be realised during the spinning process. *p*-Aramid fibre is the prime example of a high performance synthetic fibres spun from rigid (or semi-rigid) polymer chains. When poly(*p*-phenylene terehthalamid) (PPTA) is dissolved in concentrated sulphuric acid at low concentration, the rigid rod molecules are randomly distributed. These rod-like molecules will tend to arrange themselves to form nematic domains above a certain concentration. Furthermore, they can be oriented in the fibre direction when they are subject to elongational flow during spinning [8]. Using such an approach, conventional high performance *p*-aramid fibres have been produced using dry-jet wet spinning technologies taking advantage of the anisotropic properties of PPTA solutions [9, 10].

Great success has been achieved by developing through these routes high performance *p*-aramid fibres like Kevlar® and Twaron® with typical fibre diameters

of around 14 μm [11, 12]. However, until recently few efforts were devoted to the development of electrospun *p*-aramid nanofibres. Reneker and co-workers [13] attempted to electrospin 2-3 wt% of PPTA solution (isotropic phase). Although nano-scale fibres were obtained no mechanical properties were reported. Importantly, concentrations of these spinnable solutions used in their work were outside the regime (19-20 wt%) needed for high performance *p*-aramid fibres, which implies that mechanical properties of these fibres would have been rather poor.

In this chapter, we aim to develop high performance PPTA nanofibres by electrospinning anisotropic solutions. First, the electro-spinnability of both isotropic and anisotropic PPTA solutions is investigated. Subsequently, the need for using relatively high voltages in the electrospinning of these materials is analysed followed with a discussion on the difficulties and challenges in creating a continuous and technologically feasible electrospinning process. Finally, the mechanical properties of the *p*-aramid fibres obtained from the above process is discussed and correlated with the size effect.

3.2. Experimental

3.2.1. Solution preparation and electrospinning

98 wt% of concentrated sulphuric acid was prepared by diluting fuming sulphuric acid containing 20% sulphur trioxide (purchased from Sigma-Aldrich) with distilled water. For instance, in order to make 98 wt% of sulphuric acid, 100 g fuming

sulphuric containing 20g of sulphur trioxide needs to be added with 6.59g of distilled water.

A 19.46 wt% PPTA in concentrated sulphuric acid solution (kindly provided by Teijin Aramid, The Netherlands) was diluted to produce three isotropic solutions of 2 wt%, 5 wt%, 7 wt% and two anisotropic solutions of 15 wt% and 17 wt% by adding 98 wt% of sulphuric acid. All solutions were prepared using mild stirring in oil bath at 85 °C for 3 hrs.

In the electrospinning process, voltages between 0 kV and 30 kV were employed, distances from 8 to 2 cm and flow rates between 0.2 ml/h to 2 ml/h were adjusted to obtain fibres. A water bath was used to coagulate and collect the fibres. Moreover, a heating band was used to maintain the temperature of the spinning solutions between 80 °C and 90 °C.

3.2.2. Tensile testing and fibre characterization

The resulting electrospun fibres were tested using a micro-tensile tester (Agilent T150 UTM, load resolution of 50 nN) [14]. As shown in Figure 3.1, single fibres were mounted on a paper frame with a fixed internal dimension of 10 mm × 5 mm. Super glue and double-sided tapes were used to fix the single fibres to the frame and no clamp slippage was observed during testing. The strain rate during tensile testing was 0.1 mm/s. Samples that failed close to or inside the grip were discarded.

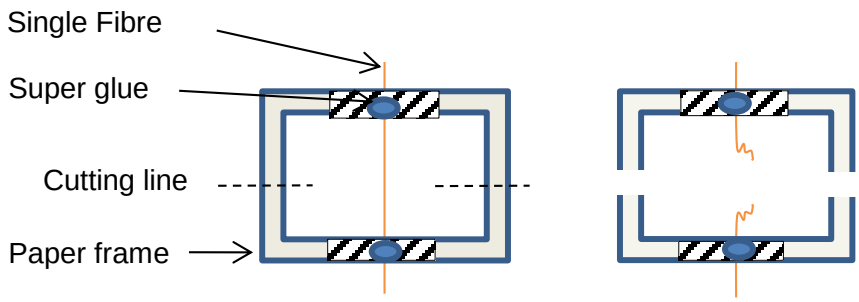

Figure 3.1. *Schematic illustration of single fibre sample preparation for mechanical tests.*

Morphological studies of the fibres were performed using a scanning electron microscope (FEI, Inspect F). All of the samples were gold-coated before observation.

3.3. Results and Discussion

3.3.1. Electrospinning from isotropic and anisotropic PPTA solutions

Figure 2.16 shows the relation of viscosity with concentration of moderate molecular weight PPTA in sulphuric acid above 80 °C [15]. An increase in solution concentration results in an increase in viscosity in the isotropic phase when PPTA molecules are randomly aligned. For this reason PPTA solutions are considered to be in their isotropic phase at low concentrations (typically less than 12 wt%). Viscosity reduces sharply at a critical concentration with a further increase in solution concentration due to the self-assembly of molecules into nematic liquid crystal domains and subsequently the viscosity reaches a minimum at a concentration of around 20 wt% when the solution becomes fully liquid crystalline. Above this

concentration, the solution viscosity will increase again with the appearance of a PPTA solid phase caused by the super-saturation of solution. Conventional *p*-aramid fibres are spun from about 20 wt% concentrations (around the lowest viscosity) by taking advantage of the anisotropic properties of PPTA solutions [16].

A typical electrospinning set-up is shown in Figure 3.2. It should be noted that these anisotropic PPTA solutions are biphasic with both nematic phase and solid phase below 80 °C while degradation of PPTA would be initiated above 90 °C. Hence, a heating band with a precise temperature control system to the syringe is necessary to ensure a spinning solution temperature of 85 °C.

Electrospinning involves charging the spinning solution using high voltage and consequently a solution jet could eject from the pending droplet on the nozzle when its surface tension is overcome by the electrostatic repulsion forces. In this work, spinning parameters such as applied voltage, distance and flow rate of solution were adjusted to make the solution spinnable. It should be noted that a water bath is needed as a collector to extract solvents and coagulate the solution jets into fibres because of the non-volatile property of sulphuric acid. Subsequently, those fibres are transported for drying at 60 °C overnight. It is important to know that the spinning solution jet in this work is relatively straight and few whipping instabilities were observed due to the use of high voltages and short spinning distances. Branched solution jets were found close to the coagulation bath, which will be discussed in the next section.

The spinnability of the PPTA solutions is of primary importance for the technological feasibility of electrospun PPTA fibres. In the case of electrospinning of isotropic solutions, only small and large droplets were deposited in the coagulation bath for 3 wt% and 5 wt% solutions, respectively. After washing and drying, these droplet morphologies are shown in Figure 3.3a and b, respectively. With increasing solution concentration, short fibres (lengths < 100 μm) of varying diameters (2 μm-20 μm) were collected from the 7 wt% solution at an applied voltage of 25 kV and a distance of 5 cm as shown in Figure 3.3c. Further increase of solution concentration would lead to rapid increase in viscosity of spinning solution but failed to lead to longer fibres.

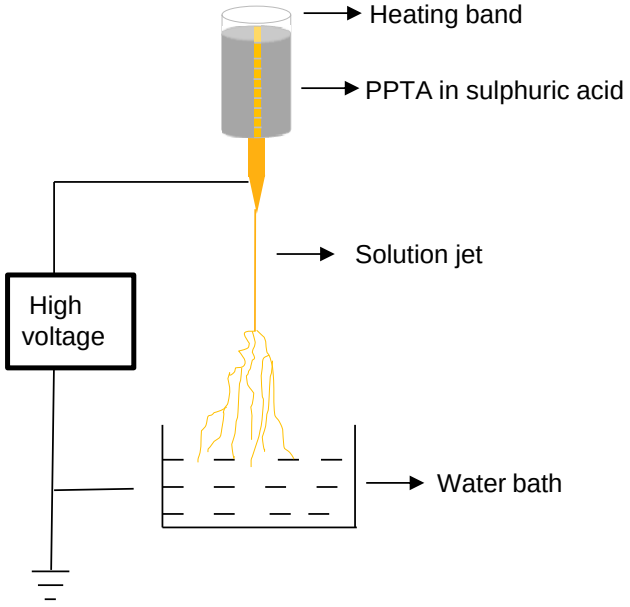

Figure 3.2. *Schematic illustration of electrospinning set-up of PPTA in concentrated sulphuric acid solutions.*

This phenomenon can be ascribed to the fact that the surface tension of solution dominates the electrospinning process at low concentrations, hence leading to the formation of droplets or stretched droplets (short fibres) [17]. Meanwhile, due to the non-volatility of sulphuric acid, no solid fibres were obtained before the coagulation bath. During the spinning process, the solution jet is prone to break when it is stretched due to the absence of chain entanglements in the low concentration solutions. Therefore, under these circumstances, the process can be considered to be electrospraying rather than electrospinning.

(a)

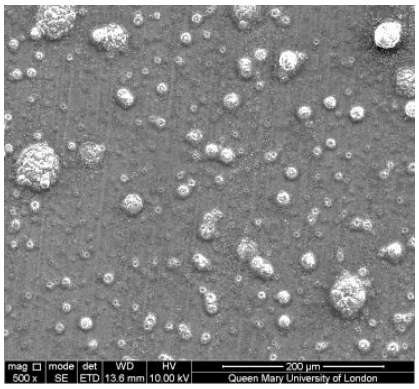

(b)

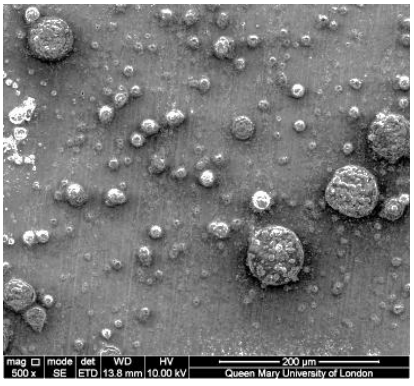

(c)

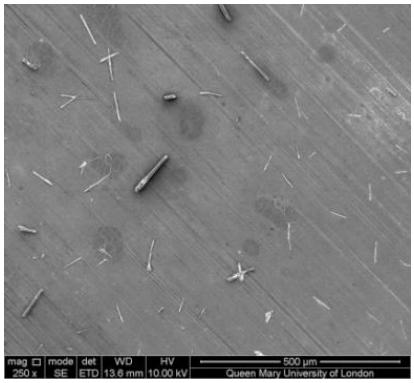

Figure 3.3. *SEM micrographs of fibres 'electrospun' from PPTA solutions with concentrations of (a) 3 wt% (b) 5 wt% and (c) 7 wt% PPTA.*

(a)

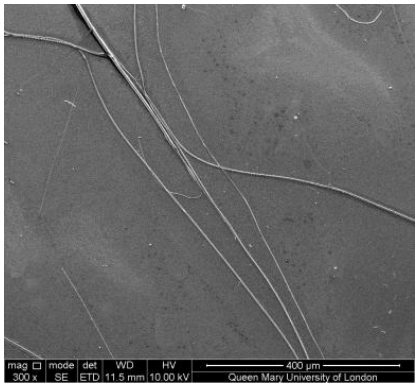

(b)

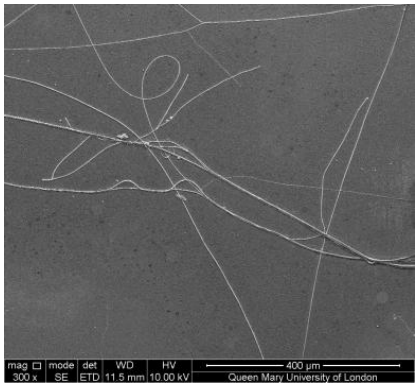

(c)

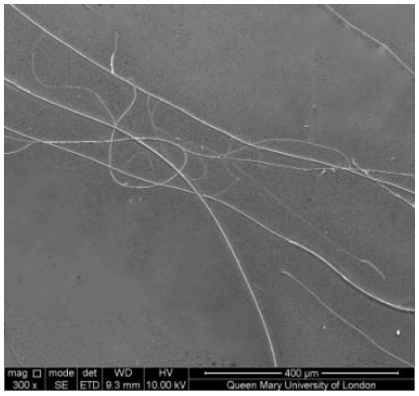

Figure 3.4. *SEM micrographs of fibres 'electrospun' from PPTA solutions with concentrations of (a) 15 wt% (b) 17 wt% and (c) 19.46 wt% PPTA.*

With respect to the electrospinning of anisotropic solutions, the solvent molecules have a tendency to interact with polymer molecules rather than congregate together, which is attributed to the high concentration of the solution. Consequently, the solution jet is stretched and fibres can be obtained without breakage of the jet owing to a sufficient level of chain entanglements in the solution. The *p*-aramid fibres electrospun from 15 wt%, 17 wt% and 19.46 wt% of anisotropic solutions are shown in Figure 3.4 (a, b, c). A broad range of fibre diameters from about 300 nm to 16 μm were found for all of the three anisotropic spinning solutions.

3.3.2. Feasibility of electrospinning conditions for p-aramid fibres

It should be noted that the electrospinning parameters (spinning voltage, distance, flowing rate, *etc.*) needed in this work to obtain fibres all varied within narrow ranges. Specifically, electric field strength (4 kV/cm) used was about threefold of that of normal electrospinning [3]. A low electric field strength leads to greater tendency of droplet formation while too high electric field strength is prone to give

rise to corona discharge. In both situations, no fibres will be obtained. Here, the electrospinning of anisotropic PPTA solutions (15 wt%, 17 wt% and 19.46 wt%) gave similar fibre diameter distributions as shown in Figure 3.4 (a, b, and c).

Three key solution parameters are listed in Table 3.1 which can significantly influence the processing parameters, *i.e.* applied voltage or potential electrical field. Compared to other commonly used electrospinning solvents, the conductivity of solvent used in this study is significantly higher. Meanwhile, the essential difference of the anisotropic PPTA solution with other common electrospinning solutions is the relatively high solution viscosity as shown in Table 3.1. Although the surface tension of 98% sulphuric acid is of the same order as surface tensions measured for common electrospinning solutions, it is not directly comparable as the surface tension of the anisotropic PPTA solution are unknown, it can still be concluded that high voltages are needed to generate sufficient electrostatic forces to stretch the electrospinning jet into micro-scale or nano-scale fibres in the case of these anisotropic PPTA solutions. The necessity of high voltage is not due to the conductivity of the solution but mainly the result of the high viscosities of the PPTA solutions. In order to better understand the role of applied high voltage (or high electrical field) in the process, a similar set-up without applied voltage was used to produce fibres from the same lyotropic solutions. It was found that large fibres with diameters varying from 2 mm to 50 μm can be collected. Mechanical properties of these fibres were found to be inferior to the largest diameter electrospun fibres collected with applied voltage as will be shown in the next section. As such this reference experiment indicated that an applied voltage is essential to fabricate thin fibres and to induce alignment of the

PPTA molecules in the fibres.

Table 3.1. *Viscosity, conductivity and surface tension of anisotropic PPTA solutions compared with common polymer solutions employed in electrospinning.*

Solutions	**Viscosity (1×10^3 cP)**	**Conductivity of solvents (mS/m)**	**Surface tension (mN/m)**	**Ref.**
Anisotropic PPTA solutions	650-1000	73.5-83.5 (80°C-90°C)	~55 (98% H_2SO_4)	[18, 19]
Common electrospun polymer solutions	0.02-300	0.05-30 (RT)	20-75	[20]

Nevertheless, two significant phenomena arise with the application of high electrical field strength. First of all, abundant branching was observed as shown in Figure 3.4. This is because the solution jet is easily disturbed by the high voltage and the high density charges tend to build up in the solution jet as a result of the high electric field. As a result, several secondary jets are formed from the primary jet during spinning in

order to reduce the local charges per unit surface area [4], leading eventually to branched fibres. Fibres with diameters ranging from 16 μm to hundreds of nanometers can be found in the deposited fibre branches and it was impossible to control the fibre diameter within a certain range independent of spinning parameters. Also fibres with diameters less than 2 μm rarely had a length above 3 mm, which makes them difficult to test but also has implications for potential applications. Branched solution jets did however lead to nano-scaled electrospun PPTA fibres.

Secondly, it is worth reminding that the electrospinning process in this work could not be operated in a controllable and continuous manner which is once again mainly attributed to the high voltage caused solution jets breakage. Therefore, strictly speaking, the spinning in this work is not electrospinning since continuous spinning is not realized and a large quantity of electrospun *p*-aramid fibre could not be collected.

3.3.3. Mechanical properties of electrospun p-aramid fibres

Conventional *p*-aramid fibre is regarded as one of the most important high performance fibres with high stiffness and tensile strength (Young's modulus > 60 GPa and tensile strength > 2 GPa).

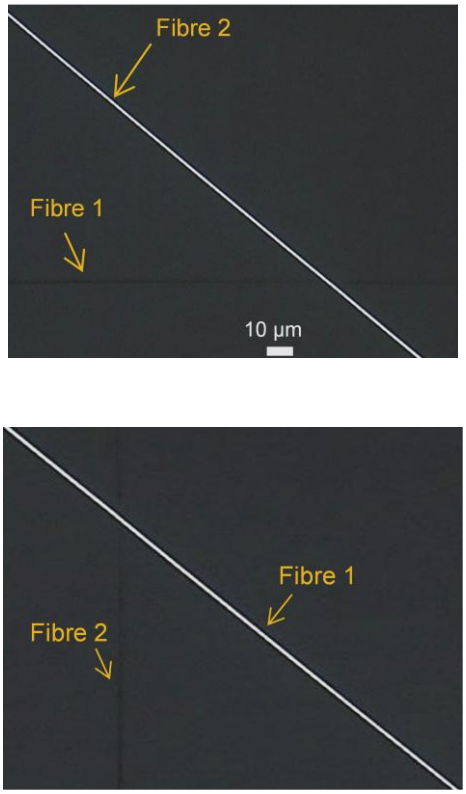

Figure 3.5. *Electrospun p-aramid fibres from 19.46 wt% anisotropic solution under crossed polarizer (a) fibre 1 is positioned parallel with one piece of polarizer whilst fibre 2 is positioned at a 45 °angle with the polarizer (b) after 45 °clockwise rotation of sample stage.*

With respect to the electrospun *p*-aramid fibres reported here, an obvious birefringence can be observed under crossed polarizers as shown in Figure 3.5, which indicates that alignment of liquid crystals in induced in the *p*-aramid fibres during electrospinning. As mentioned above, the electrospinning of PPTA resulted in branched fibre with a wide distribution in fibre diameters. Mechanical properties of a wide range of fibre diameters were evaluated in order to study a possible size effect. Single electrospun *p*-aramid fibres were carefully separated from the coagulated and

dried fibre bundles and glued to the prepared paper frame as shown in Figure 3.1 for tensile testing. Figure 3.6 and Figure 3.7 show that the Young's modulus and tensile strength of tested single fibres increased with decreasing fibre diameter, clearly indicating a significant diameter effect. Size effects on the mechanical properties of electrospun fibres have been studied extensively for flexible chain polymers [21-27]. Many studies showed that decreasing the nanofibre diameter can effectively enhance the Young's modulus of these nanofibres and is often ascribed to confinement of polymer coils forcing them to align to some extent along the fibre axis, hence leading to improvement of molecular orientation and crystallinity [6, 7], as well as orientation of amorphous regions when their sizes are comparable or larger than the nanofibre diameter [28]. Compared to bulk polymers, the Young's moduli of electrospun nanofibres can show a several folds (typically 2-4) increase with decreasing fibre diameters but these improvements are relatively small compared to improvements (typically 10-100) observed in super-drawn high performance polymer fibres [29]. Full chain extension as observed in super-drawn high performance fibres is not achieved in these fibres mainly due to the absence of a subsequent solid-state drawing process in the of as-spun nanofibres based on flexible chain polymers.

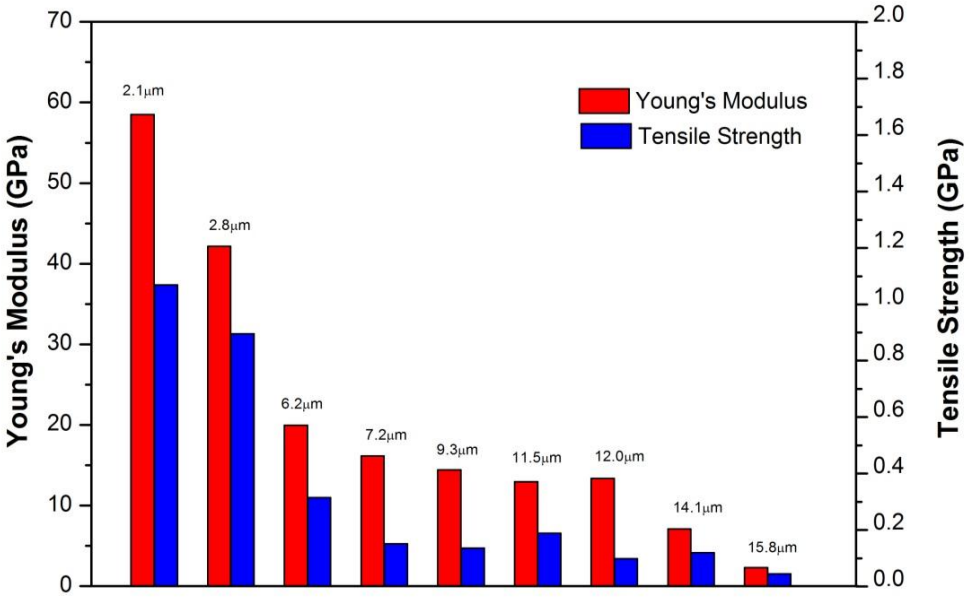

Figure 3.6. *Tensile strength and Young's modulus of electrospun PPTA fibres with varying fibre diameter.*

As discussed in Chapter 2, rigid chain polymers have a significant advantage over flexible chain polymers for the creation of high performance electrospun fibres as these systems can be oriented during the spinning process without the need of a post-drawing process to induce high levels of chain extension as here chain extension is build in by the polymer chemist. In our electrospinning work, *p*-aramid fibres are fabricated from high elongation flows where PPTA molecules are forced to align along the fibre axis. As a result, high levels of chain orientation and extension is achieved in these as-spun fibres without the need of post-drawing. However, it is also expected that thinner fibres would experience higher levels of elongational flow and better molecular orientation, leading to higher mechanical properties. For the PPTA system a 20 fold increase in Young's modulus is seen with decreasing fibre

diameter. This diameter effect is far greater than values typically reported for electrospun nanofibres based on flexible chain polymers (typically 2-4) [2], and highlights the potential of rigid rod polymers to create high performance electrospun fibres.

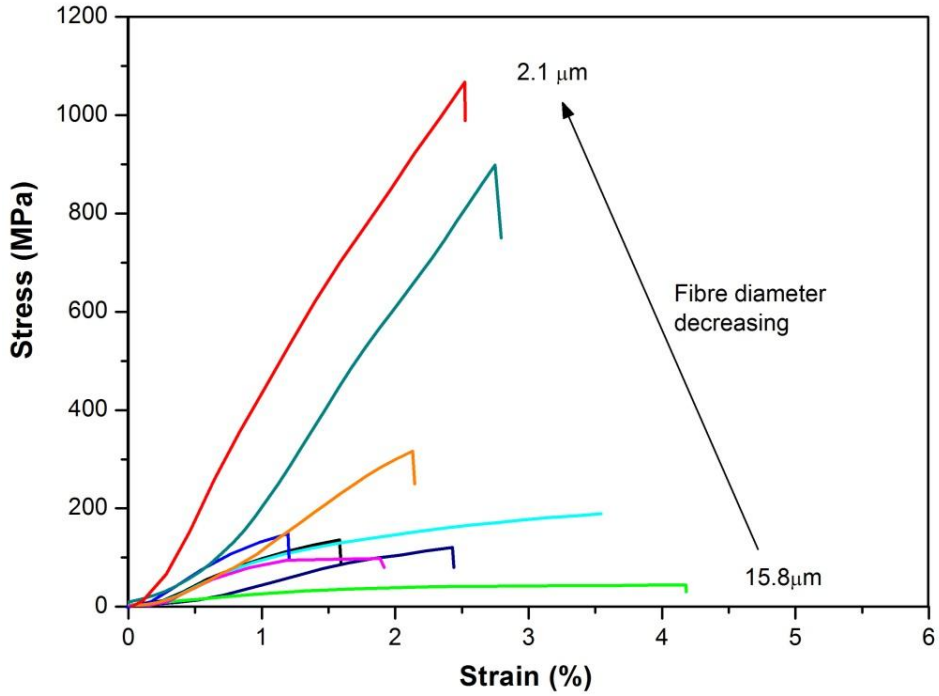

Figure 3.7. *Stress-strain curves of electrospun PPTA fibres with different diameters.*

In comparison to commercial *p*-aramid fibres, the highest Young's modulus value of 59 GPa measured for a fibre with diameter of 2.1 μm is relatively low but is similar or approaches values of Standard Twaron® 1000 or Kevlar® 29 fibres (60-80 GPa [29]). It is also interesting to mention here that nanofibres of several hundred nanometres have been produced based on Teijin's proprietary Teijinconex *m*-aramid, which is a less rigid molecule than *p*-aramid. Although no further data is reported for these *m*-aramid nanofibres, their mechanical properties are expected to be at best

similar to conventional *m*-aramid fibres (modulus < 12 GPa; strength < 600 MPa) and well below those reported in our study. *Meta*-aramid fibres are mainly used for flame-resistant technical textile applications rather than for applications requiring high mechanical properties.

Northold *et al.* developed a detailed mathematic model to describe the relation between the fibre compliance and the chain orientation distribution on the basis of single-phase crystalline model for the microstructure of PPTA fibres [30, 31]

$$S = \frac{1}{e} + A < \sin^2 \vartheta > \tag{3.1}$$

where S is the fibre compliance, e represents the theoretical modulus when the molecular chains are parallel to the fibre axis and $< \sin^2 \vartheta >$ represents the chain orientation distribution with the fibre axis and A is a factor representing the mechanical anisotropy of the crystallite. This equation has been verified experimentally by Northolt based on PPTA fibres and it was shown that the fibre compliance corresponds linearly with the chain orientation distribution [30].

On the basis of Equation 3.1, the Young's modulus of the as-spun fibre is therefore expected to scale as $(1/E) \propto (1 - \cos^2 \vartheta)$ where $\cos^2 \vartheta$ is derived from $< \sin^2 \vartheta >$ as the chains mean orientation after spinning and E is the Young's modulus of fibre which can be ascribed as the reciprocal of the fibre compliance. During spinning the chains within the fibre become more aligned as a consequence of the geometrical diameter reduction. Assuming the spinning material as incompressible, we

geometrically find $\tan\vartheta(r)=(r/R)^{\omega}\tan\vartheta(R)$. Note that for a constant volume under small elastic deformations, which is not the case for large plastic deformations as during spinning, the Poisson's ratio is $\nu=1/2$; while the other limiting case of $\nu=0$ denotes maximal compressibility and, for such a case, we find the same scaling but with the exponent $\omega=1$. For our case we expect an intermediate value of $1\le\omega\le 2$.

The Young's modulus therefore should scale as:

$$\frac{1}{E}=\frac{1}{e}+A<1-\cos^2\vartheta>=\frac{1}{e}+A(1-\frac{1}{1+\tan^2\vartheta(R)(\frac{r}{R})^{2w}}) \qquad (3.2)$$

where e is considered to be 160 GPa which is the theoretical modulus of PPTA as listed in Chapter 2.

If three sets of data (r = 2.1 μm, E = 58 GPa; R = 2.8 μm, E = 42 GPa; r = 6.2 μm, E = 20 GPa) were fitted in the equation (3.3), the values of *A, w and* $\tan\theta$ could be found as 0.055, 0.126 and 0.718, respectively.

Then one set of data (R = 2.8 μm, E = 42 GPa) was selected to fit in the Equation (3.2), it will be written as:

$$\frac{1}{E}=\frac{1}{156}+0.055(1-\frac{1}{1+0.72^2(\frac{r}{2.8})^{2.526}}) \qquad (3.3)$$

An 'S' shape curve is predicted as shown in Figure 3.8 based on Equation (3.3). Most of the experimental data are clearly well fitted by the model with little derivation. More importantly, although fibres with diameter less than 2 μm are difficult to test due to their short lengths (< 3 mm), the Young's modulus of these fibres can now be estimated from the curve with an ultimate stiffness of 160 GPa when all PPTA molecules are perfectly aligned ($\tan\theta = 0$). For example, in our branched electrospun fibres, PPTA filaments with diameters as low as 250 nm were observed but could not be tested. However, based on the above geometrical model such fibres are expected to have Young's moduli of around 150 GPa, approaching the theoretical modulus of PPTA, and exceeding moduli of commercial High Modulus Twaron® or Kevlar® 49 fibres (125 GPa).

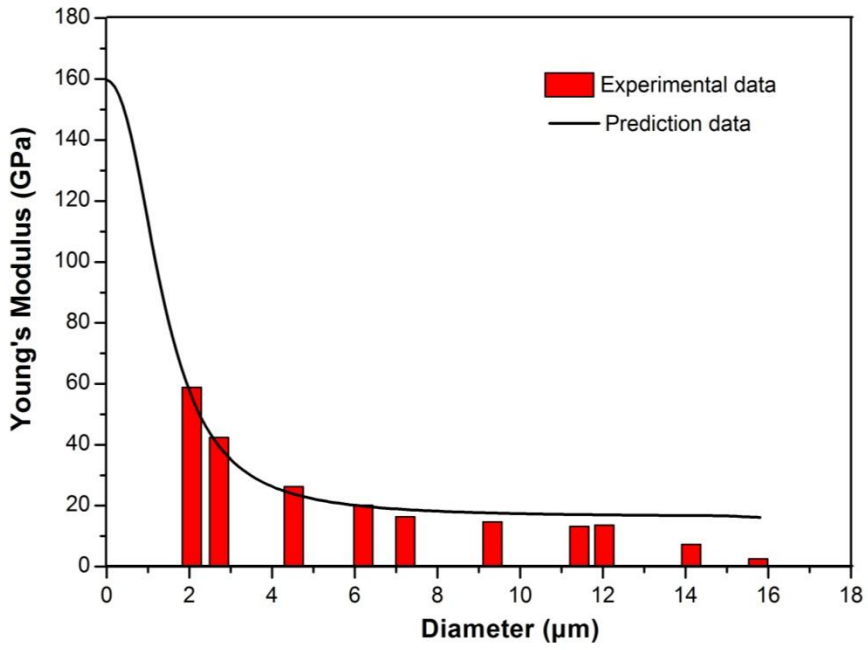

Figure 3.8. *Experimental Young's modulus of electrospun PPTA fibres and prediction data based on Equation (3.2).*

An obvious shortcoming of the electrospun fibres reported in this work is their relatively low tensile strengths compared to conventional *p*-aramid fibres. The maximum tensile strength achieved is about 1.1 GPa, which is only half that of conventional *p*-aramid fibres. Given the fact that tensile strength of fibres is sensitive to defects, any possible flaw (Figure 3.9) induced from the electrospinning process, coagulation, or handling of the fibres causing kinking can be detrimental to the final tensile strengths. Because of this it is not surprising that strengths of fibres produced under non-optimal conditions as in this work are well below those of fibres spun under fully optimized commercial spinning conditions.

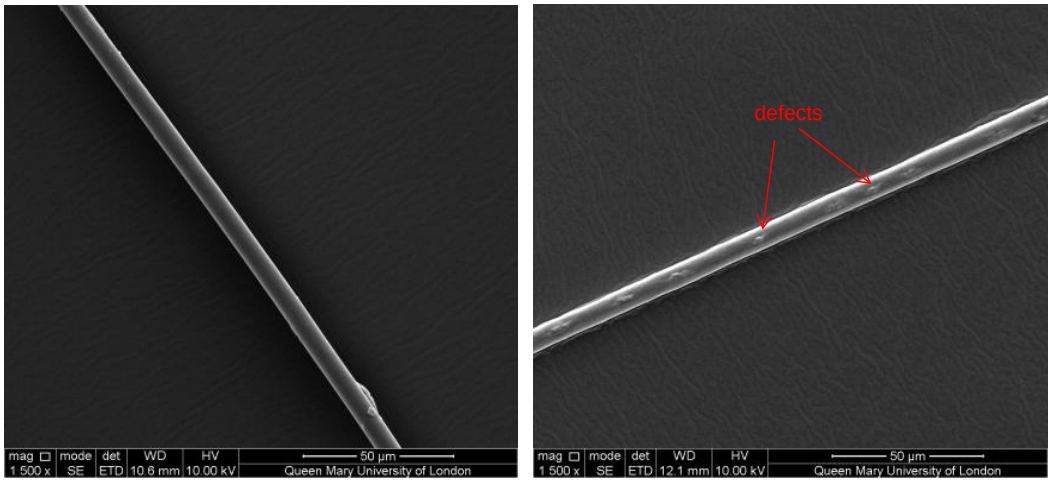

Figure 3.9. *Comparison of a smooth PPTA fibre (left) and a PPTA fibre with defects (right).*

Despite the relatively low tensile strengths and difficult spinning conditions compared to conventional *p*-aramid fibre, this work for the first time reported high performance electrospun *p*-aramid fibres from anisotropic solutions.

3.4. Conclusions

In this chapter, the electro-spinnability of isotropic PPTA solutions and anisotropic PPTA solutions has been evaluated. Fibres could be fabricated from all anisotropic solutions by adjusting spinning parameters but only droplets and short fibres were obtained from isotropic solutions. Spinning of the anisotropic PPTA solutions gave numerous secondary solution jets and fibre branching and resulted in a broad diameter distribution in as-spun fibres. The smallest diameter fibres in these branched PPTA fibres showed significantly higher mechanical properties with peak values of tensile strength and Young's modulus of 1.1 GPa and 59 GPa for fibres with a diameter of 2.1 μm. A geometrical model based on a reduction for the size-dependent Young's modulus was developed to predict the properties of fibres.

It is however worth reminding that the electrospinning process in this research work could not be operated in a well controllable and continuous manner due to the fibre branching attributed to the high voltage applied. Moreover, only small quantities of electrospun *p*-aramid fibre could be collected. However, the work did report for the first time report the use of anisotropic solutions for the electrospinning of PPTA fibres, while at the same time showing the potential of achieving high levels of property improvement in electrospun fibres using rigid rod polymers. The maximum properties achieved in this work are among the highest reported for electrospun fibres [2] and approach those of commercial *p*-aramid fibres.

3.5. References

1. Staudinger, H. Die Hochmolekularen im festen Zustand. In *Die Hochmolekularen Organischen Verbindungen-Kautschuk und Cellulose*; Springer Berlin Heidelberg: 1932; pp. 105-123.

2. Yao, J.; Bastiaansen, C.W.; Peijs, T. High strength and high modulus electrospun nanofibers. *Fibers* **2014**, *2*, 158-186.

3. Greiner, A.; Wendorff, J.H. Electrospinning: a fascinating method for the preparation of ultrathin fibers. *Angewandte Chemie International Edition* **2007**, *46*, 5670-5703.

4. Greiner, A.; Wendorff, J. Functional self-assembled nanofibers by electrospinning. In *Self-Assembled Nanomaterials I*; Springer Berlin Heidelberg: Berlin, Germany, 2008; pp. 107-171.

5. Huang, C.; Chen, S.; Reneker, D.H.; Lai, C.; Hou, H. High-strength mats from electrospun poly(*p*-phenylene biphenyltetracarboximide) nanofibers. *Advanced Materials* **2006**, *18*, 668-671.

6. Zong, X.; Ran, S.; Fang, D.; Hsiao, B.S.; Chu, B. Control of structure, morphology and property in electrospun poly (glycolide-co-lactide) non-woven membranes via post-draw treatments. *Polymer* **2003**, *44*, 4959-4967.

7. Wu, S.Z.; Yang, X.P.; Zhang, F.; Hou, X.X. Stretching-induced orientation for improving the mechanical properties of electrospun polyacrylonitrile nanofiber sheet. *Advanced Materials Research* **2008**, *47*, 1169-1172.

8. Yang, H. *Kevlar Aramid Fiber*; John Wiley & Sons: Chichester, NH, USA: 1993; pp. 1-22.

9. Kwolek, S.; Morgan, P.; Schaefgen, J.; Gulrich, L. Synthesis, anisotropic solutions, and fibers of poly (1, 4-benzamide). *Macromolecules* **1977**, *10*, 1390-1396.

10. Morgan, P.W.; Kwolek, S.L.; Pletcher, T.C. Aromatic azomethine polymers and fibers. *Macromolecules* **1987**, *20*, 729-739.

11. Dobb, M.; Johnson, D.; Saville, B. Supramolecular structure of a high-modulus polyaromatic fiber (Kevlar 49). *Journal of Polymer Science: Polymer Physics Edition* **1977**, *15*, 2201-2211.

12. Bair, T.; Morgan, P.; Killian, F. Poly (1, 4-phenyleneterephthalamides). polymerization and novel liquid-crystalline solutions. *Macromolecules* **1977**, *10*, 1396-1400.

13. Srinivasan, G.; Reneker, D.H. Structure and morphology of small diameter electrospun aramid fibers. *Polymer International* **1995**, *36*, 195-201.

14. Lepore, E.; Marchioro, A.; Isaia, M.; Buehler, M.J.; Pugno, N.M. Evidence of the Most Stretchable Egg Sac Silk Stalk, of the European Spider of the Year Meta menardi. *PloS one* **2012**, *7*, e30500.

15. Lewin, M. *Handbook of Fiber Chemistry, 3rd ed.*; Taylor & Francis Group: Boca Raton, FL, USA: 2006; pp. 812-958.

16. Hearle, J.W. *High-Performance Fibres*; Woodhead Publishing: Cambridge, England: 2001; Vol. 15, pp. 93-155.

17. Ramakrishna, S. *An Introduction to Electrospinning and Nanofibers*; World Scientific Publishing Co. Pte. Ltd: Singapore: 2005; pp. 90-154.

18. Darling, H.E. Conductivity of Sulfuric Acid Solutions. *Journal of Chemical & Engineering Data* **1964**, *9*, 421-426.

19. Bolz, R.E. *CRC Handbook of Tables for Applied Engineering Science*; Chemistry Rubber Company: Boca Raton, FL: 1973; pp. 93-94.

20. Wendorff, J.H.; Agarwal, S.; Greiner, A. *Electrospinning: Materials, Processing, and Applications*; Wiley-VCH: Weinheim, Germany: 2012; pp. 69-104.

21. Tan, E.; Lim, C. Physical properties of a single polymeric nanofiber. *Applied Physics Letters* **2004**, *84*, 1603-1605.

22. Lim, C.; Tan, E.; Ng, S. Effects of crystalline morphology on the tensile properties of electrospun polymer nanofibers. *Applied Physics Letters* **2008**, *92*, 141908-141908-3.

23. Bashur, C.A.; Dahlgren, L.A.; Goldstein, A.S. Effect of fiber diameter and orientation on fibroblast morphology and proliferation on electrospun poly (D, L-lactic-co-glycolic acid) meshes. *Biomaterials* **2006**, *27*, 5681-5688.

24. Pai, C.-L.; Boyce, M.C.; Rutledge, G.C. Mechanical properties of individual electrospun PA 6(3)T fibers and their variation with fiber diameter. *Polymer* **2011**, *52*, 2295-2301.

25. Chew, S.Y.; Hufnagel, T.C.; Lim, C.T.; Leong, K.W. Mechanical properties of single electrospun drug-encapsulated nanofibres. *Nanotechnology* **2006**, *17*, 3880.

26. Shin, M.K.; Kim, S.I.; Kim, S.J.; Kim, S.-K.; Lee, H.; Spinks, G.M. Size-dependent elastic modulus of single electroactive polymer nanofibers. *Applied Physics Letters* **2006**, *89*, 231923-231929.

27. Fennessey, S.F.; Farris, R.J. Fabrication of aligned and molecularly oriented electrospun polyacrylonitrile nanofibers and the mechanical behavior of their twisted yarns. *Polymer* **2004**, *45*, 4217-4225.

28. Arinstein, A.; Burman, M.; Gendelman, O.; Zussman, E. Effect of supramolecular structure on polymer nanofibre elasticity. *Nature Nanotechnology* **2007**, *2*, 59-62.

29. Ajji, A.; Coates, P.; Dumoulin, M.; Ward, I. *Solid Phase Processing of Polymers*; Carl Hanser Verlag: Munich, Germany: 2000; pp. 85-210.

30. Northold M.G.; Tensile deformantion of poly(*p*-phenylene terephthalamide) fibres, an esperimental and theoretical analysis. *Polymer* **1980**, 21, 1199-1204.

31. Northold M.G. and Aartsen J.J.; Chain orientation distribution and elastic properties of poly(p-phenylene terephthalamide), a "rigid rod" polymer. *Journal of Polymer Science: Polymer Symposia* **1977**, 58, 283-296.

Chapter 4

Electrospinning of Reactive Mesogens

4.1 Introduction

Reactive mesogens (RMs) are liquid crystalline monomers with polymerizable end groups which tend to orient parallel to each other in their liquid crystalline phases. UV-light exposure induced photo-polymerization of reactive mesogens with two or more end groups can be used to chemically fixate the ordered liquid crystalline structure leading to highly oriented polymer networks [1, 2].

Aligned RMs giving polarized emissions have been explored for potential applications in amongst others full-colour organic light-emitting diodes (OLEDs) [3]. One example was a pixelated liquid crystal OLED which emitted red, green and blue light by the use of three different light-emitting RMs which was fabricated by Aldred *et al.* [4]. Besides, RMs can be used in organic field effect transistors (OFETs) [5],

viewing-angle compensation films for LCDs [6], fluidic applications as liquid crystal polymer spheres [7], *etc*.

However, reactive mesogens haven't been used in fibre application. As discussed in Chapter 3, electrospinning has the potential to induce molecular alignment in systems based on rigid rod polymers such as PPTA, potentially leading to high performance *p*-aramid fibres. However, continuous spinning was not realized as a result of the necessary high voltage causing fibre breakage and branching with nano-scale fibres being relatively short (< 3 mm). A potential alternative approach to produce high performance fibres through electrospinning is the use of reactive liquid crystal monomers as the high molecular orientation induced during spinning can be fixated in the fibre after photo-polymerization.

Because of the rheological properties of RMs, it is impossible to directly electrospin the liquid crystal monomers into fibres as the absence of viscoelasticity in these liquids would lead to electrospraying rather than electrospinning.

In order to create spinnable systems, in this chapter, the electrospinning of liquid crystal monomers respectively blended with PMMA and PA6 at different ratios is presented. Their corresponding nanofibre morphologies, thermal properties and mechanical properties were evaluated and discussed. This work potentially provides a new concept towards designed nanofibres with oriented morphologies, and could lead to high strength and high modulus electrospun nanofibres. It needs to be pointed out that this study mainly focuses on the investigation of the electrospinning of

RM/polymer composite nanofibres, their mechanical properties and the reinforcing efficiency of RM257 in composite nanofibres.

4.2 Experimental

4.2.1 Materials and solution preparation

7 wt% of poly(methyl methacrylate) (M_w = 996,000g/mol, Sigma-Aldrich) in solvent mixture of DMF (Anhydrous, 99.8%, Sigma-Aldrich) and chloroform (Anhydrous, 99%, Sigma-Aldrich) with a ratio of 7/3 (w/w) was prepared by overnight stirring at 60 ℃. Reactive diacrylate liquid crystal monomer RM257 (Merck) was blended with PMMA in different weight contents (20%, 33%, 50%, 66%) in the same solvent mixture as above to prepare spinning solutions. In addition, two solutions for spin-coating were prepared using PMMA/RM257 blends and PMMA/RM82 (Merck) blends. In both cases, the PMMA concentration is 1 wt% and the weight ratio of PMMA to liquid crystal monomer is 1/1.

14 wt% of polyamide 6 (PA6 or Nylon 6, Ultramid B33L, BASF) in formic acid (puriss. ≥ 98%, Sigma-Aldrich) and acetic acid (puriss. ≥ 99.7%, Sigma-Aldrich) mixture with a weight ratio of 1/1 was prepared by stirring at 70 ℃ for 3 hrs. Similar to the PMMA/RM257 blends, a variety of RM257 contents (20%, 33%, 50%, and 66%).were also blended to PA6.

Furthermore, 40 wt% of RM257 and RM82 in 1,2-Dichloroethane (Sigma-Aldrich) were also prepared to make aligned neat RM films by spin-coating the solutions on rubbed PI film substrates [8].

In all solutions, photo-initiator Irgacure184 (1-Hydroxy-cyclohexyl-phenyl-ketone, Ciba) was added at a 1/50 ratio (w/w) to RMs.

4.2.2 Spin-coating, electrospinning and UV-induced photo-polymerization

In the spin-coating process, 20 mm × 20 mm square glass-slides were used as substrates and all samples were prepared at a speed of 1000 rpm/min for 30 sec.

A flow rate of 0.5 ml/h, distance of about 20 cm, and voltage of around 20 kV was applied for the electrospinning of the PMMA solutions and PMMA/RM257 solutions. Similar flow rates and distances but slightly lower voltage levels of about 18 kV were used for the electrospinning of PA6 solutions and PA6/RM257 solutions.

RMs or polymer/RM blends are capable of undergoing photo-initiated radical reaction under UV-light exposure (Omnicure S2000®, Lumen Dynamics) with the obtained fibres being subsequently heated to 90 ℃ at which the liquid crystal monomers are in their nematic phase as shown in Figure 4.1. The exposure time was 20 min and the UV-light dosage is 1.5 J cm^{-2} at a distance of 20 cm. The sample cell was purged with nitrogen gas during the whole process to inhibit oxygen induced oxidization.

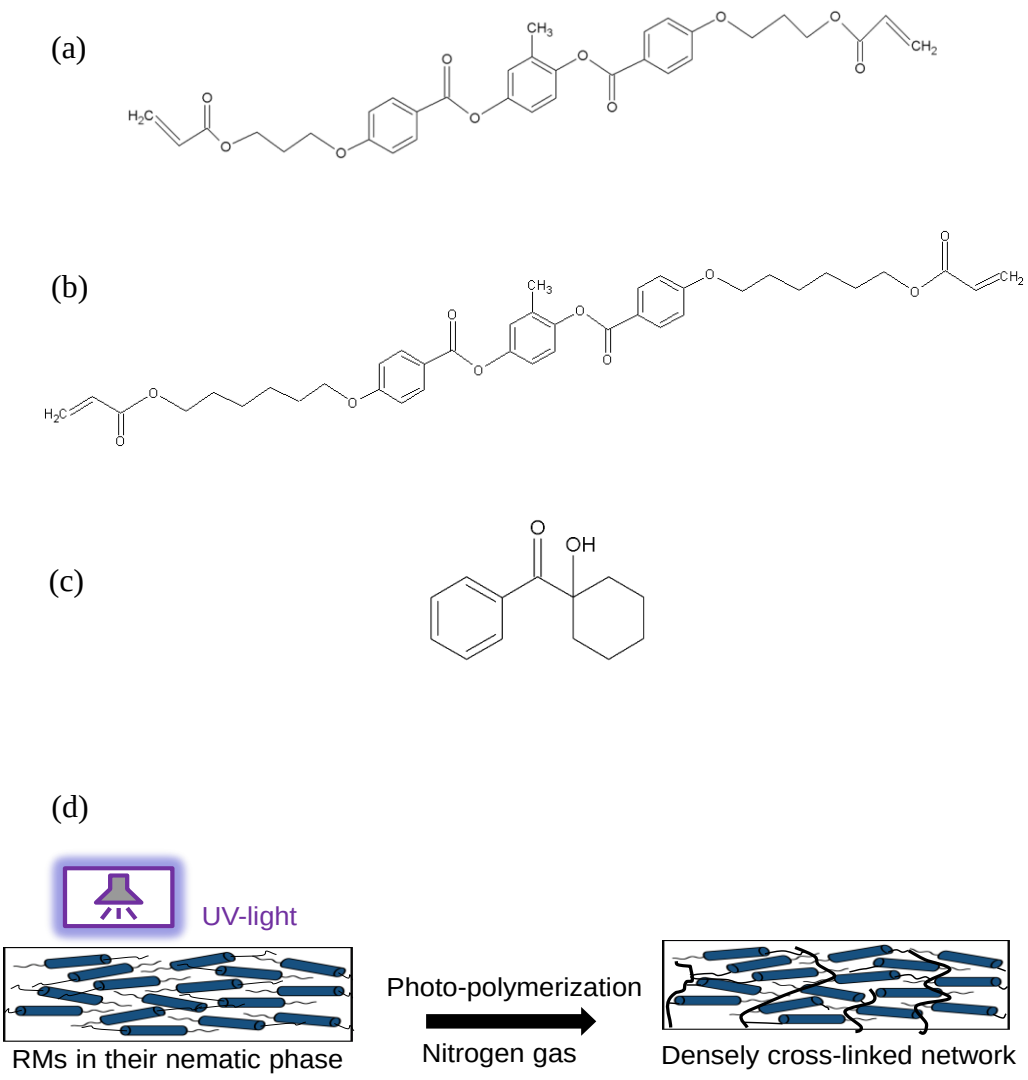

Figure 4.1. *Chemical structure of (a) RM257 (b) RM82 and (c) Irgacure184 along with (d) UV-light exposure induced photo-polymerization of RMs in their nematic phase forming an anisotropic structure.*

4.2.3 Characterization

The surface morphology of nanofibre samples was characterized using SEM (Jeol JSM-6300F) after Au coating. An optical microscope (OM) incorporated with a high resolution digital camera was used to check the morphology of spin-coated films and

a polarized optical microscope (POM) was used to characterize the birefringence of electrospun fibres.

Phase-transition temperatures of the nanofibres were determined using differential scanning calorimetry (DSC) (Q-1000, TA Instruments). Approximately 5-10 mg samples were sealed into aluminum DSC pans and measurements were carried out in the temperature range of 25 ℃ to 140 ℃ at a heating and cooling rate of 5 ℃/min.

All electrospun nanofibre samples and UV-cured RM257 and RM82 neat films were cut into rectangular strips along the alignment direction with a length of 40 mm and width of 5 mm for mechanical tests using an Instron 5566 universal testing machine with a load cell of 100 N. It should be noted that all nanofibre samples were directly clamped between two flat clamps whilst the pure liquid crystal films were first glued on a paper frame as ascribed in Chapter 3 and then kept in place between two flat clamps to avoid any clamping induced damage to the brittle films. The testing speed was 2 mm/min for all samples.

4.3 Result and Discussion

4.3.1 Spinning-coating, electrospinning and characterization of PMMA with RM257

Thin films were prepared from the PMMA/RM257 and PMMA/RM82 solutions using a high speed spinning coater, respectively. As shown in Figure 4.2, compared to the PMMA/RM82 spin-coating film, the PMMA/RM257 film has a much finer

morphology with polymer dispersed in the liquid crystals, indicating less phase separation of PMMA with RM257.

This phenomenon is confirmed by Figure 4.3, where the UV-cured electrospun PMMA/RM82 fibres show discontinuous birefringences whilst the UV-cured electrospun PMMA/RM257 fibres exhibit homogenous birefringences under crossed polarizers. Phase separation of polymer carrier with RM is vital for electrospinning as it can result in RM agglomeration and fibres with inhomogeneous RM dispersions could be found. This will be detrimental to the mechanical properties of such blend nanofibres as continuous and ordered liquid crystal networks after UV-curing are difficult to achieve. Similar phenomenon were observed in the case of PA6/RM82 but pictures are not shown.

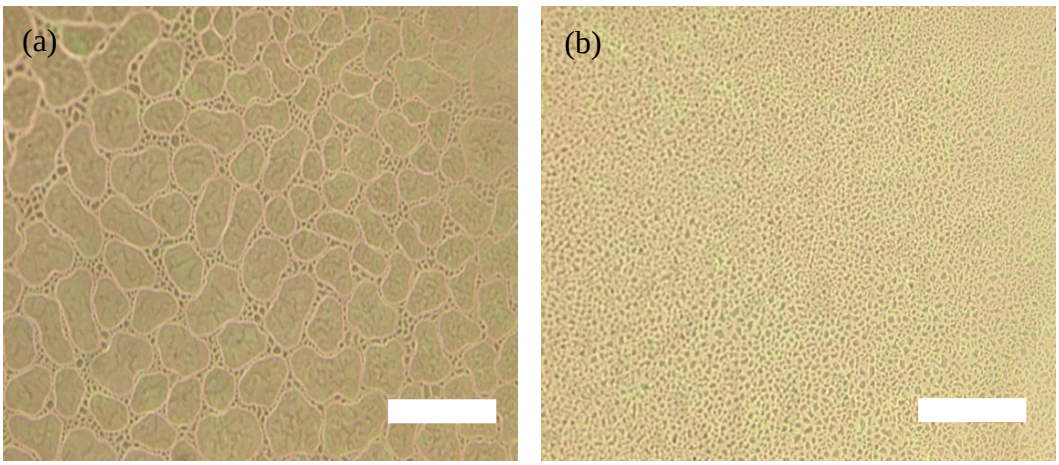

Figure 4.2. *Optical microscopy pictures of spin-coated films (scale bar 50 μm) of (a) PMMA/RM82 and (b) PMMA/RM257.*

In addition, neat RM films with preferred orientations were also fabricated. Pure RM257 film after photo-polymerization displayed better mechanical properties in

comparison with polymerized RM82 film as revealed by the stress-strain curves in Figure 4.4. Young's modulus of about 7.5 GPa and tensile strength up to 133 MPa were found (Table 4.1). As a result, only nanofibres electrospun from polymer and RM257 blends were investigated in this work.

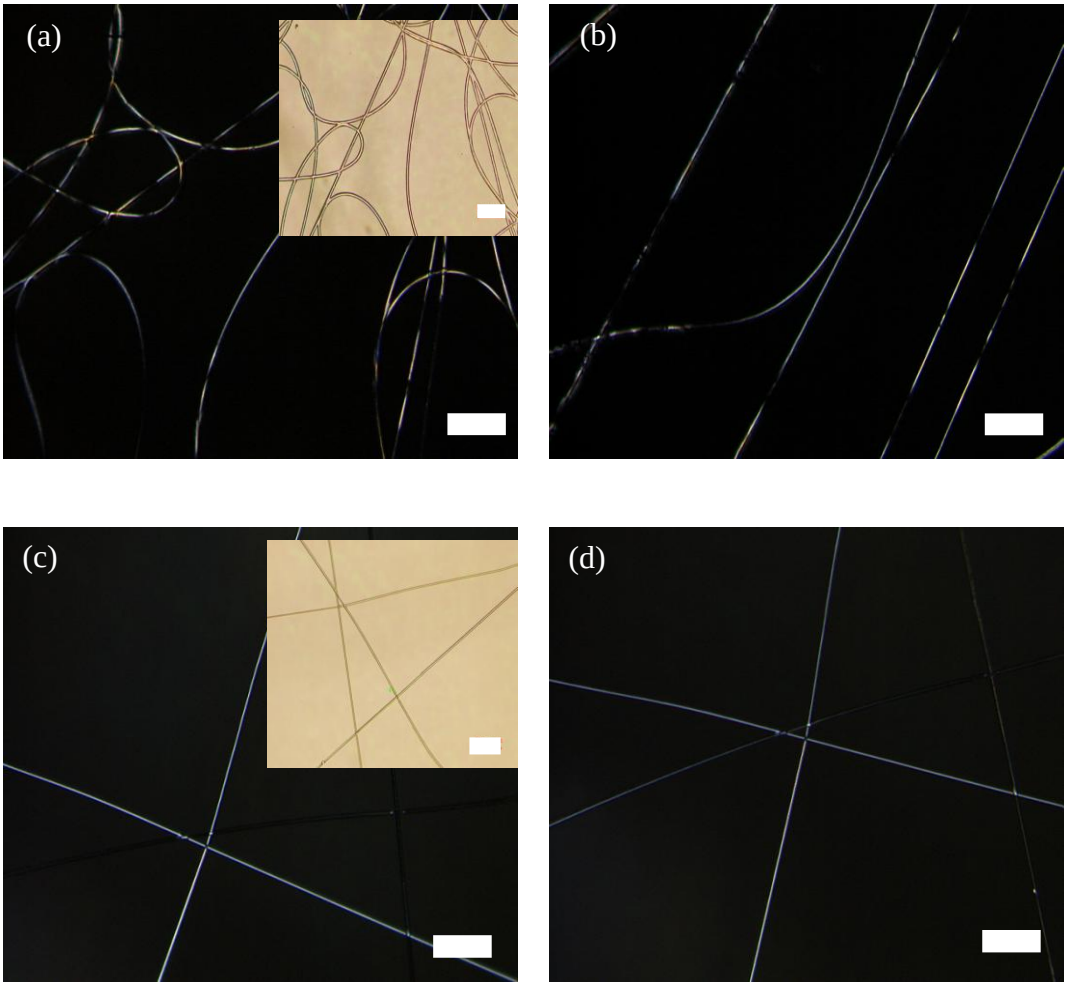

Figure 4.3. *Polarized optical micrographs of electrospun PMMA/RM82 (1/1, weight ratio) fibres (scale bar 50 µm); (a) at 45° angle with crossed polarizers (corresponding optical micrograph, inset); (b) at 135° angle with crossed polarizers and electrospun PMMA/RM257 (1:1, weight ratio) fibres; (c) at 45° angle with*

crossed polarizers (corresponding optical micrograph, inset); (d) at 135 °angle with crossed polarizers.

Electrospinning of PMMA/RM257 blends with different compositions were carried out. Before photo-polymerization, smooth and homogenous nanofibres obtained are shown in the left-hand side of Figure 4.5. All nanofibres exhibited diameters ranging from 220 nm to 450 nm with average diameters at around 350 nm.

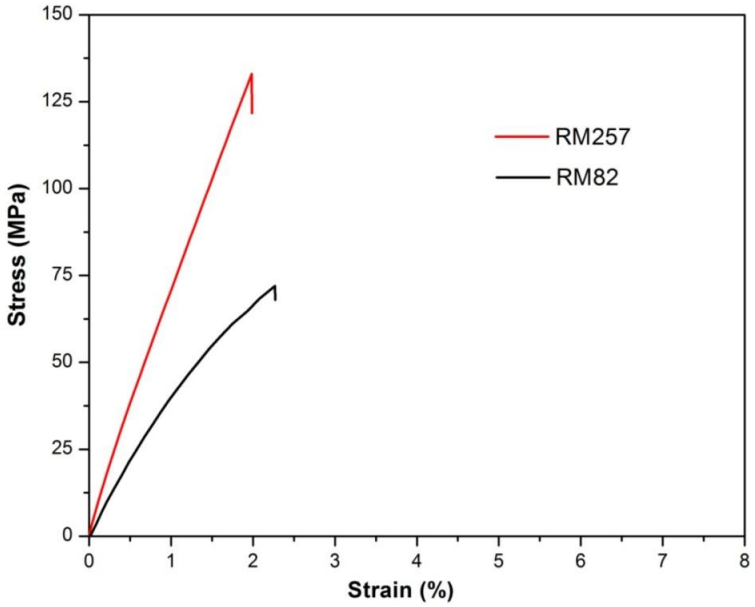

Figure 4.4. *The stress-strain curves of neat RM257 and RM82 films after UV-light exposure induced photo-polymerization.*

The phase transition of RMs in polymer blends and the glass transition temperature (T_g) of PMMA in these blends were investigated using DSC. DSC traces of 0, 20, 33, 50, 66 wt% of RM257 in PMMA and pure RM257 were shown in Figure 4.6. The glass transition temperature of PMMA decreased with increasing RM257 content (Figure 4.7). This depression in T_g was attributed to size of the monomer as

well as the interaction between the monomer and the polymer [9]. The monomer size can be considered constant as only RM257 was used here. Hence, the depression of T_g can be mainly ascribed to the weak interactions between polymer and monomer [10]. This is supported by the fact that a phase transition temperature of RM257 was not detected until a monomer content of 66 wt%.

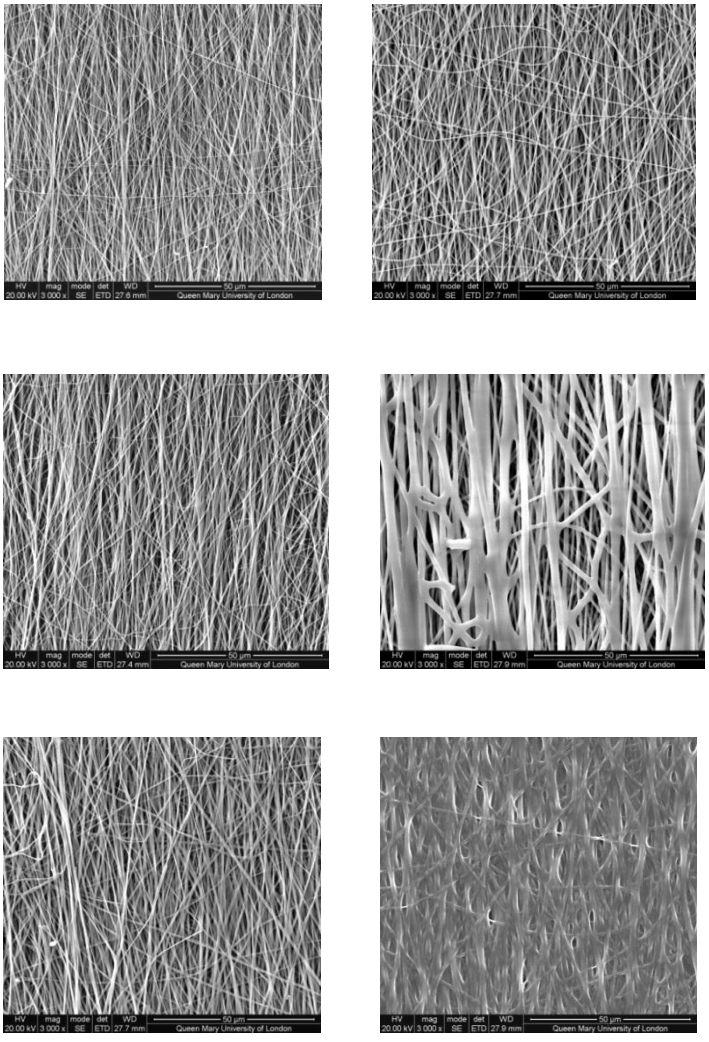

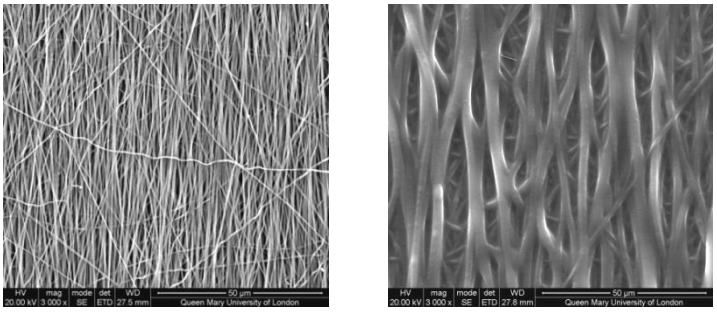

Figure 4.5. *Electrospun PMMA/RM257 nanofibre with RM257 content of 20, 33, 50, 66 wt% (from top to bottom) before and after UV-curing (from left to right).*

The depression of T_g is profound when the monomer content was increased from 0 wt% to 20 wt% as a steep depression in T_g was found. A mild depression was found which is not surprising as increasing monomer content will not enhance the interaction with PMMA. However, when the RM257 content increased to 66 wt%, the crystalline to nematic phase transition of RM257 started to appear and the T_g of PMMA increased to 105 ℃, suggesting phase separation of RM257 and PMMA.

PMMA/RM257 blend nanofibres of various compositions were transported to a sample cell which was kept at 85 ℃ for UV-light exposure to induce photo-polymerization. Here, ordered RM257 molecules in their nematic phase should be fixed into a densely cross-linked network. The SEM graphs of PMMA/RM257 after UV-curing were shown in the right-hand side of Figure 4.5. The morphologies of nanofibre with 20 wt% of RM257 were found to be similar before and after UV-curing. Fibre fusion was found in the nanofibres with 66 wt% of RM257 after photo-polymerization, which is consistent with the phase separation indicated in the DSC trace above.

However, slight fibre fusion and severe fusion were found in nanofibres with RM257 contents of 33 wt% and 50 wt%, respectively. Here nanofibre fusion is attributed to the flowing of RM257 during UV irradiation in their nematic phase but results are not yet fully understood as the phase separation causing RM257 flow is contradictory with the DSC traces of PMMA/RM257 as here phase separation between PMMA and RM257was not detected at these two concentrations.

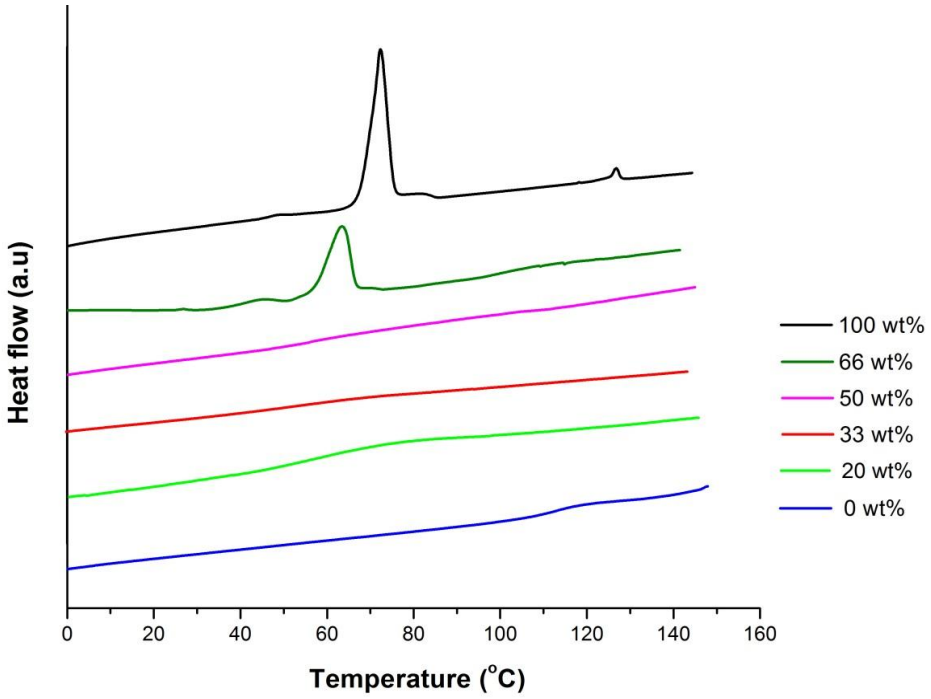

Figure 4.6. *DSC curves of 0, 20, 33, 50, and 66 wt% RM257 in PMMA nanofibre samples along with DSC curves of pure RM257 film (100 wt%).*

Moreover, the UV-cured PMMA/RM257 nanofibre samples were too brittle for tensile testing. Samples easily broke during handling or clamping, thus no reliable and repeatable data were found.

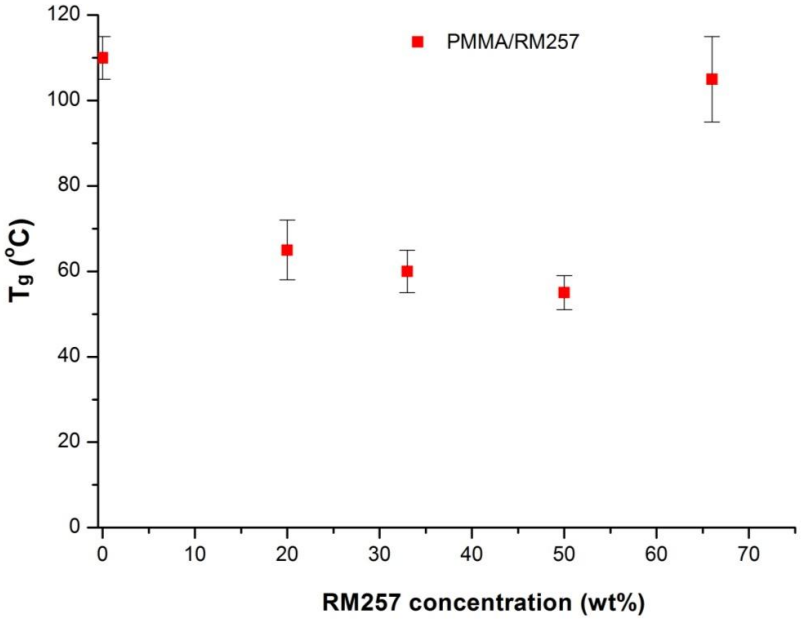

Figure 4.7. *DSC traces of PMMA/RM257, showing the shifting of T_g for PMMA with the increasing content of RM257.*

4.3.2 Electrospinning and characterization of PA6 with RM257

Electrospinning of different weight ratios of PA6/RM257 solutions were also performed. A high speed rotating disc with a velocity of about 2800 rpm was used to collect aligned nanofibres. Smooth and homogenous nanofibres with a preferred diameter distribution around 400 nm were obtained from the solutions containing 20 wt% and 33 wt% RM257 as shown from the top two SEM graphs in the left-hand side of Figure 4.8. It is worth mentioning that RM257 has poor solubility in formic acid and acetic acid mixtures although they are good solvents for PA6. When the content of RM257 increased to 50 wt%, poor solubility of RM257 in formic acid and acetic acid mixtures caused inhomogeneous spinning solutions and potentially leads to nanofibre fusion after electrospinning.

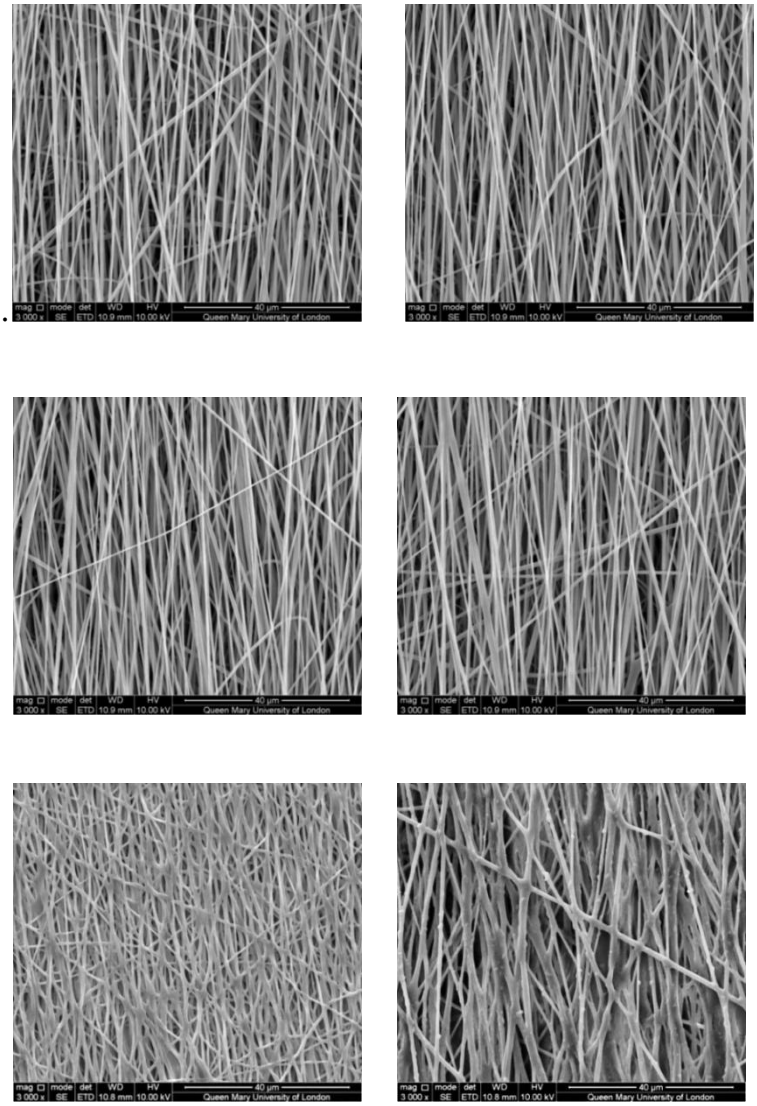

Figure 4.8. *Electrospun PA6/RM257 nanofibre with 20, 33 and 50 w% RM257 in PA6 (from top to bottom) before and after UV-curing (from left to right).*

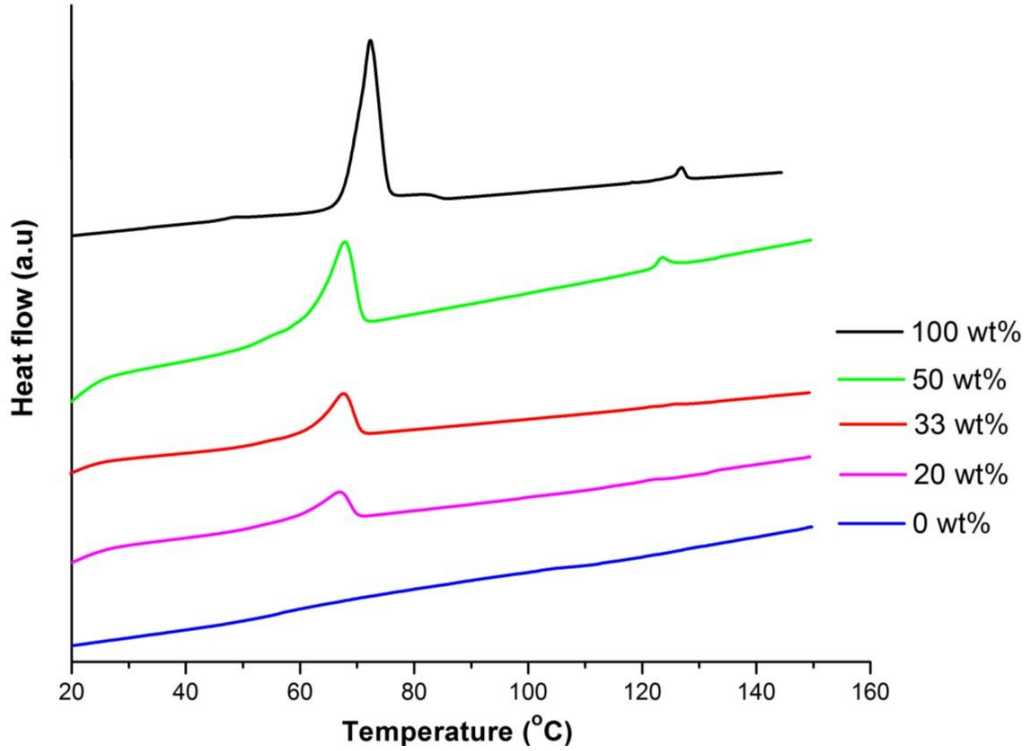

Figure 4.9. *DSC curves of 0, 20, 33 and 50 wt% RM257 in PA6 nanofibre samples along with DSC curves of pure RM257 film (100 wt%).*

The glass transition temperature of PA6 in the blends was also investigated using DSC. DSC traces of 0, 20, 33, 50 and 100 wt% of RM257 in PA6 are shown in Figure 4.9. A T_g shift with increasing RM257 content as shown for the PMMA blends (see Figure 4.6) was not observed for the PA6/RM257 blends. One possible explanation for this apparent absence is that the endothermic step which appears at the glass transition temperature is hidden behind the broad peak of the crystalline to liquid crystalline phase transition for RM257 in blends as the T_g of PA6 (55 ℃) is within the temperature range of this phase transition (50 ℃--72 ℃). Hence, phase separation could exist in all PA6/RM257 blend nanofibres although this is hardly observed in the micrographs after UV curing at low RM257 content (20 wt% and 33

wt%) but more profound at the higher concentration of 50 wt%. Figure 4.8 also indicated that liquid crystals are present on the surface of the nanofibres as the fibre fusion observed after curing could be due to a combination of RM flow during UV-curing and/or inhomogeneous solutions causing fibre fusion during electrospinning.

Table 4.1. *Mechanical properties of pure RM films and PA6/RM257aligned composite nanofibres along with effective RM257 contributions to the modulus of composite nanofibres.*

Materials	**Young's modulus (GPa)**	**Tensile strength(MPa)**	**Effective modulus contribution of RM257 (GPa)**
RM82	7.5	134	-
RM257	3.8	74	-
PA6 nanofibres	1.15	101	-
20 wt% RM257 in PA6	1.7	97	3.9
33 wt% RM257 in PA6	2.8	121	6.1
50 wt% RM257 in PA6	1.9	58	2.6

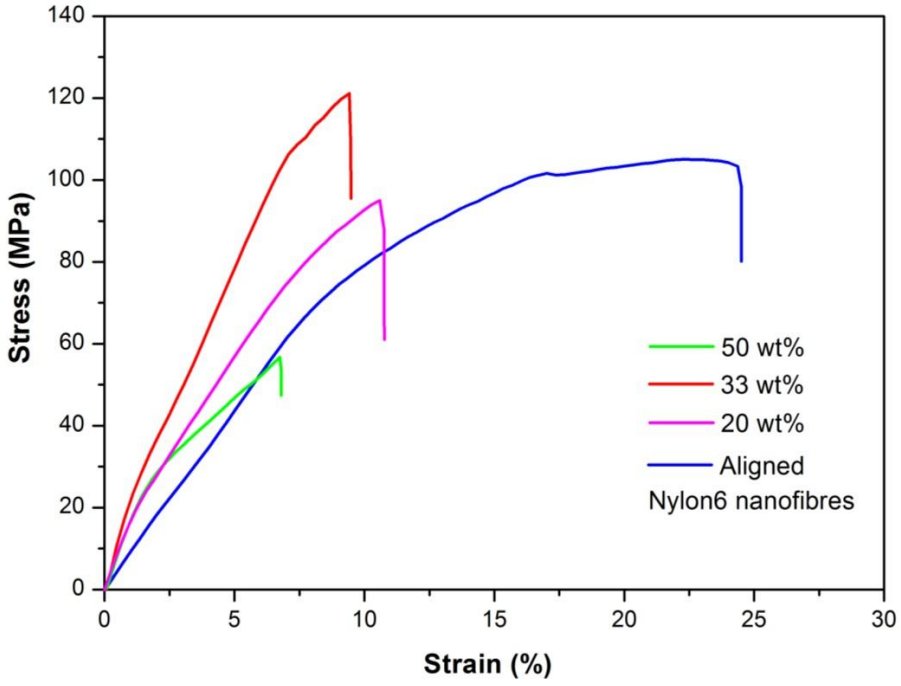

Figure 4.10. *The stress-strain curves of aligned PA6 electrospun nanofibre mat and PA6/RM257 blend nanofibre mats with different RM257 content.*

The mechanical properties of aligned PA6/RM257 nanofibres mats with different RM257 content after UV-curing were evaluated. Stress-strain curves are shown in Figure 4.10 and their Young's moduli and tensile strengths are listed in Table 4.1. Aligned nanofibre mats with 33 wt% of RM257 content exhibit the highest Young's modulus and tensile strength. Since these blend fibres can be considered as composite fibres with RM257 as reinforcement and PA6 as a matrix, a simple back-calculation to derive the effective RM257 contribution [11] to the Young's modulus of those composite nanofibres was made in Table 4.1 using the 'Rule of Mixture':

$$E_c = E_r V_r + E_m (1-V_r)$$

where E_c, E_m, and E_r are the Young's modulus of the composite, matrix and the

reinforcement, respectively, and V_r is the volume fraction of the RM257. The effective modulus contribution of RM257 to the composite nanofibre was found to increase from 3.9 GPa (20 wt% of RM257) to 6.1 GPa (50 wt% of RM257) and then decrease sharply to 2.6 GPa at higher loadings (66 wt% of RM257). The results indicate that an RM257 network after UV-curing can effectively enhance the nanofibre stiffness at low concentrations but that the effective contribution of RM257 to the modulus of the composite nanofibres decreases significantly at high concentrations due to phase separation, which is in agreement with morphological and thermal analysis. Furthermore, it should be noted that the strength contribution of RM257 was not investigated in this chapter as the tensile strengths of RM257, PA6 and the composite nanofibres (20 wt% and 33 wt% of RM257) are all of a similar level. With respect to the composite nanofibre with 50 wt% of RM257, a tensile strength as low as 58 MPa was found which is hardly surprising because the excessive flow of the RM257 during UV-curing can significantly reduce their orientation induced during the electrospinning process.

4.4 Conclusions

In this chapter, the reactive mesogens RM257 rather than RM82 were selected to be blended with polymers in order to create an electrospinnable system. RM257 was selected and electrospun into nanofibres due to two reasons; (1) Significant phase separation occurred in the electrospun RM82/PMMA nanofibres and spin-coated films and (2) Pure aligned RM257 possessed better mechanical properties than

RM82. Electrospinning of different compositions of PMMA/RM257 and PA6/RM257 blends were carried out followed by UV radiation induced photo-polymerization. DSC results showed that the T_g shifts towards lower temperatures with increasing RM257 content, indicating weak interactions between PMMA and RM257 whilst no T_g shift was found in the case of PA6/RM257 blends. The latter indicating phase separation, which was further confirmed by surface morphology studies of nanofibres after UV-curing. The mechanical properties of the composite fibres were enhanced with increasing RM 257 content from 20 wt% to 33 wt% followed with a drop when further increasing the RM257 content. Composite fibres containing 33 wt% of RM257 showed the best mechanical properties with Young's moduli up to 2.8 GPa and tensile strengths up to 121 MPa and an effective modulus contribution of the RM257 to the composite fibre of 6.1 GPa. However, although this study showed that reactive mesogens can induce some levels of reinforcement in electrospun polymer fibres the properties obtained were rather modest and well below those required for high performance fibres.

4.5 References

1. Broer, D.; Crawford, G.P.; Zumer, S. *Cross-linked Liquid Crystalline Systems: From Rigid Polymer Networks to Elastomers*; CRC Press, Taylor & Francis Group: Boca Raton, FL: 2011; pp. 3-48.

2. Thiem, H.; Strohriegl, P.; Shkunov, M.; McCulloch, I. Photopolymerization of reactive mesogens. *Macromolecular Chemistry and Physics* **2005**, *206*, 2153-2159.

3. O'Neill, M.; Kelly, S.M. Liquid crystals for charge transport, luminescence, and photonics. *Advanced Materials* **2003**, *15*, 1135-1146.

4. Aldred, M.P.; Contoret, A.E.; Farrar, S.R.; Kelly, S.M.; Mathieson, D.; O'Neill, M.; Tsoi, W.C.; Vlachos, P. A Full-Color Electroluminescent Device and Patterned Photoalignment Using Light-Emitting Liquid Crystals. *Advanced Materials* **2005**, *17*, 1368-1372.

5. Huisman, B.H.; Valeton, J.J.; Nijssen, W.; Lub, J.; ten Hoeve, W. Oligothiophene-Based Networks Applied for Field-Effect Transistors. *Advanced Materials* **2003**, *15*, 2002-2005.

6. Amimori, I.; Suzuki, S.; Obata, F.; Ruslim, C. Deformed nanostructure of photo-induced biaxial cholesteric films and their application in VA-mode LCDs. *Journal of the Society for Information Display* **2005**, *13*, 799-804.

7. Cairns, D.R.; Sibulkin, M.; Crawford, G.P. Switching dynamics of suspended mesogenic polymer microspheres. *Applied Physics Letters* **2001**, *78*, 2643-2645.

8. Hikmet, R.; Broer, D. Dynamic mechanical properties of anisotropic networks formed by liquid crystalline acrylates. *Polymer* **1991**, *32*, 1627-1632.

9. Hughes-Brittain, N.; Picot, O.; Dai, M.; Peijs, T.; Bastiaansen, C. Effect of polymer binder on surface texturing by photoembossing. *Applied Surface Science* **2012**, *258*, 8609-8612.

10. Stukalin, E.B.; Douglas, J.F.; Freed, K.F. Plasticization and antiplasticization of polymer melts diluted by low molar mass species. *The Journal of Chemical Physics* **2010**, *132*, 084504.

11. Wang, Z.; Ciselli, P.; Peijs, T. The extraordinary reinforcing efficiency of single-walled carbon nanotubes in oriented poly (vinyl alcohol) tapes. *Nanotechnology* **2007**, *18*, 455709.

Chapter 5

Electrospinning of Co-polyimide Nanofibres

5.1 Introduction

As discussed in Chapter 2, flexible chain polymers can be relatively easy electrospun from solution into nanofibres but only with poor mechanical properties due to insufficient levels of chain orientation and chain extension. In contrast, the electrospinning of a rigid-rod polymer like PPTA as reported in Chapter 3 can exhibit good mechanical properties, the main drawback being related to the actual electrospinning process with continuous spinning and uniform fibre diameters being difficult to realize. Conversely in Chapter 4 it was shown that when blended with thermoplastic polymers, rigid molecules like reactive mesogens could be readily

electrospun into fibres, albeit with inferior mechanical properties compared to typical high performance fibres.

An alternative method to produce high performance nanofibres is by using soluble flexible chain polyimide precursors for electrospinning and subsequently converting these into chain extended polyimide nanofibres. Polyimides are normally not soluble in common organic solvent because of their high rigidity of molecular chains hence electrospinning the corresponding polyamic acid solution followed with imidizing the polyamic acid precursor nanofibres is the main route to produce polyimide nanofibres. Huang *et al.* electrospun well-aligned poly(*p*-phenylenebiphenyl tetracarboxamide (BP-PAA) nanofibres and then imidized these homopolymers into poly(*p*-phenylene biphenyltetracarboximide) (BPDA/PDA) nanofibres [1]. The Young's modulus, tensile strength and elongation at break of their well-aligned BPDA/PDA nanofibre mat were about 15 GPa, 660 MPa and 4.9%, respectively. Enhancement of mechanical properties compared to the BP-PAA precursor nanofibres (Young's modulus of 2.1 GPa, tensile strength of 187 MPa and elongation at break of 10.3%) is mainly ascribed to the imidization process where the flexible BP-PAA chains are transformed into rigid-rod molecular chains of BPDA/PDA which become oriented and extended along the fibre axis. Co-polyimides are also suitable for producing nanofibres by using BPDA/BPA/ODA (composition mole ratio can be found in Table 5.1). Nanofibres with Young's moduli of 6 GPa, tensile strengths of 980 MPa and elongation at break of 22.2% were found and the resulting nanofibres had greater toughness compared to the homo-polyimide nanofibres but at the expense of stiffness [2].

The focus of this chapter is to develop an electrospun co-polyimide nanofibre with greater stiffness then reported BBO co-polyimide nanofibres and higher tensile strength than the reported BPDA/PDA nanofibres with the aim of using these fibres as reinforcements for high performance nanocomposites. For this, attempts were made to introduce the flexible moiety ODA the rigid homo-polyimide structure of BPDA/PDA. Its corresponding polyamic acid was synthesized and electrospun into aligned nanofibre mats and then imidized to BPO co-polyimide nanofibres. Both the PAA nanofibres and BPO nanofibres were characterized by means of SEM, FTIR, and XRD. Mechanical properties of both BPO nanofibre UD-mats (unidirectional mats) and UD-bundles were evaluated. Subsequently, the tensile strength of a single BPO nanofibre was estimated from the bundle data by applying Daniel's theory based on Weibull statistics.

5.2 Experimental

5.2.1 Materials

3, 3', 4, 4'-Biphenyltetracarboxylic dianhydride (BPDA), 4, 4'-oxydianiline (ODA) and *p*-Phenylenediamine (PDA) were purchased from Sigma-Aldrich. N, N-Dimethylformamide (DMF, 99.8%, anhydrous) was supplied by Sigma-Aldrich. All materials were used without further purification.

5.2.2 Synthesis of co-polyimide BPDA/PDA/ODA polyamic acid

2.942 g (0.01 mol) BPDA, 0.545 g (0.005 mol) PDA and 1.001 g (0.005 mol) ODA were mixed together in 40.400 g of DMF within a three-neck flask which was ventilated with dry nitrogen gas. Intense stirring was applied in the polycondensation process at low temperature (0 ℃) for 20 hrs. A 10 wt% solution of the polyamic acid product in DMF was obtained eventually.

5.2.3 Electrospinning of BPDA/PDA/ODA polyamic acid

The 10 wt% solution synthesized above was diluted to 4.5 wt% by adding anhydrous DMF to get a homogenous spinning solution. Then the spinning solution was placed inside a syringe and pumped through a metallic needle acting as one electrode at a controlled flow rate of 0.5 ml/h. A voltage of 25 kV was applied to the needle of which then a solution jet was ejected and collected on a rotating drum with a speed of 2200 rpm wrapped with aluminium foil acting as the ground electrode. Evaporation of solvent and stretching of solution jet occurred and solid nanofibres were collected on the surface of the drum. The nanofibre mat could be easily peeled off from the aluminium foil and was dried in a vacuum oven at 70 ℃ for 3 hrs to remove all residual solvent.

5.2.4 Conversion from BPDA/PDA/ODA polyamic acid to polyimide

To obtain BPDA/PDA/ODA polyimide from its precursor fibres, these as-spun nanofibres were heated in a nitrogen atmosphere using the following procedure:

(1) Heating up to 240 ℃ at a rate of 10 ℃/min and annealing for 2 hrs. (2) Heating up to 380 ℃ at a rate of 1.5 ℃/min and annealing for 1 hr. (3) Cooling down to room temperature.

5.2.5 Characterization

The UD nanofibre mat was cut into rectangular strips with width of 4 mm and length of 50 mm. Mechanical tests of nanofibre mats were performed using an Instron 5566 universal testing machine with a load cell of 100 N. Each sample was griped directly in the clamps with the gauge length being determined by the distance between the two clamps.

The thickness of pure solid nanofibre strip (without consideration of voids between nanofibres) is determined using the Equation (5.1).

$$T_f = W_f / D L \rho_f \tag{5.1}$$

where W_f, D and L represent the weight, width and length of PI nanofibre strip respectively. ρ_f is the density of solid PI nanofibres without air which is measured to be 1.48g/cm^3 using a gas pycnometer (AccuPyc 1330 He, U.S.A.).

Nanofibre bundles containing ~30 filaments were prepared by carefully removing them from the UD-mat using a sharp tweezer and then glued on 1 mm × 1 mm paper frames. As a micro-tensile tester, an Agilent T150 with a maximum load of 500 mN and load resolution of 50 nN was applied to test the mechanical properties of the nanofibre bundles. Every series of samples was measured five times. Samples which

failed close to or inside the grips were discarded. The surface morphology of the nanofibres was investigated using a scanning electron microscope (Jeol JSM-6300F). All samples were gold-coated before observation. 2D wide-angle X-ray diffraction (WAXD) patterns were recorded using an APEX II detector in transmission mode with Cu Kα radiation from the Incoatec microfocus source. Diffraction patterns were collected with 30 sec exposure and calibrated with an Al_2O_3 filled capillary.

5.3 Results and Discussion

5.3.1 Synthesis of BPO polyamic acid

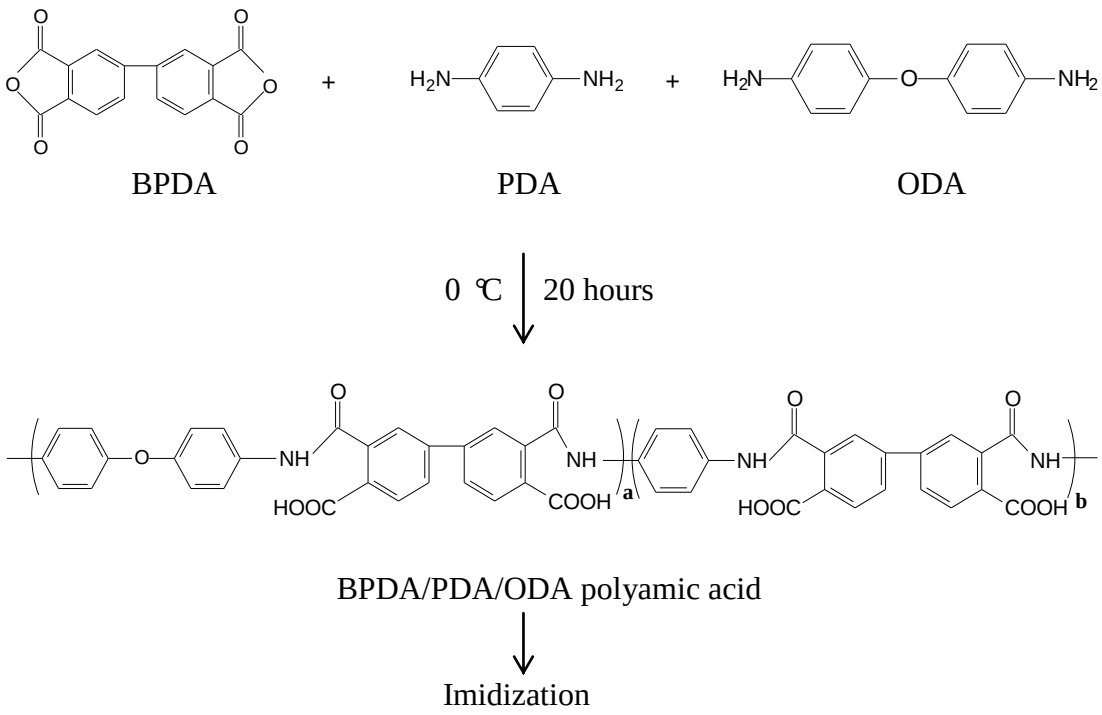

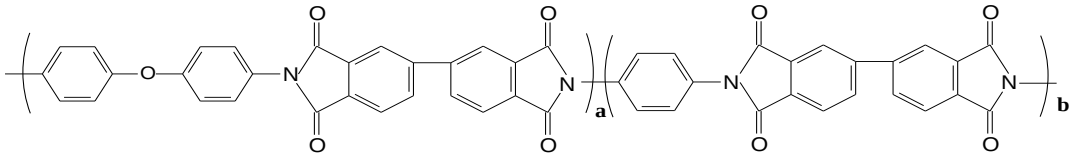

BPDA/PDA/ODA co-polyimide

Figure 5.1. *Low temperature polycondensation and imidization process.*

The polycondensation process (Figure 5.1) of monomers BPDA, PDA and ODA with a mole ratio of 2:1:1 in organic solvent is effective and rapid. Hence, the synthesis should be performed at low temperatures (0 ℃) to inhibit side reactions. A 10 wt% solution of polyamic acid in DMF was obtained after 20 hrs.

5.3.2 Electrospinning of polyamic acid, imidization process and characterization

In order to produce nanofibre reinforced composites with good mechanical properties it is vital to produce high performance electrospun nanofibre mats which are well aligned along one direction as nanofibre misalignment in a non-woven mat will significantly reduce the mechanical properties of such mats [1, 3]. In this study, a high speed rotating disc (diameter of 10 cm) with a speed of 2200 rpm was used to collect nanofibres. It should be also mentioned that the morphology of nanofibres plays an important role in their final mechanical properties. Beaded and non-uniform nanofibres should be avoided by optimizing the spinning solution (conductivity, concentration, *etc*.) and spinning parameters (applied voltages, spinning distance, temperature, rotating speed of collector, *etc*.). Figure 5.2a shows a representative

morphology of an aligned polyamic acid (PAA) nanofibre mat electrospun from 4.5 wt% spinning solution, as prepared by diluting the 10 wt% polyamic acid solution with DMF. Electrospinning of lower concentrations would lead to beaded fibres whilst higher concentrations result in bigger fibres or a solution that is too viscous to spin. The electrospun polyamic acid nanofibres produced from the well-prepared PAA solution were reasonably well-aligned, uniform and smooth. They possess diameters ranging from 180 nm to 300 nm with the majority the nanofibres having a diameter of around 275 nm.

(a) (b)

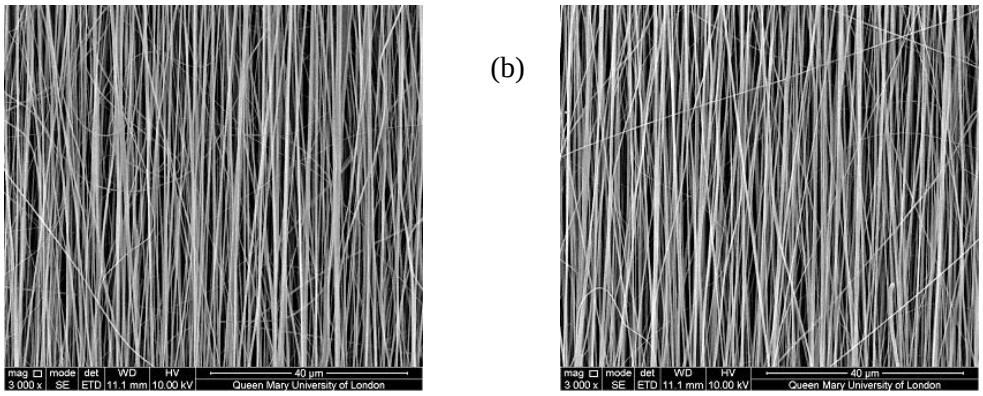

Figure 5.2. *SEM micrographs of; (a) polyamic acid nanofibres before imidization; (b) polyimide nanofibres after imidization.*

Before imidization, the polyamic acid nanofibres needed to be dried in a vacuum oven to avoid fibre fusion during the following imidization step [4]. Next, the solvent-free PAA nanofibre mat was imidized at elevated temperatures (see experimental procedure). Figure 5.2b shows that there are no obvious differences in fibre orientation in the nanofibre mats before and after imidization.

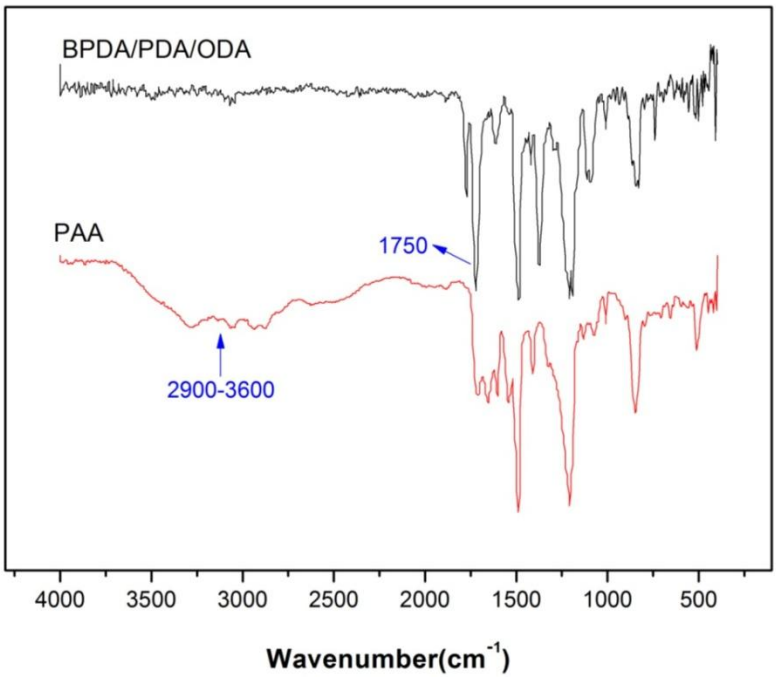

Figure 5.3. *FTIR spectrum of nanofibres before and after imidization.*

(a)

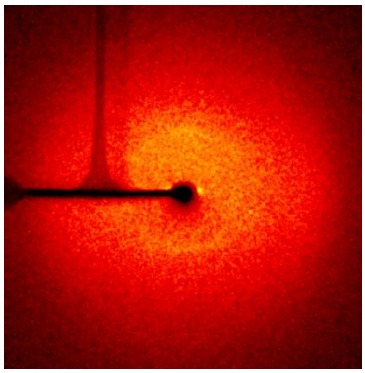

(b)

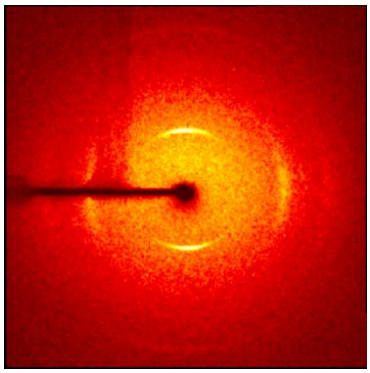

Figure 5.4. *WAXD patterns of (a) polyamic acid nanofibres before imidization (b) co-polyimide nanofibres after imidization.*

FTIR was used to study the imidization process. The most obvious difference in the FTIR spectrums as shown in Figure 5.3 is the disappearance of the broad absorption peak in the range of 2900 to 3600 cm^{-1} after imidization, which is attributed to

stretching vibration of carboxyl group and amide group of polyamic acid. This implies that the BPDA/PDA/ODA polyamic acid has been completely transferred to BPDA/PDA/ODA co-polyimide. Also, the absorption peak around 1340 cm^{-1} which is attributed to stretching of -C-O- confirms the existence of flexible ODA units in the molecular chain. In addition, the peak around 1750 cm^{-1} which results from the C=O in the five-membered imide cycle appears upon imidization [2].

From the 2D WAXD patterns of aligned polyamic acid nanofibre mats (Figure 5.4a), a typical pattern for random chain orientation is observed. In contrast, distinct bright diffreaction arcs are clearly seen from the pattern of the aligned co-polyimide nanofibre mat in Figure 5.4b, revealing preferred crystal orientation along the fibre axis in these materials.

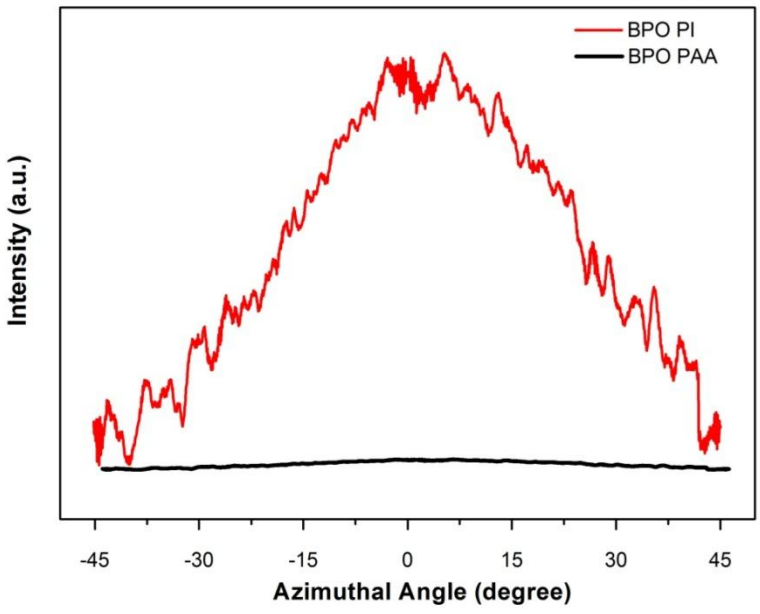

Figure 5.5. *X-ray intensity versus the azimuth angle for BPO nanofibre mats before (black) and after (red) imidization.*

Herman's orientation factor, *f*, was introduced here to better quantify the orientation of crystals before and after imidization and was determined from the fully corrected azimuthal intensity distribution diffracted from the (110) reflection [5] at d = 3.03 Å.

$$f = \frac{3 < \cos^2 \phi > -1}{2} \tag{5.2}$$

$$< \cos^2 \phi > = \frac{\int_0^{\frac{\pi}{2}} I(\phi) \sin \phi \cos^2 \phi d\phi}{\int_0^{\frac{\pi}{2}} I(\phi) \sin \phi d\phi} \tag{5.3}$$

where $I(\phi)$ is the intensity distribution of the (110) reflection at that angle of ϕ which is the azimuthal angle between the axis of the crystal plane and of the fibre. For a given crystallographic axis, $< \cos^2 \phi >$ assumes values of 1 for perfect alignment, 1/3 for random orientations, and 0 for precise perpendicularity, which corresponds to a Herman's orientation factor with respective values of 1, 0 and -1/2 [6].

In this study, the X-ray intensity as a function of azimuthal angle was plotted in Figure 5.5 with a Herman's orientation factor of about 0 and 0.7 for BPO nanofibres before and after imidization, respectively. These results confirm that the PAA precursor nanofibre shows isotropic behaviour while the imidized BPO nanofibre possesses a high degree of chain orientation.

5.3.3 Mechanical properties of co-polyimide nanofibres

The imidization of polyamic acid is considered to be a molecular chain self-ordering process which is to transform a non-oriented structure into an extended and oriented

structure [1] by the formation of rigid five-membered imide cycles in the molecular structure upon imidization. This is usually accompanied with increasing mechanical properties of the nanofibre mats. It is clearly seen from Figure 5.6 that the mechanical properties of the UD nanofibre mat after imidization improved dramatically when compared to its precursor nanofibre mat. The average Young's modulus increased from 2.5 GPa to 10 GPa whilst the average tensile strength increased from 132 MPa to 1040 MPa.

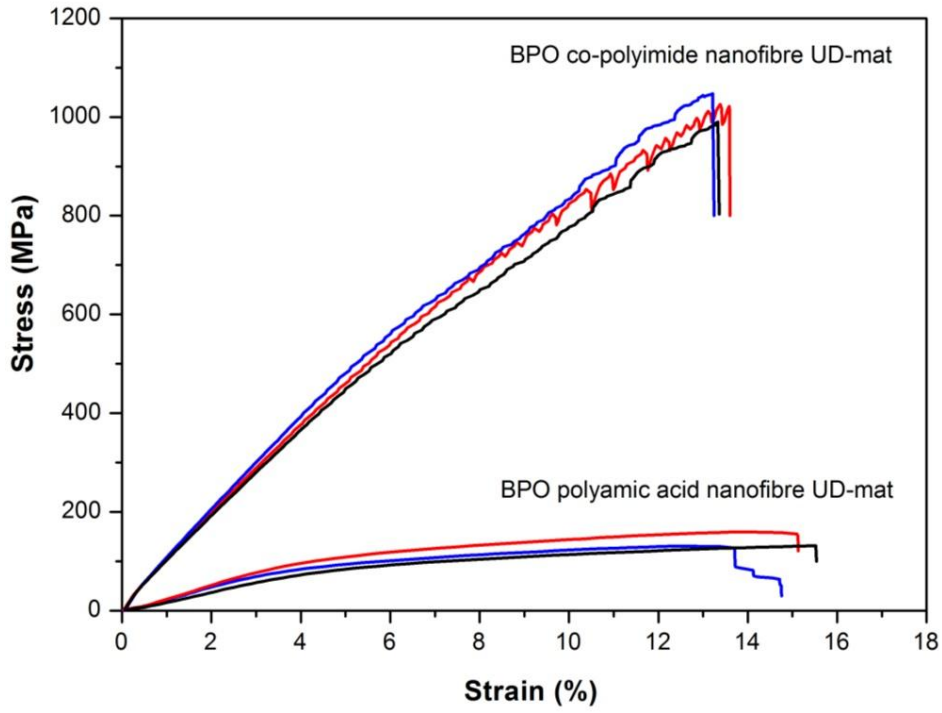

Figure 5.6. *Stress-strain curves of UD nanofibre mats before and after imidization.*

Compared to the reported co-polyimide BPDA/BPA/ODA (BBO) electrospun nanofibres listed in Table 5.1, they have higher values for Young's modulus and tensile strength, which is important for application in high performance composites.

The mechanical properties also compare very favourable to those of homo-polyimide BPDA/PDA nanofibres. Particularly, the moderate strain-at-break (~13.5%) in combination with the higher tensile strength ensures that the BPO co-polyimide nanofibre has a greater toughness than homo-polyimide BPDA/PDA nanofibres as listed in Table 5.1 and Table 5.2. A reasonable explanation for this is that the mole ratio of rigid BPDA/PDA units to flexible BPDA/ODA units in the co-polyimide has a significant influence to the resulting nanofibres. It can be concluded from Chen *et al.* [2] that with increasing rigid unit content in co-polyimide, the Young's moduli and strain-at-break of the corresponding nanofibres will increase and decrease, respectively. Meanwhile, the co-polyimide fibres can have a higher tensile strength than homo-polyimide. In our work, the BPO co-polyimide fibres possess an excellent balance of tensile strength and Young's modulus with their tensile strength being much higher than that of homo-polyimide nanofibres [7]. Interestingly, the co-polyimide nanofibres reported in this work also exhibit moderate strain-at-break, which in combination with high strength and stiffness, results in a good level of toughness. The toughness of spider silk and Kevlar® 49 are listed in Table 5.2 for comparison. The toughness of our high performance BPO nanofibres approaches Kevlar® 49 fibre, which is commonly used for anti-ballistic applications [8]. Although the BPO nanofibres have lower toughness than spider silk they have favourable levels of strength and stiffness for advanced composite applications.

Table 5.1. *Mechanical properties of three different types of electrospun polyimide nanofibre unidirectional mats. [1, 2].*

Material (mole ratio)	**Young's modulus (GPa)**	**Tensile strength (MPa)**	**Strain (%)**
BPDA/PDA/ODA (2:1:1) (this work)	10	1040	13.5
BPDA/BPA/ODA (2:1:1)	6.3	983	22.2 [2]
BPDA/PDA (1:1)	15	660	4.97 [1]

It is important to note that the toughness of UD mat is not the same as that of individual fibres. Provided the fact that the toughness of UD mat is calculated from the enclosed area under the stress-strain curve, strain-at-break significantly influences the resulting toughness. In the case of electrospun non-woven mats the random orientation of the nanofibres or fibre entanglements in these mats can lead to extensive nanofibre sliding and deformation during tensile testing. Hence, there is little correlation between the toughness of individual nanofibres and random non-woven nanofibre mats, while the toughness of UD mats represents better the intrinsic toughness of single fibres.

Table 5.2. *Toughness of the three different types of nanofibre from Table 5.1 together with spider silk and Kevlar® 49.*

Materials		**Toughness (MJ/m^3 or MPa)**
BPDA/PDA/ODA co-polyimide (this work)	Nonwoven UD nanofibre mat	77 ± 3
	Multifilament bundle	39 ± 4
BPDA/PDA polyimide	Nonwoven UD nanofibre mat	~ 20 [8]
	Single nanofibre	~ 22 [8]
BPDA/BPA/ODA co-polyimide	Nonwoven UD nanofibre mat	~120 [2]
Spider silk	Single fibre	160 (MA silk) [9] 150 (Viscid silk) [9] 221 (*Nephila edulis* silk) [10]
Kevlar® 49	Single fibre	50 [9]

It should also be noted that even in the case of electrospun aligned mats discrepancies exist between the mechanical properties of these UD mats and those of single nanofibres. In most aligned electrospun mats some level of misalignment exist in these mats and because of this aligned mats typically have inferior mechanical properties compared to single electrospun fibres. For the tensile testing of individual electrospun nanofibres two main techniques have been reported. The first one

involves *in-situ* tensile testing using atomic force microscopy (AFM) for force measurement and SEM for imaging. Typical stress-strain behaviour can be obtained by this method on single nanofibres [11]. Mechanical properties of electrospun poly(vinyl alcohol) (PVA), polyamide 6 and mineralized collagen fibrils have been successfully tested via this technique. A second method involved the use of a high resolution nano-tensile tester that allows for the testing of single nanofibres. This method has been used by Tan *et al.*, Leong *et al.* and Chen *et al.* [5, 12, 13].

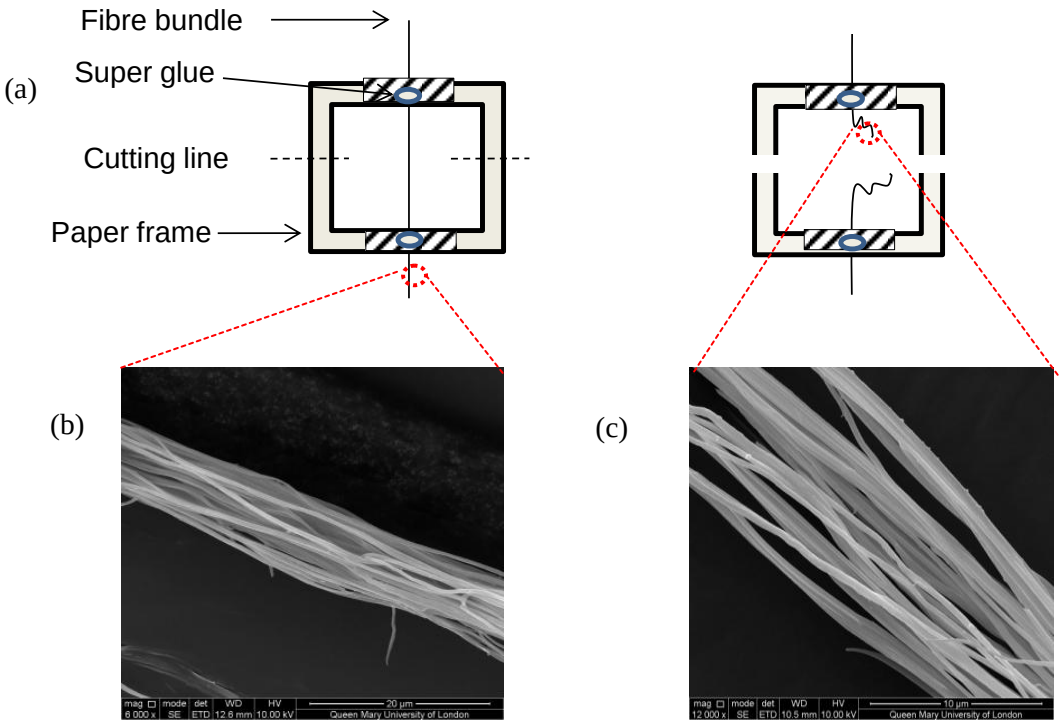

Figure 5.7. *(a) Schematic illustration of bundle sample preparation for mechanical testing and SEM micrographs of a multifilament nanofibre bundle of 29 filaments (b) before testing and (c) after testing.*

For the testing of single nanofibres two main challenges have to be faced. The first one involves the separation of single nanofibres from aligned mats and the other one

is manipulating and transporting single nanofibres to the tensile tester. In both cases, the single nanofibre can easily be damaged. A relatively convenient alternative method to evaluate the mechanical property of nanofibres is to test aligned multifilament bundles. Compare to aligned nanofibre mats, such bundles have much less fibres and have nearly perfect fibre alignment so that they reflect better the intrinsic mechanical properties of corresponding single nanofibres.

Before tensile testing, multifilament nanofibre bundles were mounted on a paper frame using double-sided sticky tapes and epoxy glue as shown in Figure 5.7a. Figure 5.7b shows a well aligned nanofibre bundle before tensile testing and Figure 5.7c presents a nanofibre bundle including 29 filaments after testing. Once the specimen is prepared, it needs to be gripped between two clamps to ensure the gauge length is equal to the inner length (10 mm) of the paper frame. In this work, we used a high resolution (50 nN) universal micro-tensile testing machine (Agilent T150) [14]. The cross-section area of a multifilament bundle is determined by counting the number of filaments and then multiplying this by the cross-section area of the individual nanofibres. Here, 275 nm is considered as the average filament diameter as detected by SEM and taking into account the ~5 nm thickness of the gold coating. It is worth mentioning that the number of filaments in a bundle is determined from the number of broken fibre ends in a bundle (Figure 5.7c) rather than from the multifilament bundle before testing (Figure 5.7b) in case any broken fibre ends exists in the bundle before testing. The Young's modulus and tensile strength of the aligned co-polyimide nanofibre bundles are found to be 38 ± 2 GPa and 1550 ± 70 MPa, respectively (Figure 5.8). The relatively high mechanical properties in

comparison to the UD mats are the result of a better alignment of individual nanofibres in the bundles compared to the mats.

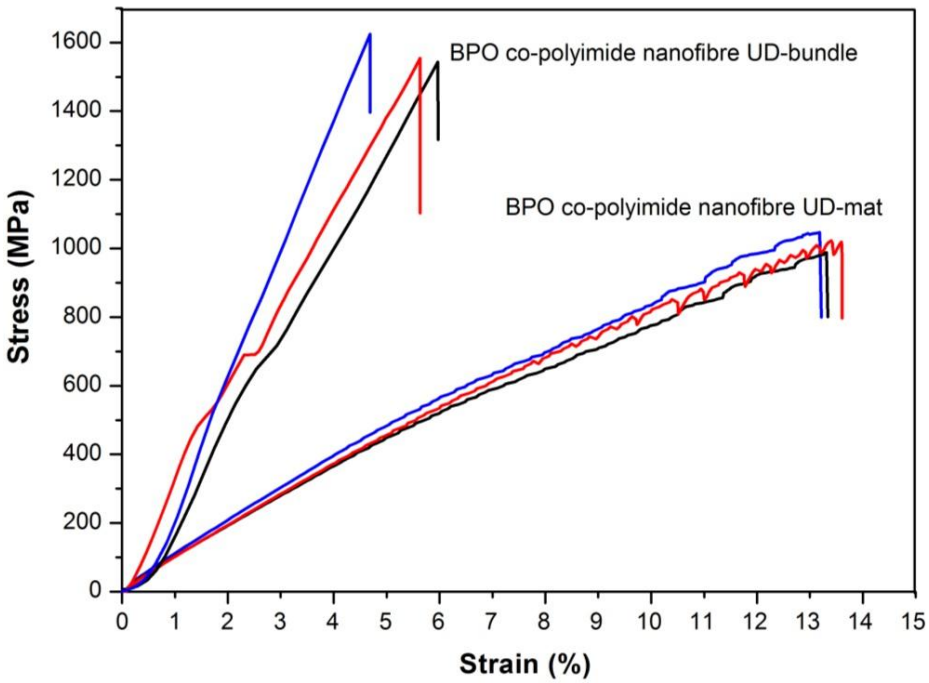

Figure 5.8. *Stress-strain curves of UD nanofibre mats and bundles.*

In order to estimate the single nanofibre properties from the bundle data we applied Daniel's bundle theory based on Weibull statistics, which was recently extended for considering hierarchical [15], composite [16], and even self-healing materials [17].

Accordingly, describing the nanofibre strength statistics with the classical Weibull statistics, having unknown mean strength σ_f and Weibull modulus *m*, we deduce:

$$m = \frac{1}{\ln\left(1 + \frac{\vartheta_b^2}{\sigma_b^2} N\right)} \tag{5.4}$$

$$\sigma_f = \sigma_b m^{1/m} e^{1/m} \Gamma\left(1 + \frac{1}{m}\right) \tag{5.5}$$

where σ_b, ϑ_b, N are respectively the bundle mean strength, standard deviation and number of nanofibres in the bundle (Γ is the gamma function).

Since the tensile strength of the aligned co-polyimide nanofibre bundles composed with *N*=30 (average of 28, 29 and 33 from three bundles), individual nanofibre strength was found to be 1550 ± 70 MPa. From the Equation (5.4) we estimated *m*=16.8, whereas from Equation (5.5) $\sigma_f = 1.9\,\text{GPa}$.

Note that although the experimental estimation of ϑ_b could be not very accurate due to the relative small number of tests (*n*=3), the Weibull modulus of 16.8 is in agreement with Weibull moduli reported for polymeric fibres. Weibull moduli for polymeric fibres were found to be in the range of 8 to 18 [18], which in turn confirms the reliability of ϑ_b and thus the reliability of the single BPO nanofibre strength data.

5.4 Conclusions

In this chapter, BPO co-polyimide precursor polyamic acid was first synthesized and electrospun into nanofibres and then imidized to high strength and high modulus co-

polyimide nanofibres. Aligned co-polyimide nanofibre mats possessed a mean Young's modulus, strength and strain-at-break of respective 10 GPa, 1.04 GPa, and 13.5 %. In comparison with reported co-polyimide nanofibres (BBO) of similar chemical structure, these BPO co-polyimide nanofibres were both strong and stiff, while at the same time exhibiting high levels of toughness. Because of their relatively high strain-at-break these BPO co-polyimide nanofibres exhibit greater toughness than homo-polyimide (BPDA/PDA) nanofibres with comparable toughness to Kevlar® 49.

Mechanical properties of multifilament nanofibre bundles (~30 filaments) were tested by virtue of a micro-tensile tester. Young's moduli of 38 ± 2 GPa and tensile strengths of 1550 ± 70 MPa were found. Further analysis of this bundle data using of Daniel's fibre bundle theory based on Weibull statistics lead to a predicted tensile strength for single co-polyimide nanofibres of about 1.9 GPa.

The high performance co-polyimide electrospun fibres reported here are expected to make interesting nano-reinforcements for composites and this will be the focus of the following chapter.

5.5 References

1. Huang, C.; Chen, S.; Reneker, D.H.; Lai, C.; Hou, H. High-strength mats from electrospun poly(*p*-phenylene biphenyltetracarboximide) nanofibers. *Advanced Materials* **2006**, *18*, 668-671.

2. Chen, S.; Hu, P.; Greiner, A.; Cheng, C.; Cheng, H.; Chen, F.; Hou, H. Electrospun nanofiber belts made from high performance copolyimide. *Nanotechnology* **2008**, *19*, 015604.

3. Kongkhlang, T.; Tashiro, K.; Kotaki, M.; Chirachanchai, S. Electrospinning as a new technique to control the crystal morphology and molecular orientation of polyoxymethylene nanofibers. *Journal of the American Chemical Society* **2008**, *130*, 15460-15466.

4. Goponenko, A.V.; Hou, H.; Dzenis, Y.A. Avoiding fusion of electrospun 3, 3', 4, 4'-biphenyltetracarboxylic dianhydride-4, 4'-oxydianiline copolymer nanofibers during conversion to polyimide. *Polymer* **2011**, *52*, 3776-3782.

5. Chen, F.; Peng, X.; Li, T.; Chen, S.; Wu, X.-F.; Reneker, D.H.; Hou, H. Mechanical characterization of single high-strength electrospun polyimide nanofibres. *Journal of Physics D: Applied Physics* **2008**, *41*, 025308.

6. Bilotti, E. Polymer/Sepiolite Clay Nanocomposites. Ph.D Thesis, Queen Mary University of London, UK, 2009.

7. Sukhanova, T.; Baklagina, Y.G.; Kudryavtsev, V.; Maricheva, T.; Lednický, F. Morphology, deformation and failure behaviour of homo-and copolyimide fibres: 1. Fibres from 4, 4'-oxybis (phthalic anhydride)(DPhO) and *p*-phenylenediamine (PPh) or/and 2, 5-bis (4-aminophenyl)-pyrimidine (2, 5PRM). *Polymer* **1999**, *40*, 6265-6276.

8. Zhang, J.M.; Mousavi, Z.; Soykeabkaew, N.; Smith, P.; Nishino, T.; Peijs, T. All-aramid composites by partial fiber dissolution. *ACS Applied Materials & Interfaces* **2010**, *2*, 919-926.

9. Tirrell, D.A. Putting a new spin on spider silk. *Science* **1996**, *271*, 39-40.

10. Vollrath, F.; Knight, D.P. Liquid crystalline spinning of spider silk. *Nature* **2001**, *410*, 541-548.

11. Hang, F.; Lu, D.; Bailey, R.J.; Jimenez-Palomar, I.; Stachewicz, U.; Cortes-Ballesteros, B.; Davies, M.; Zech, M.; Bödefeld, C.; Barber, A.H. In situ tensile testing of nanofibers by combining atomic force microscopy and scanning electron microscopy. *Nanotechnology* **2011**, *22*, 365708.

12. Tan, E.; Lim, C. Physical properties of a single polymeric nanofiber. *Applied Physics Letters* **2004**, *84*, 1603-1605.

13. Chew, S.Y.; Hufnagel, T.C.; Lim, C.T.; Leong, K.W. Mechanical properties of single electrospun drug-encapsulated nanofibres. *Nanotechnology* **2006**, *17*, 3880.

14. Lepore, E.; Marchioro, A.; Isaia, M.; Buehler, M.J.; Pugno, N.M. Evidence of the most stretchable egg sac silk stalk, of the European spider of the year Meta Menardi. *PloS One* **2012**, *7*, e30500.

15. Pugno, N.M.; Bosia, F.; Abdalrahman, T. Hierarchical fiber bundle model to investigate the complex architectures of biological materials. *Physical Review E* **2012**, *85*, 011903.

16. Pugno, N.M.; Abdalrahman, T. Multimodal Daniels' theory: An application to carbon nanotube twisted strands. *Composites Part B: Engineering* **2013**, *45*, 303-307.

17. Bosia, F.; Abdalrahman, T.; Pugno, N.M. Investigating the role of hierarchy on the strength of composite materials: evidence of a crucial synergy between hierarchy and material mixing. *Nanoscale* **2012**, *4*, 1200-1207.

18. Bosia, F.; Abdalrahman, T.; Pugno, N.M. Self-Healing of Hierarchical Materials. *Langmuir* **2014**, *30*, 1123-1133.

Chapter 6

Co-Polyimide Nanofibre Reinforced Composites

6.1 Introduction

Traditionally, fibres such as glass [1], carbon [2-4], cellulose [5-7] or synthetic [8, 9] have been used to reinforce softer polymer matrices such as epoxy and polyester resins or thermoplastic resins. Nowadays, fibre reinforced composites are available in a range of properties with applications varying from aircraft to military, from bridges to automotive and to sporting goods.

In recent years, electrospun nanofibres have attracted interest as reinforcements for composite materials due to their small diameter (20 nm-1 μm) and high aspect ratio. Such nanocomposites have potentially great impact properties as a result of the high interfacial area, leading to high fibre debonding and pull-out energies during

composite fracture [10-12]. Fibre orientation, fibre aspect ratio as well as interfacial bonding between fibre and matrix can all greatly influence mechanical properties of fibre reinforced composites. In theory, the high aspect ratio of electrospun fibres can be of significant advantage as reinforcement efficiency increases with fibre aspect ratio. For example, for a nanofibre with a diameter of 100 nm, the critical fibre length is only 1/100 of that for a micro-fibre of the same strength and a diameter of 10 μm [11]. As electrospun fibres are generally continuous their aspect ratios are extremely high and much greater than that of other nanoreinforcements such as nanoclays, whiskers, carbon nanotubes or graphene, making them great candidates for composite reinforcement.

Electrospun nanofibres have been evaluated as reinforcements in polymer matrices such as styrene-butadiene rubber [13], epoxy resin [13, 14], melamine-formaldehyde resin [15], thermoplastic polyurethane [16], *etc*. Nevertheless, their potential research in the area of polymer nanofibre reinforced composites is still rather limited due to some key challenges. First, as mentioned previously, the mechanical properties of electrospun nanofibres are often very poor compared to traditional reinforcing fibres such as glass and carbon fibres or even corresponding synthetic micro-fibres made from the same polymer. So far very few studies have reported mechanical properties for electrospun nanofibres which are approaching those of e.g. glass fibres with moduli of 70 GPa and tensile strengths of 2 GPa [17, 18]. Secondly, electrospun nanofibres are almost exclusively available in non-woven form and textile fabrics (knitted, woven, *etc.*) have not yet been realized which restricts the development of nanofibres for composite applications. Finally, so far systematic

studies and analysis of polymer nanofibre reinforced composites using traditional composite theories are inadequate.

In the previous chapter, co-polyimide polyamic acid based on BPO was synthesized and then electrospun to nanofibres. After imidization, the mechanical properties of the tested multifilament nanofibre bundles were as high as 40 GPa for the Young's modulus and a tensile strength of 1.55 GPa. The low density of these fibres compared to glass fibres leads to very interesting specific mechanical properties making them great candidates for composite reinforcement. However, whether these mechanical properties can be translated into effective composite reinforcement remains unclear. In the work reported here, a triblock Kraton G1643MS thermoplastic elastomer exhibiting low viscosity and easy processing in solutions was used as a soft matrix. The BPO co-polyimide nanofibre described in Chapter 5 was used as reinforcement. As such a novel strong and flexible unidirectional composite was obtained, which was fully characterized. The off-axis mechanical properties of these nanofibre reinforced composites with two fibre volume fractions (45% and 25%) were investigated and compared with predicted data using classical composite theories. Meanwhile, the influence of nanofibre misalignment in a these unidirectional composites was studied and the Young's modulus of single nanofibres was predicted from composite data.

6.2. Experimental

6.2.1. Materials

Tetrahydrofuran (THF, ≥ 99.9%, anhydrous) was purchased from Sigma-Aldrich without further purification. Kraton G1643MS resin was kindly supplied by Kraton Performance Polymers, Inc.

6.2.2. Fabrication of UD BPO co-polyimide nanofibre reinforced composites

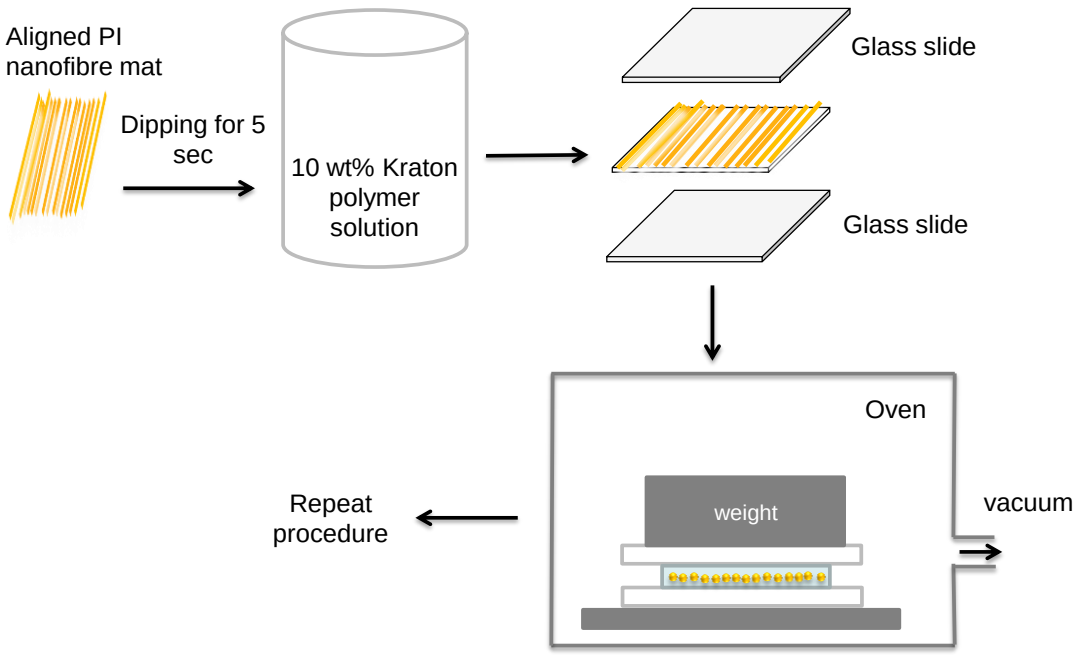

Figure 6.1. *Schematic of the fabrication process of unidirectional BPO co-polyimide nanofibres reinforced composites.*

All aligned nanofibre mat samples were cut into strips of rectangular shape with a width of 4 mm and length of 30 mm. The fabrication process of BPO co-polyimide nanofibre reinforced composite is illustrated in Figure 6.1. A well aligned PI nanofibre mat was dipped into a 10 wt% matrix in THF solution for 5 sec until voids between the nanofibres were eliminated. Then the wetted mat was pressed first between two flat glass slides followed by placing weights (5 kg) on top of them. Subsequently, the specimen was left in a vacuum oven for drying at 70 ℃ for 2 min. After that, the above steps were repeated until the required fibre volume fraction was reached.

6.2.3. Characterization

Mechanical tests of the composite laminates were performed by using an Instron 5566 universal testing machine with a load cell of 100 N. Every series of samples were measured five times. Samples failing close to or inside the grips were discarded.

The thickness of the neat aligned nanofibre mat (without consideration of voids between the nanofibres) is determined by:

$$T_f = W_f / (D L \rho_f) \tag{6.1}$$

where W_f, D and L represent the weight, width and length of the UD co-polyimide nanofibre sample, respectively. ρ_f is the density of solid BPO nanofibres without air and is measured to be 1.45 g/cm^3 using a gas pycnometer (AccuPyc 1330 He, U.S.A.). It should be noted that the matrix between nanofibres is regarded as homogenously dispersed. Therefore, the matrix thickness can be considered to be the

thickness of a rectangular matrix strip which has the same width and length as the nanofibre strips, which is given by:

$$T_m = W_m / (D\ L\ \rho_m) \tag{6.2}$$

where W_m and ρ_m are the weight and density of the matrix, respectively. ρ_m equates to 0.89 g/cm^3 which is measured based on casting neat matrix films. Therefore, the thickness of the UD co-polyimide nanofibre reinforced composite T_c can be determined as:

$$T_c = T_f + T_m \tag{6.3}$$

The porosity of the UD nanofibre mat was determined from:

$$P_f = 1 - V_f / V \tag{6.4}$$

where V_f is the volume of solid nanofibres without consideration of voids between nanofibres and V is the total volume of nanofibres plus voids. More specifically, the porosity can be written as:

$$P_f = 1 - (W_f / \rho_f) / (D\ L\ T) = 1 - [(W_f / (\rho_f\ D\ L)] / T = 1 - T_f / T \tag{6.5}$$

where T stands for the thickness of nanofibre strip which is measured using a micrometre without visible compression of the specimen. In the same way, the porosity of composites is given by:

$$P_c = 1 - (T_f + T_m) / T_{measured} \tag{6.6}$$

Where $T_{measured}$ is also measured by using a micrometer without visible compression.

The average degree of orientation (AD) of the nanofibres in the aligned mats is calculated based on the misalignment angles of 500 randomly selected nanofibres, and is given by:

AD = Sum of the product of individual fibre angles with its frequency / 500

The surface and fracture surface morphology studies of the composites were investigated using a scanning electron microscope (Jeol JSM-6300F). All samples were gold-coated before observation.

6.3. Results and Discussion

6.3.1. Mechanical properties of UD BPO nanofibre reinforced composites

Providing the respective Young's modulus and volume fractions of fibre and matrix are known, the stiffness of unidirectional composite can be calculated from the 'Rule of Mixtures'. Furthermore, it can also be used to back-calculate the stiffness contribution of the reinforcement and as such be used to evaluate the efficiency of nanoreinforcements [19, 20]. The Young's modulus of the UD co-polyimide composites as a function of nanofibre volume fractions are shown in Figure 6.2, with experimental data in good agreement with predictions using the 'Rule of Mixtures' ($E_c = E_f V_f + E_m V_m$) assuming equal strain in fibre and matrix (Voigt model).

It should be noted that the composites reported here are not all free of voids. About 25 vol% voids are present in the composite specimen. Void-free composites were difficult to achieve due to the numerous confined spaces caused by misalignment of nanofibres. In this situation, the ROM can be rewritten into $E_c = E_f V_f + E_m V_m + E_v V_v$ in where E_v is the modulus of voids which is considered to be zero and V_v is the volume fraction of voids (porosity) in the composites, with the sum of V_f, V_m, V_v being 100%. Because of this, although voids do not contribute to the stiffness, the approximate 25 vol% voids actually reduces the effective nanofibre volume fraction in the composites.

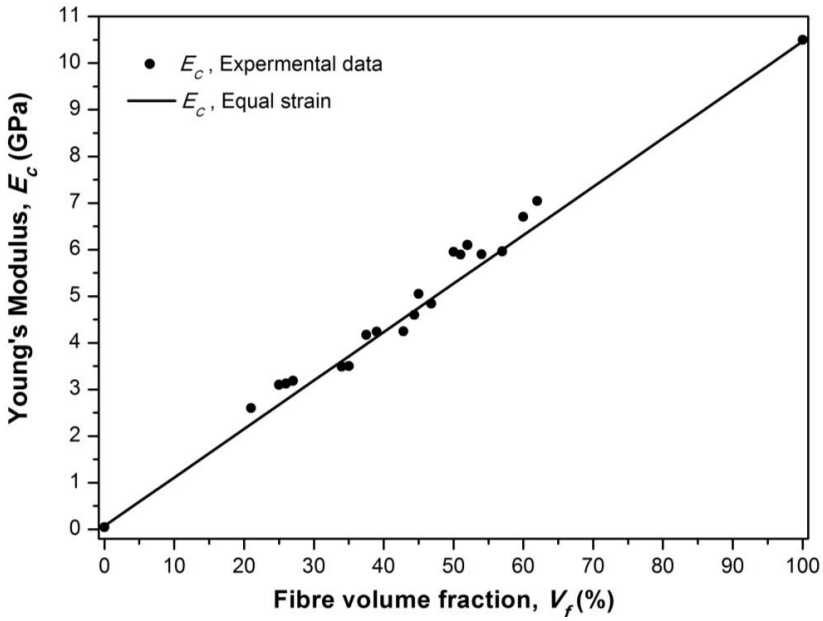

Figure 6.2. *Young's modulus of unidirectional BPO co-polyimide nanofibre reinforced composites with different nanofibre volume fractions.*

Nevertheless, BPO nanofibre reinforced composites still have fibre volume fractions ranging from 21% up to 62%, which is far higher than of most other nanocomposites

based on clays or nanotubes with typical nanofiller loadings < 5%. Figure 6.2 shows good agreement between measurements and prediction (assuming equal strains of nanofibre and matrix), indicating a good stress transfer and limited interfacial sliding when the composite is loaded along the fibre axis.

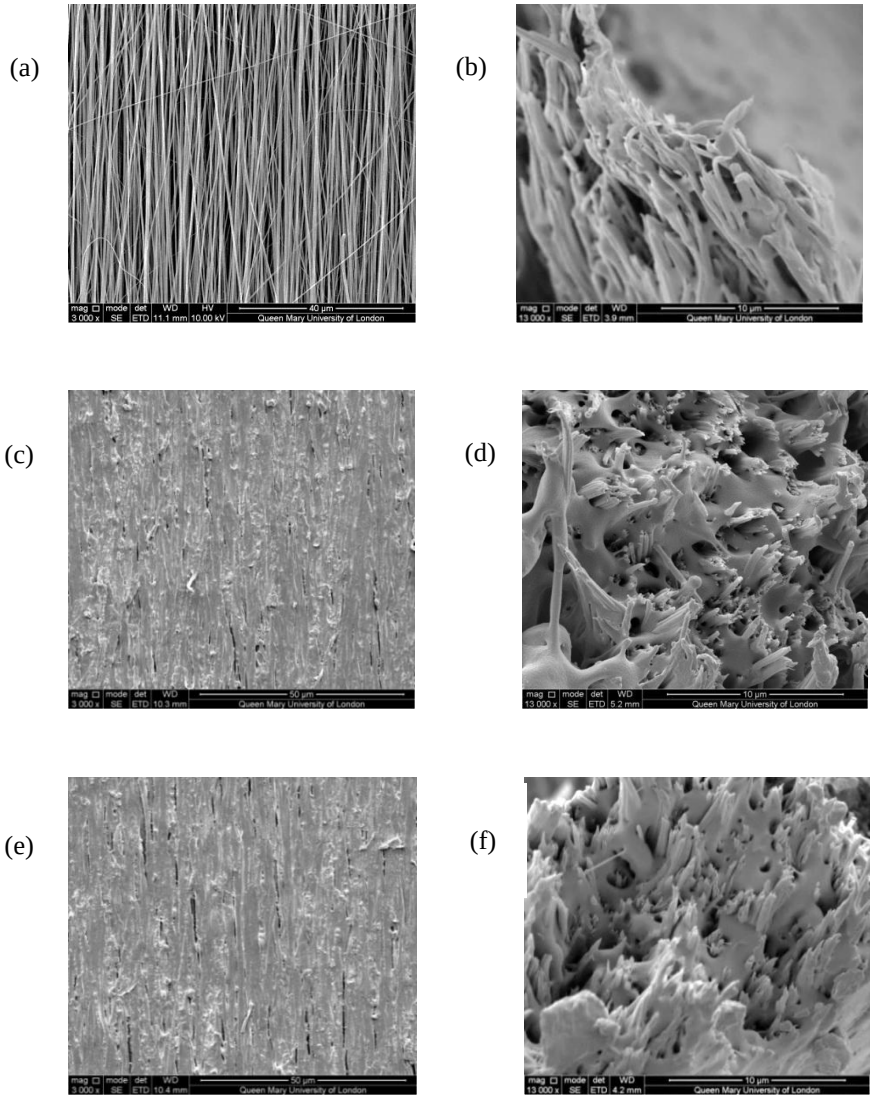

Figure 6.3. *SEM micrographs showing the surface of UD BPO nanofibre reinforced composite and fracture surface of (a), (b) neat polyimide UD nanofibre mat. (c), (d) 25 vol% nanofibre composite. (e), (f) 45 vol% nanofibre composite.*

Further morphological studies of the composite and fracture surface lead to more information of the composite failure modes. Figure 6.3a, c and e show the surfaces of pure BPO nanofibre UD-mat, UD composites with 25 vol% and 45 vol% of nanofibre, respectively. It can be seen that the nanofibre mat is reasonable well impregnated by the matrix. Intimate contact between nanofibres and matrix can be found by observing the corresponding fracture surfaces of Figure 6.3d and f. Meanwhile, ends of broken nanofibres are still covered with matrix, implying good interfacial bonding between nanofibres and matrix. Furthermore, numerous shallow holes resulting from fibre pull-out after fibre breakage manifest itself in the composite, indicating that nanofibre composites can absorb significant amounts of energy through pull-out and debonding during the failure process [21].

6.3.2. Off-axis properties of UD BPO nanofibre reinforced composites

The Young's modulus E_θ of unidirectional composites at different loading angles can be described by Equation (6.7) [22, 23].

$$\frac{1}{E_\theta} = \left[\frac{1}{E_{11}}\right]\cos^4\theta + \left[\frac{1}{G_{12}} - 2\frac{\nu_{12}}{E_{11}}\right]\cos^2\theta\sin^2\theta + \left[\frac{1}{E_{22}}\right]\sin^4\theta \tag{6.7}$$

where G_{12} = shear modulus, ν_{12} = Poisson's ratio, θ = angle between loading direction and nanofibre direction and E_{11} = longitudinal tensile modulus, E_{22} = transverse tensile modulus.

When θ =45 °, the shear modulus can be calculated from Equation (6.8).

$$\frac{1}{G_{12}} = \left[\frac{4}{E_{45}}\right] - \left[\frac{1-2\nu_{12}}{E_{11}}\right] - \left[\frac{1}{E_{22}}\right] \tag{6.8}$$

In the above two equations, both E_{11} and E_{22} are experimental data. Meanwhile, ν_{12} is considered to be 0.4 which is usually applied for rubbery polymer materials.

The tensile strength, σ_θ, of UD composites at different loading angles can be predicted using the Tsai-Hill criterion [18, 19] as below.

$$\sigma_\theta = \left[\frac{\cos^2\theta(\cos^2\theta - \sin^2\theta)}{\sigma_{11}^2} + \frac{\sin^4\theta}{\sigma_{22}^2} + \frac{\cos^2\theta\sin^2\theta}{\tau_{12}^2}\right]^{-1/2} \tag{6.9}$$

where σ_{11} and σ_{22} are the longitudinal and transverse tensile strength. τ_{12} is the in-plane shear strength which can be obtained from $\sigma_\theta = \tau_{12} / (\cos\theta \sin\theta)$ by loading a 10 ° off-axis specimen.

Table 6.1. *A list of values used for off-axis Young's modulus and tensile strength predictions (V_f is the volume fraction of nanofibre).*

V_f (%)	E_{11} (GPa)	E_{22} (GPa)	G_{12} (GPa)	ν_{12} (-)	σ_{11} (MPa)	σ_{22} (MPa)	τ_{12} (MPa)
45	5.10	0.16	0.37	0.40	385.40	9.10	23.12
25	3.10	0.09	0.14	0.40	265.30	6.60	15.05

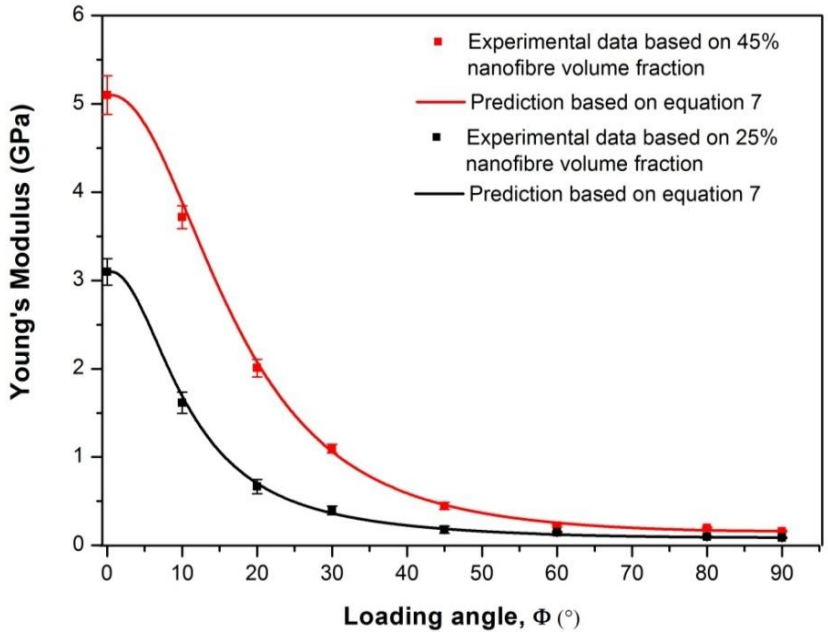

Figure 6.4. *Young's modulus vs. loading angles for unidirectional BPO co-polyimide nanofibre reinforced composites based on two fibre volume fractions.*

Both the off-axis Young's modulus and tensile strength of unidirectional composites in this work are investigated based on two nanofibre loadings (45 vol% and 25 vol%).

Table 6.1 lists values used for Young's modulus calculations using Equation (6.7) based on two nanofibre volume fractions. Young's modulus against loading angle for composites with 45 vo% and 25 vol% nanofibre are plotted in Figure 6.4. Both prediction curves are in close agreement with the experimental modulus data. Meanwhile, the experimental strength data also shows a good fit with the Tsai-Hill model for both two volume fractions (Figure 6.5).

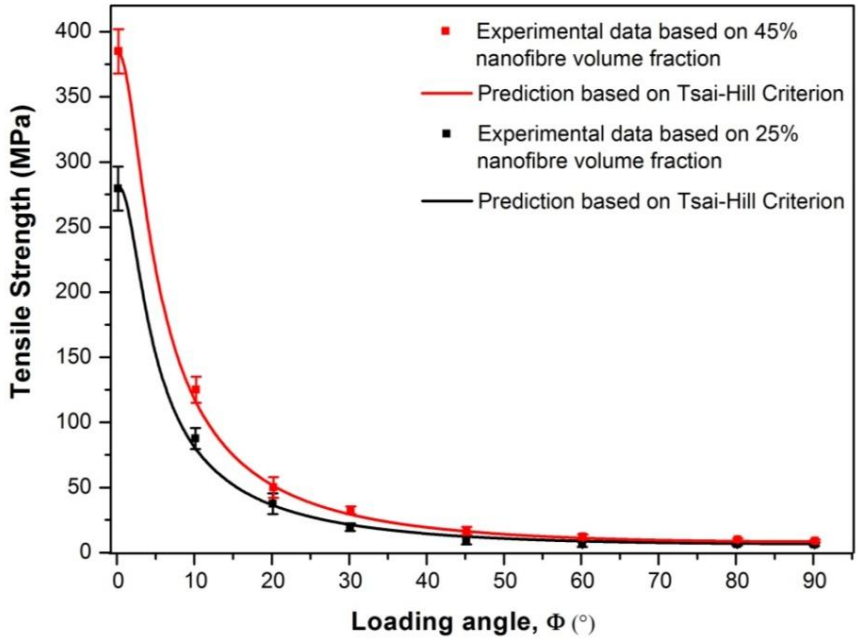

Figure 6.5. *Tensile strength vs. loading angles of unidirectional BPO co-polyimide nanofibre reinforced composite based on two fibre volume fractions.*

6.3.3. Young's modulus evaluation of single nanofibres

The previous section clearly showed that fibre misalignment significantly reduces the mechanical performance of the composites. Figure 6.6 shows predicted Young's moduli of UD BPO nanofibre mat reinforced composites and aligned multifilament bundle reinforced composites based on ROM calculations. However, in practice nanofibres are not perfectly aligned in UD mats, leading to relatively low mechanical properties of the corresponding composite laminates. If a composite was to be made from better aligned nanofibre bundles, the composite Young's moduli can be predicted to be higher as shown in Figure 6.6b (where at V_f = 100% the Young's modulus of the composite is equal to that of the bundle at 38 GPa). Mechanical properties of the composites could be even more improved if nanofibres were

perfectly aligned. More importantly, the mechanical properties of a single nanofibre can be predicted or back-calculated from composite data if the longitudinal Young's modulus of a perfectly aligned nanofibre reinforced composite is known.

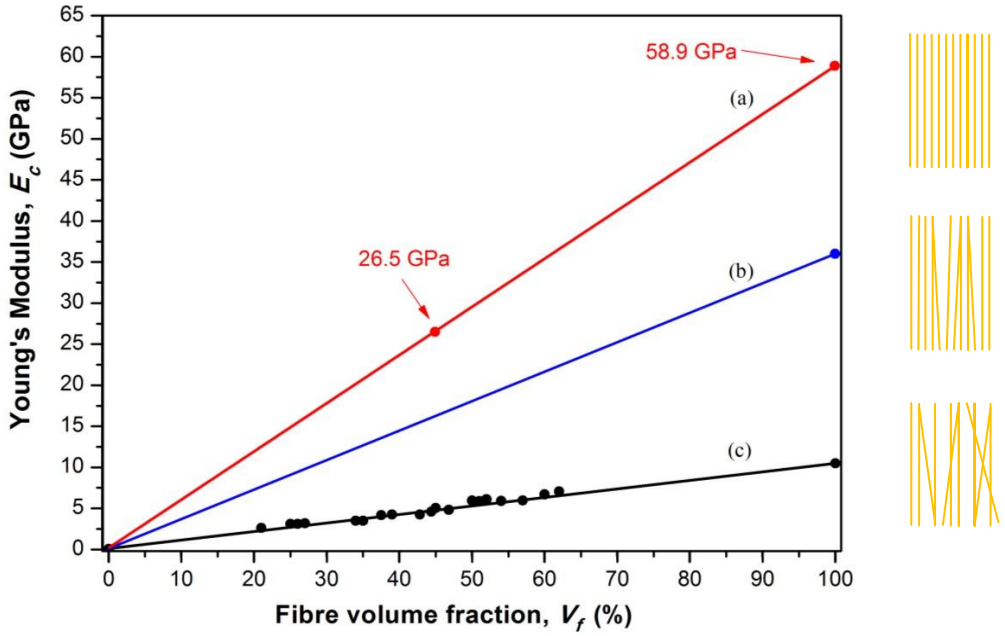

Figure 6.6. *Predicted Young's modulus of unidirectional BPO co-polyimide nanofibre reinforced composites with different nanofibre volume fractions based on; (a) perfectly aligned nanofibres (b) aligned nanofibres in a bundle (c) aligned nanofibres in a UD mat with significant misalignment.*

Figure 6.7 shows an orientation distribution plot of 500 individual nanofibres in an aligned spun mat with an average fibre angle of 14 °. Based on this observed off-axis angle the Young's modulus of a perfectly aligned BPO co-polyimide nanofibre reinforced composite (Vf = 45%) can now be predicted using Equation (6.7). E_θ is the Young's modulus at θ = 14° and the Young's modulus of the (non-perfectly) aligned UD mat reinforced composite with a nanofibre volume fraction of 45%.

Assuming the values of E_{22}, G_{12}, ν_{12} for perfectly aligned composites are the same as for non-perfectly aligned UD mat reinforced composites, the longitudinal Young's modulus of a perfectly aligned BPO co-polyimide nanofibre reinforced composite can be calculated at 26.5 GPa using Equation (6.7).

Table 6.2. *A list of values used for predicting Young's moduli as a function of various loading angles.*

V_f **(%)**	E_θ **(θ = 14°)** ***(GPa)***	E_{22} **(GPa)**	G_{12} **(GPa)**	ν_{12} **(-)**
45	5.1	0.16	0.37	0.4

Using now the predicted Young's modulus data of perfectly aligned BPO co-polyimide nanofibre composites (Figure 6.5(a)) in combination with the 'Rule of Mixtures', gives us Young's modulus data for the single nanofibres. The intersection point of the prediction line (a) with Y-axis (V_f = 100%) provides a direct value of Young's modulus for perfectly aligned nanofibres of 59 GPa. In other words, the expected Young's modulus of single BPO co-polyimide nanofibres is approximately 59 GPa. As such the proposed method, for the first time, presents an indirect method to determine the intrinsic Young's modulus of single nanofibres from composite data using composite theories.

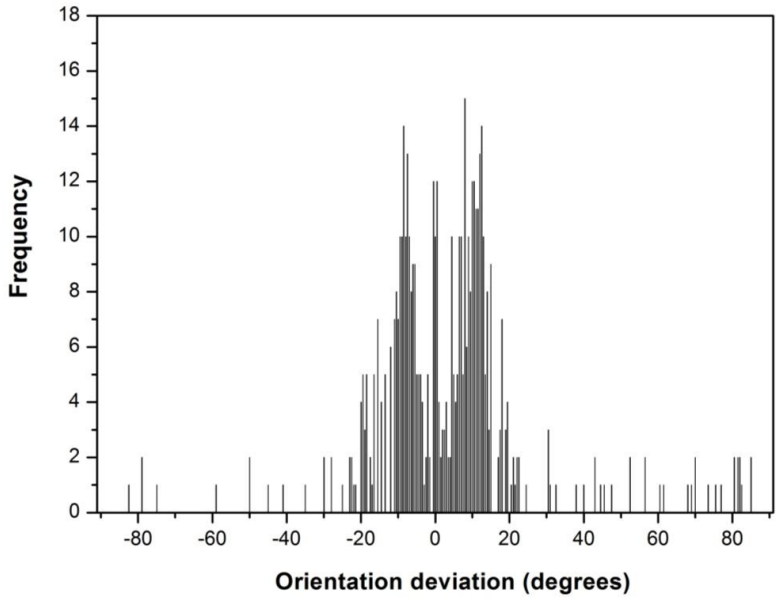

Figure 6.7. *Histogram representing the average orientation angles of 500 individual nanofibres along the nanofibre alignment direction in electrospun aligned mats.*

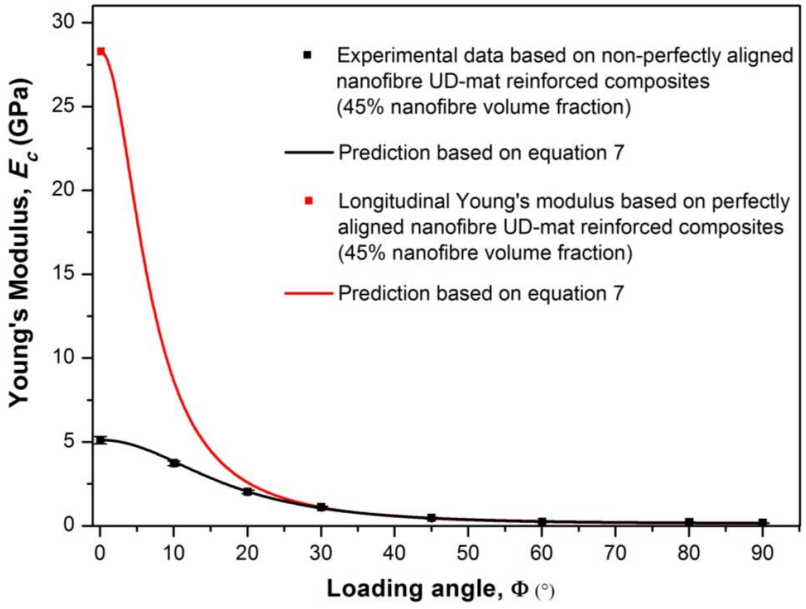

Figure 6.8. *Young's modulus vs. loading angles of unidirectional BPO nanofibre composites with perfect alignment (theory) (upper) and non-perfect alignment (experimental mat data) (lower).*

6.4. Conclusions

In this research, unidirectional BPO co-polyimide nanofibres reinforced composites were fabricated by impregnating aligned nanofibre mats with 10% of matrix solutions. Classical composite laminate and 'Rule of Mixtures' theory were for the first time applied to nanofibre reinforced composites. It was found that the Young's modulus and tensile strength of off-axis loaded composites could be well described using classical laminate theory. Meanwhile, the mechanical behaviour of the composites was also in agreement with 'Rule of Mixture' behaviour (Voigt model). More importantly, the study also provided a novel indirect method to evaluate the Young's modulus of single nanofibres using a combination of laminate analysis and 'Rule of Mixtures'. Aligned nanofibre mats produced in this study exhibited an average nanofibre orientation of 14 °and from this the longitudinal Young's modulus of a perfectly aligned (0 °) nanofibre composite was calculated. Using this data the Young's modulus of a single nanofibre was back-calculated at 59 GPa by applying the 'Rule of Mixtures'.

6.5. References

1. Van den Oever, M.; Peijs, T. Continuous-glass-fibre-reinforced polypropylene composites II. Influence of maleic-anhydride modified polypropylene on fatigue behaviour. *Composites Part A: Applied Science and Manufacturing* **1998**, *29*, 227-239.

2. Choi, N.; Kinloch, A.; Williams, J. Delamination fracture of multidirectional carbon-fiber/epoxy composites under mode I, mode II and mixed-mode I/II loading. *Journal of Composite Materials* **1999**, *33*, 73-100.

3. Van den Heuvel, P.; Goutianos, S.; Young, R.; Peijs, T. Failure phenomena in fibre-reinforced composites. Part 6: a finite element study of stress concentrations in unidirectional carbon fibre-reinforced epoxy composites. *Composites Science and Technology* **2004**, *64*, 645-656.

4. Schultz, J.; Lavielle, L.; Martin, C. The role of the interface in carbon fibre-epoxy composites. *Journal of Adhesion* **1987**, *23*, 45-60.

5. Bledzki, A.; Gassan, J. Composites reinforced with cellulose based fibres. *Progress in Polymer Science* **1999**, *24*, 221-274.

6. Wambua, P.; Ivens, J.; Verpoest, I. Natural fibres: can they replace glass in fibre reinforced plastics? C*omposites Science and Technology* **2003**, *63*, 1259-1264.

7. Peijs, T. Natural fiber based composites. *Materials Technology(UK)* **2000**, *15*, 281-285.

8. Zhang, J.M.; Peijs, T. Self-reinforced poly(ethylene terephthalate) composites by hot consolidation of Bi-component PET yarns. *Composites Part A: Applied Science and Manufacturing* **2010**, *41*, 964-972.

9. Zhang, J.M.; Mousavi, Z.; Soykeabkaew, N.; Smith, P.; Nishino, T.; Peijs, T. All-aramid composites by partial fiber dissolution. *ACS Applied Materials & Interfaces* **2010**, *2*, 919-926.

10. Teo, W.; Ramakrishna, S. A review on electrospinning design and nanofibre assemblies. *Nanotechnology* **2006**, *17*, R89.

11. Greiner, A.; Wendorff, J.H. Electrospinning: a fascinating method for the preparation of ultrathin fibers. *Angewandte Chemie International Edition* **2007**, *46*, 5670-5703.

12. Reneker, D.H.; Chun, I. Nanometre diameter fibres of polymer, produced by electrospinning. *Nanotechnology* **1996**, *7*, 216.

13. Kim, J.s.; Reneker, D.H. Mechanical properties of composites using ultrafine electrospun fibers. *Polymer Composites* **1999**, *20*, 124-131.

14. Bergshoef, M.M.; Vancso, G.J. Transparent nanocomposites with ultrathin, electrospun nylon-4, 6 fiber reinforcement. *Advanced Materials* **1999**, *11*, 1362-1365.

15. Jiang, S.; Hou, H.; Greiner, A.; Agarwal, S. Tough and transparent nylon-6 electrospun nanofiber reinforced melamine-formaldehyde composites. *ACS Applied Materials & Interfaces* **2012**, *4*, 2597-2603.

16. Jiang, S.; Duan, G.; Hou, H.; Greiner, A.; Agarwal, S. Novel layer-by-layer procedure for making nylon-6 nanofiber reinforced high strength, tough, and transparent thermoplastic polyurethane composites. *ACS Applied Materials & Interfaces* **2012**, *4*, 4366-4372.

17. Chen, F.; Peng, X.; Li, T.; Chen, S.; Wu, X. F.; Reneker, D.H.; Hou, H. Mechanical characterization of single high-strength electrospun polyimide nanofibres. *Journal of Physics D: Applied Physics* **2008**, *41*, 025308.

18. Papkov, D.; Zou, Y.; Andalib, M.N.; Goponenko, A.; Cheng, S.Z.; Dzenis, Y.A. Simultaneously strong and tough ultrafine continuous nanofibers. *ACS Nano* **2013**, *7*, 3324-3331.

19. Wang, W.; Ciselli, P.; Kuznetsov, E.; Peijs, T.; Barber, A. Effective reinforcement in carbon nanotube-polymer composites. *Philosophical*

Transactions of the Royal Society A: Mathematical, Physical and Engineering Sciences **2008**, *366*, 1613-1626.

20. Wang, Z.; Ciselli, P.; Peijs, T. The extraordinary reinforcing efficiency of single-walled carbon nanotubes in oriented poly (vinyl alcohol) tapes. *Nanotechnology* **2007**, *18*, 455709.

21. Fong, H. Electrospun nylon 6 nanofiber reinforced BIS-GMA/TEGDMA dental restorative composite resins. *Polymer* **2004**, *45*, 2427-2432.

22. Hull, D.; Clyne, T. *An Introduction to Composite Materials*; Cambridge university press: 1996; pp. 66-125.

23. Alcock, B.; Cabrera, N.; Barkoula, N.-M.; Loos, J.; Peijs, T. The mechanical properties of unidirectional all-polypropylene composites. *Composites Part A: Applied Science and Manufacturing* **2006**, *37*, 716-726.

Chapter 7

Conclusions and Future Work

7.1 Conclusions

Electrospinning has proven to be an efficient method to produce ultra-thin fibres with diameters down to the nano-scale. However, the mechanical properties of these nanofibres are often well below those of fibres made by conventional processes such melt- or solution spinning. The main reason for this is the competition between flow-induced chain orientation and chain relaxation before fibre solidification, leading to low degrees of molecular orientation in as-spun flexible chain polymer fibres. In conventional polymer fibre processing, chain alignment and chain extension is induced by super-drawing or stretching the as-spun fibre in the solid-state below the melting temperature into a highly oriented structure as here relaxation times are infinite.

After a full review of mechanical properties of various electrospun nanofibres, it was concluded in Chapter 2 that, although some evidence exists of confinement induced molecular orientation in the case of ultra-fine nanofibres, the orientation and particularly chain extension achieved in electrospun fibres based on flexible chain polymers is often rather limited, leading to only moderate improvements in Young's modulus (typically 2–4 times bulk polymer), well below those attainable in commercial melt- or solution spun fibres (typically 10–100 times bulk polymer).

As the introduction of a post-drawing step in commercial electrospinning processes may prove technologically challenging, the use of rigid-rod polymers as an alternative to flexible chain polymers may be more promising as here chains have already build in chain extension can be readily oriented during spinning. Other alternative routes worth pursuing are the use of nano-reinforcements such as carbon nanotubes or transforming polymer precursor fibres into carbon nanofibres, which is not further discussed in this thesis.

In this thesis, rigid (or semi-rigid) polymers showing liquid crystalline properties and reactive liquid crystal monomers have been selected for electrospinning in order to produce nanofibre with high mechanical properties.

Rigid (semi-rigid) liquid crystalline polymer PPTA in its isotropic and anisotropic phase solutions were attempted for electrospinning in Chapter 3. Although after process optimization, fibres could be spun from anisotropic solutions, these fibres had a broad distribution of fibre diameters as a result of numerous secondary solution jets and branching. Thinner fibres in these mats exhibited higher mechanical

properties, with the smallest diameter fibres (2.1 μm) that could be measured reaching peak values of tensile strength and Young's modulus of 1.1 GPa and 58.6 GPa, respectively. An equation linking geometry reduction to Young's modulus was developed to predict properties of fibres with diameters less than 2.1 μm. Despite the fact that the electrospinning of PPTA could not be operated in a controllable and continuous manner, the work still showed that for the first time high performance *p*-aramid fibres can be electrospun from anisotropic solutions.

Since the uncontrollable manner of electrospinning PPTA solutions is mainly caused by the use of sulphuric acid as a solvent, liquid crystal monomers, which can be oriented in their nematic phase and subsequently 'frozen-in' by UV-radiation induced photo-polymerization was investigated.. It was intended to electrospun this into nanofibres which was described in Chapter 4. A reactive mesogen RM257 was selected for blending with thermoplastic polymers as a carrier and electrospinning into nanofibres. Electrospinning of different weight ratios of PMMA/RM257 blends and PA6/RM257 blends was carried out followed with UV-radiation induced photo-polymerization. DSC results showed that the glass transition temperature shifted with increasing RM 257 content, indicating a weak interaction between PMMA and RM257, whilst no such T_g shift was found in the case of PA6/RM257, indicating phase separation which was further confirmed by morphological studies of the resulting nanofibres after UV-curing. The mechanical properties of the composite fibres were enhanced with increasing content of RM257 from 20 wt% to 33 wt% followed with a subsequent drop upon further increasing RM257 content. The composite fibre containing 33 wt% of RM257 shows the best mechanical

performance with a Young's modulus up to 2.8 GPa and a tensile strength up to 121 MPa and a highest effective modulus contribution of RM257 of 6.1 GPa. Although this chapter exhibits a controllable manner of electrospinning liquid crystalline materials into fibres the resulting mechanical properties achieved through this route are well below those of required for high performance fibres. This is mainly because pure electrospun reactive mesogens nanofibres could not be obtained because of the absence of viscoelasticity in these monomer liquids, leading to electrospraying rather than electrospinning. At the same time the mechanical properties of the pure RMs seem not sufficient to achieve properties comparable to high performance fibres. Despite that, this chapter still provides some insight into routes to creat oriented fibres via electrospinning incorporating RMs with potentially interesting functional and optical properties.

Chapter 5 presents a high performance co-polyimide electrospun nanofibre which can be produced in a controllable and continuous manner. The BPO co-polyimide precursor polyamic acid was first synthesized and electrospun into nanofibres and then imidized to co-polyimide nanofibres. It was found that the aligned co-polyimide nanofibre mats possesses a mean modulus, strength and strain-at-break of respective 10 GPa, 1.04 GPa, and 13.5 %. In comparison with previously reported co-polyimide nanofibres (BBO) with similar chemical structures, the BPO co-polyimide nanofibres can be as stiff and strong while at the same time exhibiting moderate ductility. On the other hand, the BPO co-polyimide nanofibres are tougher than homo-polyimide (BPDA/PDA) nanofibres due to their relatively high strain-at-break and exhibited similar levels of toughness as Kevlar fibres. This study also reported a

novel and efficient way to evaluate mechanical properties of aligned nanofibre bundles (~30 nanofibres in a bundle) by virtue of a micro-tensile tester. Young's modulus of 38 ± 2 GPa and tensile strength of 1550 ± 70 MPa were found. Further evaluation based on the bundle data by using of Daniel's theory based on Weibull statistics was used to predict the tensile strength of single fibres at about 1.9 GPa.

In Chapter 6, BPO co-polyimide nanofibre reinforced composites were fabricated by impregnating aligned mats with a 10% of matrix solution. Laminate theory and 'Rule of Mixtures' were used for the evaluation of the mechanical properties of these nanofibre reinforced laminates. It is found that the Young's modulus and tensile strength of off-axis loaded composites could be well described using classical composite theories. Meanwhile, the longitudinal mechanical behaviour of the UD composites with different nanofibre volume fractions corresponded well with the 'Rule of Mixture' (Voigt model). More importantly, this study also introduced a novel method to evaluate the Young's modulus of single nanofibres from composite data. Aligned nanofibre mats produced in this study exhibited an average nanofibre orientation of 14 ° and from this the longitudinal Young's modulus of a perfectly aligned composite and that of a single nanofibre could be back-calculated at 59 GPa.

A new mechanical property comparison graph can be made based on the one shown in Chapter 2 including the mechanical properties of the electrospun fibres reported in this thesis. It clearly shows that the electrospun BPO co-polyimide nanofibres and *p*-aramid fibres possess among the highest mechanical properties reported for electrospun fibres so far.

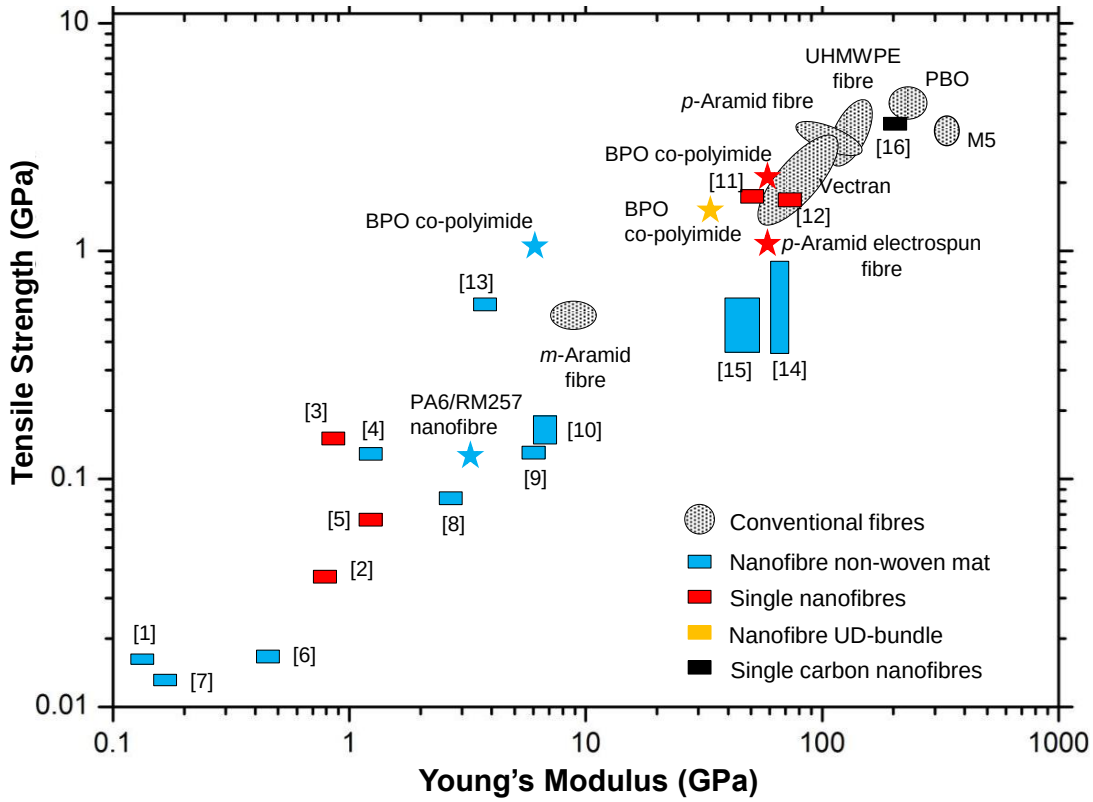

Figure 7.1. *Mechanical property comparison chart of traditional high performance fibres, reported electrospun nanofibres and the nanofibres investigated in this thesis with respect to Young's modulus and tensile strength. Commercial high-performance fibres show typical tensile strengths of 2–4 GPa and moduli of around 100–300 GPa, while most electrospun fibres typically possess tensile strengths < 0.3 GPa and Young's moduli < 3 GPa [1-10]. Some high performance electrospun nanofibres have been reported in literature based on polyimide [11], polyacrylonitrile [12] and carbon nanofibres from electrospun PAN precursors [13-16].*

7.2 Future Work

Based on a full understanding of the production of traditional high performance fibres, the electrospinning process and recently reported mechanical properties of electrospun nanofibres, this thesis presents several routes to electrospun fibres with highly oriented molecular structures. Although the electrospun BPO nanofibre has been proven to be among the best nanofibres with regards to mechanical properties, there is still a big gap between the mechanical properties achieved here and those of conventional high performance polyimide fibres such as BPDA/PPD/PMR whose tensile strength can be as high as 5.1 GPa with Young's moduli up to 282 GPa [17, 18]. The significantly lower mechanical properties of our electrospun co-polyimide fibres can again be mainly ascribed to the relatively poor molecular chain orientation in these fibres as reflected by a Herman's orientation factor of BPO nanofibres of about 0.8, compared to orientation factors in commercial PI fibres approaching 1. Thus, a potential way to further improve mechanical properties is through improved molecular orientation in these electrospun fibres.

Although post-drawing of single nanofibres is hardly technologically feasible, a certain degree of stretching of nanofibre bundles or UD mats could be used to further improve molecular orientation or even increase crystallinity [19]. Some preliminary data is shown in Figure 7.2. Here, a certain degree of stretching (3%, 5%, 7%, 10%) on electrospun BPO polyamic acid nanofibre UD mats was applied in a universal testing machine enclosed in an oven at different temperatures ranging from room temperature to 120 °C (i.e. below the imidization temperature). Young's modulus of

all samples was significantly enhanced to about twice its initial value from 2.1 GPa to 3.9 GPa. It should be noted that PAA nanofibre can only be stretched to about 7% at 100 °C and 3% at 120 °C, respectively. Further stretching would lead to fibre breakage. However, the modulus of all stretched UD nanofibre mats only increased by about 10% to 20% as shown in Figure 7.3, which is well below our expectations. A possible reason for this could be that stretching barely improved the molecular orientation but only improved the nanofibre orientation in the mat.

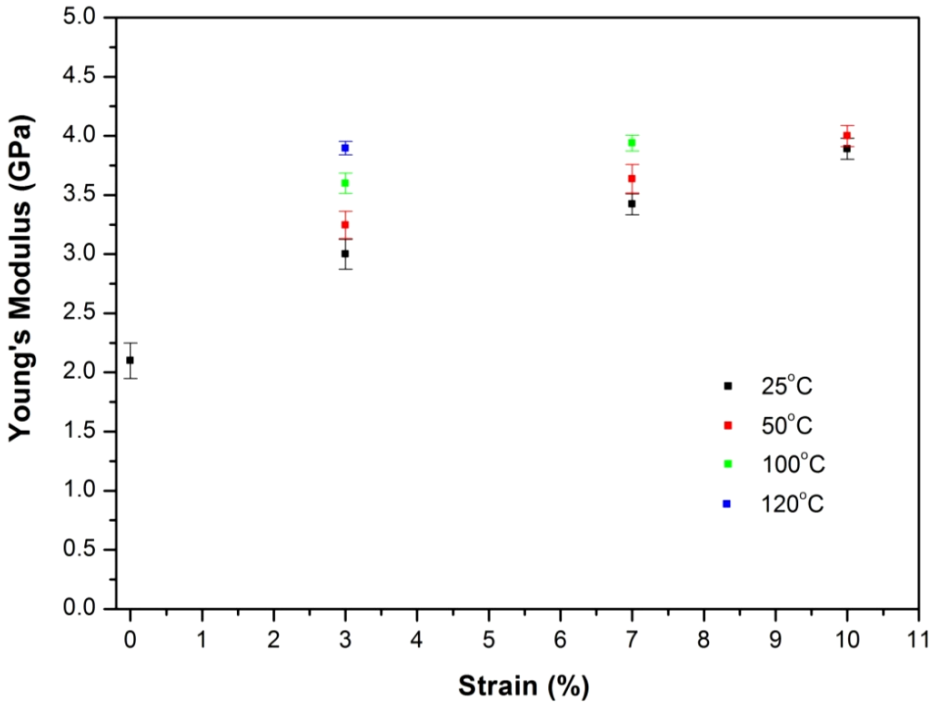

Figure 7.2. *The Young's modulus of electrospun BPO polyamic acid nanofibres after stretching at different extensions and temperatures.*

An alternative approach worthy of trying is to apply tension to the fibre during the imidization process. For this, PAA fibres were stretched at room temperature or 50 °C to about 10% extension, with subsequently a certain degree of pre-tension

being applied to the stretched nanofibre mats during the imidization process. It is expected that this could further improve the orientation during the molecular self-ordering process from flexible to rigid chain structure.

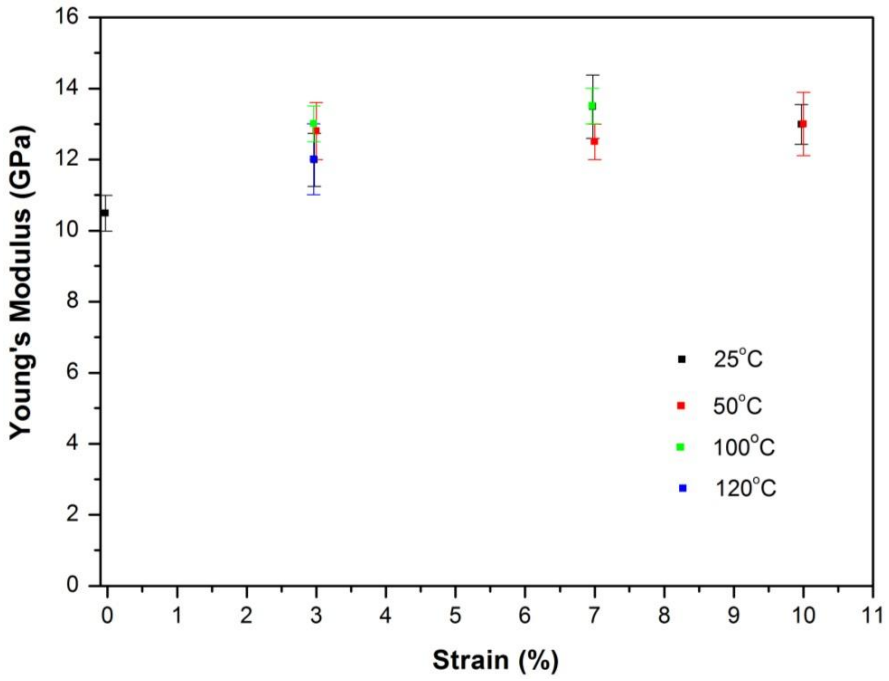

Figure 7.3. *The corresponding Young's modulus of stretched electrospun BPO nanofibres after imidization.*

As described in Section 4.3.1, after UV-curing, the blend nanofibres tended to fuse together, as the liquid crystals were prone to leach out from the blend fibre. Bi-component electrospinning has been successfully applied to produce core-shell fibres with a polymer [20] or liquid crystal [21-23] core. Hence, some preliminary bi-component electrospinning studies were performed to evaluate to potential of this technique while at the same time solving the leaching problem as the RMs would be contained in a thermoplastic shell.

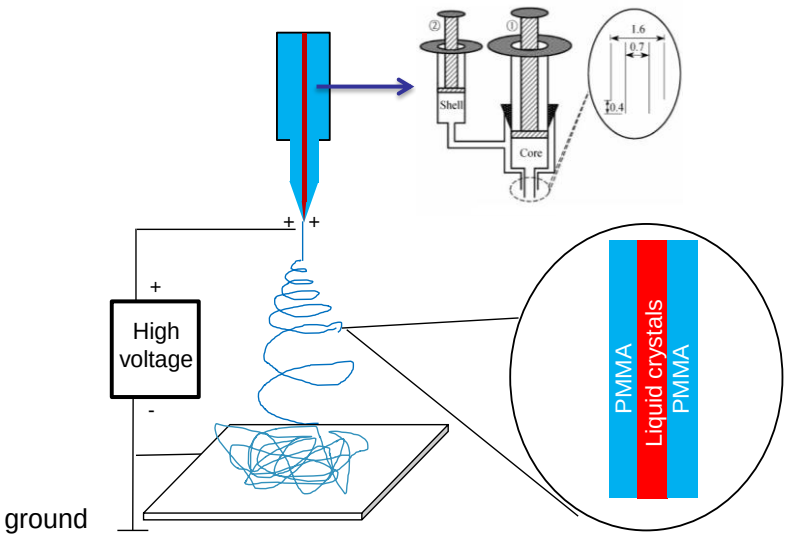

Figure 7.4. *Schematic illustration of the experimental set up for bi-component electrospinning. The insets show the diameter of co-axial spinneret and a core-shell structure of nanofibres.*

7 wt% PMMA in formic acid and acetic acid (1/1, w/w) and 21 wt% of RM257 dissolved in chloroform and *p*-xylene (1/1, w/w) were used as outer and inner solutions, respectively. Feeding rate was about 1 ml/h for both solutions, voltage around 20 kV and distance of 20 cm were adjusted to obtain good quality nanofibres.

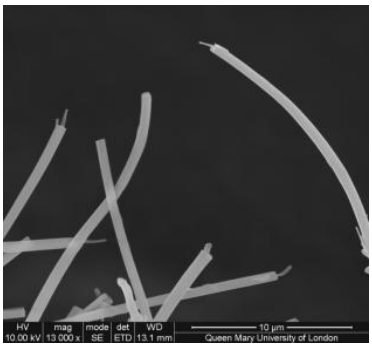

Figure 7.5. *SEM micrograph of core-shell nanofibres with RM257 as core and PMMA as shell.*

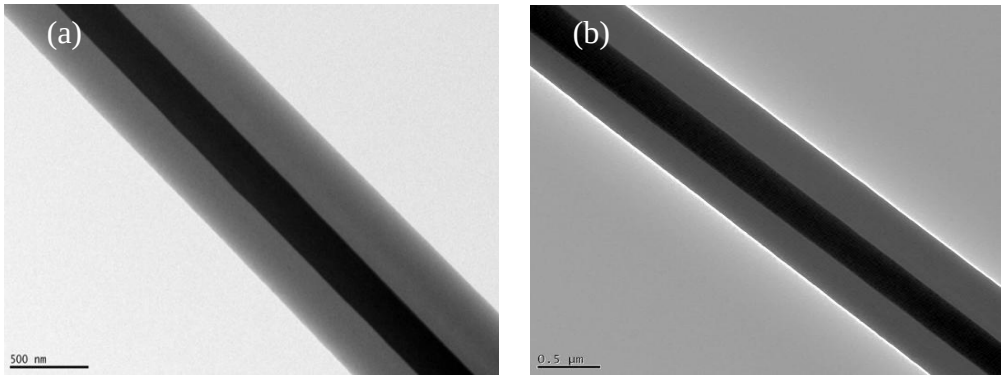

Figure 7.6. *TEM micrographs of electrospun nanofibres showing clear contrast between core (RM257) and shell structures (PMMA); (a) before UV-curing and (b) after UV-curing.*

Core-shell nanofibres composed of a liquid crystal core (RM257) and a polymer shell (PMMA) were created using an electrospinning set-up incorporating a bi-component spinneret as shown in Figure 7.4. Figure 7.5 clearly displays the core-shell structures of these electrospun nanofibres after photo-polymerization by means of SEM and Figure 7.6 presents two TEM graphs with clear contrast of a core-shell morphology before and after UV-curing. No nanofibre fusion was observed because the polymer shell now inhibits flow of the liquid crystals.

However, the numerous process parameters including solvent selection (miscible or non-miscible) [24] for both core and shell, evaporation rate mismatch between both solvent systems (which can result in re-dissolving of core or shell) and the flow rate adjustment of both solutions caused great complexity in the bi-component electrospinning process for RM257 and PMMA. Nevertheless, the capability of embedding liquid crystals inside a bi-component nanofibre could prove to be a

potential way to create neat liquid crystal fibres with interesting functional and optical properties after removal of the polymer sheath.

7.3 References

1. Carrizales, C.; Pelfrey, S.; Rincon, R.; Eubanks, T.M.; Kuang, A.; McClure, M.J.; Bowlin, G.L.; Macossay, J. Thermal and mechanical properties of electrospun PMMA, PVC, Nylon 6, and Nylon 6, 6. *Polymers for Advanced Technologies* **2008**, *19*, 124-130.

2. Bazbouz, M.B.; Stylios, G.K. The tensile properties of electrospun nylon 6 single nanofibers. *Journal of Polymer Science Part B: Polymer Physics* **2010**, *48*, 1719-1731.

3. Zussman, E.; Burman, M.; Yarin, A.; Khalfin, R.; Cohen, Y. Tensile deformation of electrospun nylon-6, 6 nanofibers. *Journal of Polymer Science Part B: Polymer Physics* **2006**, *44*, 1482-1489.

4. Sanatgar, R.H.; Borhani, S.; Ravandi, S.A.H.; Gharehaghaji, A.A. The influence of solvent type and polymer concentration on the physical properties of solid state polymerized PA66 nanofiber yarn. *Journal of Applied Polymer Science* **2012**, *126*, 1112-1120.

5. Hang, F.; Lu, D.; Bailey, R.J.; Jimenez-Palomar, I.; Stachewicz, U.; Cortes-Ballesteros, B.; Davies, M.; Zech, M.; Bödefeld, C.; Barber, A.H. In situ tensile testing of nanofibers by combining atomic force microscopy and scanning electron microscopy. *Nanotechnology* **2011**, *22*, 365708.

6. Stachewicz, U.; Peker, I.; Tu, W.; Barber, A.H. Stress delocalization in crack tolerant electrospun nanofiber networks. *ACS Applied Materials & Interfaces* **2011**, *3*, 1991-1996.

7. Veleirinho, B.; Rei, M.F.; Lopes-DA-Silva, J. Solvent and concentration effects on the properties of electrospun poly (ethylene terephthalate) nanofiber mats. *Journal of Polymer Science Part B: Polymer Physics* **2008**, *46*, 460-471.

8. Wu, S.Z.; Yang, X.P.; Zhang, F.; Hou, X.X. Stretching-induced orientation for improving the mechanical properties of electrospun polyacrylonitrile nanofiber sheet. *Advanced Materials Research* **2008**, *47*, 1169-1172.

9. Pai, C.-L.; Boyce, M.C.; Rutledge, G.C. Mechanical properties of individual electrospun PA 6(3)T fibers and their variation with fiber diameter. *Polymer* **2011**, *52*, 2295-2301.

10. Naraghi, M.; Arshad, S.; Chasiotis, I. Molecular orientation and mechanical property size effects in electrospun polyacrylonitrile nanofibers. *Polymer* **2011**, *52*, 1612-1618.

11. Papkov, D.; Zou, Y.; Andalib, M.N.; Goponenko, A.; Cheng, S.Z.; Dzenis, Y.A. Simultaneously strong and tough ultrafine continuous nanofibers. *ACS Nano* **2013**, *7*, 3324-3331.

12. Chen, F.; Peng, X.; Li, T.; Chen, S.; Wu, X.-F.; Reneker, D.H.; Hou, H. Mechanical characterization of single high-strength electrospun polyimide nanofibres. *Journal of Physics D: Applied Physics* **2008**, *41*, 025308.

13. Baji, A.; Mai, Y.-W.; Wong, S.-C.; Abtahi, M.; Du, X. Mechanical behavior of self-assembled carbon nanotube reinforced nylon 6, 6 fibers. *Composites Science and Technology* **2010**, *70*, 1401-1409.

14. Zussman, E.; Chen, X.; Ding, W.; Calabri, L.; Dikin, D.; Quintana, J.; Ruoff, R. Mechanical and structural characterization of electrospun PAN-derived carbon nanofibers. *Carbon* **2005**, *43*, 2175-2185.

15. Zhou, Z.; Lai, C.; Zhang, L.; Qian, Y.; Hou, H.; Reneker, D.H.; Fong, H. Development of carbon nanofibers from aligned electrospun polyacrylonitrile

nanofiber bundles and characterization of their microstructural, electrical, and mechanical properties. *Polymer* **2009**, *50*, 2999-3006.

16. Arshad, S.N.; Naraghi, M.; Chasiotis, I. Strong carbon nanofibers from electrospun polyacrylonitrile. *Carbon* **2011**, *49*, 1710-1719.

17. Kaneda, T.; Katsura, T.; Nakagawa, K.; Makino, H.; Horio, M. High-strengthhigh-modulus polyimide fibers I. One-step synthesis of spinnable polyimides. *Journal of Applied Polymer Science* **1986**, *32*, 3133-3149.

18. Kaneda, T.; Katsura, T.; Nakagawa, K.; Makino, H.; Horio, M. High-strength-high-modulus polyimide fibers II. Spinning and properties of fibers. *Journal of Applied Polymer Science* **1986**, *32*, 3151-3176.

19. Sikkema, D.J. Design, synthesis and properties of a novel rigid rod polymer, PIPD or M5: high modulus and tenacity fibres with substantial compressive strength. *Polymer* **1998**, *39*, 5981-5986.

20. Sun, Z.; Zussman, E.; Yarin, A.L.; Wendorff, J.H.; Greiner, A. Compound core-shell polymer nanofibers by co-electrospinning. *Advanced Materials* **2003**, *15*, 1929-1932.

21. Lagerwall, J.P.; McCann, J.T.; Formo, E.; Scalia, G.; Xia, Y. Coaxial electrospinning of microfibres with liquid crystal in the core. *Chemical Communications* **2008**, 5420-5422.

22. Buyuktanir, E.A.; Frey, M.W.; West, J.L. Self-assembled, optically responsive nematic liquid crystal/polymer core-shell fibers: Formation and characterization. *Polymer* **2010**, *51*, 4823-4830.

23. Wu, Y.; An, Q.; Yin, J.; Hua, T.; Xie, H.; Li, G.; Tang, H. Liquid crystal fibers produced by using electrospinning technique. *Colloid and Polymer Science* **2008**, *286*, 897-905.

24. Longson, T.J.; Bhowmick, R.; Gu, C.; Cruden, B.A. Core–shell interactions in coaxial electrospinning and impact on electrospun multiwall carbon nanotube core, poly (methyl methacrylate) shell fibers. *The Journal of Physical Chemistry C* **2011**, *115*, 12742-12750.